UNIVERSITÀ DEGLI STUDI DI PADOVA

SCUOLA DI SCIENZE
Dipartimento di Geoscienze
Direttrice Prof.ssa Cristina Stefani

TESI DI LAUREA MAGISTRALE
IN
GEOLOGIA E GEOLOGIA TECNICA

CHARACTERIZATION OF THE NEW DIAMONDS COMING FROM CENTRAL AFRICAN REPUBLIC

Relatore: Prof. Fabrizio Nestola

Laureanda: Sofia Lorenzon

N° matricola:1144503

ANNO ACCADEMICO 2017/2018

Abstract

This thesis work focuses on the characterization of a diamond set coming from secondary alluvial deposits of the Ubangy River, natural border between The Democratic Republic of Congo and The Central African Republic; these deposits are far about 150 km to North-East from the capital Bangui (Central African Republic).

At present, there are no available scientific investigations of gem-quality diamonds from this locality and therefore the main aim of this work is to characterize for the first-time diamonds from CAR.

In the Central African Republic, Kimberlite pipes (primary sources of diamonds) are not present and the diamonds have been recovered in two Cretaceous sandstone formations, the Carnot Formation and the Mouka-Ouadda Formation, considered secondary host rocks of diamonds, and in recent alluvial deposits.

The analysis of the paleocurrents through the study of the sedimentary structures and the provenance of the other heavy minerals both in the Carnot Formation and the Mouka-Ouadda Formation suggest that the primary source of the diamonds could be located at South of the two formations, apparently in the northern Democratic Republic of Congo.

The diamonds found in the alluvial deposits probably have derived from the alteration of the sandstone formation (in the past their extension was wider) and following transport and deposition in other places.

Previous studies about diamonds coming from Democratic Republic of Congo show the lithospheric nature of the these.

The characterization of the diamonds consists in the determination of their lithospheric (about 120-230 km depth) or sub-lithospheric (about 300-800 km depth) origin.

This occurs through the identification of the mineral inclusions within the diamonds, the study of the stable isotopes (C and N), the study of the impurities; thanks to the formation depth of the diamonds, it provides information about the

mineralogy, petrography, geochemistry and geodynamics of the upper mantle, transition zone and lower mantle.

The diamond set studied in this work is composed by twelve diamonds: the shape is different from pseudo-octahedral to irregular; the size is about 1 cm along the longest direction and the colour is variable, from grey to yellow sometimes vivid.

The identification of the inclusions was performed by the Micro-Raman spectroscopy, since the size of inclusions did not allow us to obtain satisfying results through the Single-crystal X-ray Diffraction.

Moreover, the Fourier Transform InfraRed (FTIR) spectroscopy permitted us to calculate the nitrogen amount in the diamonds and their aggregation state.

The main inclusions are anatase, calcite, dolomite, olivine and a fluid phase.

Such inclusions are typical of the lithospheric diamonds, but the finding of only one possible inclusion of ringwoodite opens the possibility that these diamonds formed at sub-lithospheric conditions, in the deeper part of transition zone (about 525-660 km depth).

Moreover, the amount of nitrogen impurities in the diamonds and its aggregate state do not provide a definitive proof of lithospheric or sub-lithospheric nature of the samples.

Further studies are necessary for a definitive identification of the most important inclusion, which is ringwoodite.

Riassunto

L’obiettivo di questa tesi è stato caratterizzare una serie di diamanti provenienti da dei depositi fluviali del fiume Ubangy, confine naturale tra la Repubblica Democratica del Congo e la Repubblica Centrafricana; questi depositi sono situati a circa 150 km a Nord-Est dalla capitale Bangui (Repubblica Centrafricana).

Ad oggi non sono presenti investigazioni scientifiche su diamanti provenienti da questa località e quindi l’obiettivo principale di questa tesi è caratterizzare per la prima volta i diamanti provenienti dalla Repubblica Centrafricana.

In Repubblica Centrafricana, non vi è la presenza di kimberliti (sorgente primaria dei diamanti) e i diamanti sono stati ritrovati in due formazioni arenacee Cretacee, la Carnot Formation e la Mouka-Ouadda Formation, considerate rocce ospiti di diamanti secondarie, e in recenti depositi fluviali.

L’analisi delle paleocorrenti attraverso lo studio delle strutture sedimentarie e la provenienza degli altri minerali pesanti, sia nella Carnot Formation che nella Mouka-Ouadda Formation indicano che la possibile sorgente primaria dei diamanti potrebbe essere collocata a Sud delle due formazioni, evidentemente a Nord della Repubblica Democratica del Congo.

I diamanti trovati nei depositi fluviali probabilmente derivano dall’alterazione delle formazioni arenacee (la loro estensione in passato era maggiore) e il successivo trasporto e deposizione in altri luoghi.

Studi precedenti su diamanti provenienti dalla Repubblica Democratica del Congo mostrano origine litosferica dei diamanti.

La caratterizzazione dei diamanti consiste nella determinazione della loro origine litosferica (120-230 km di profondità) o sub-litosferica (300-800 km di profondità). Questo è possibile attraverso l’identificazione delle inclusioni mineralogiche all’interno dei diamanti, lo studio degli isotopi stabili (C e N) e lo studio delle impurità; grazie alla profondità di formazione dei diamanti, questo permette di avere informazioni sulla mineralogia, petrografia, geochimica e geodinamica del mantello superiore, zone di transizione e mantello inferiore.

I campioni studiati sono dodici, la loro forma varia da pseudo-ottaedrica ad irregolare, sono grandi circa 1 cm e il loro colore è variabile.

L'identificazione delle inclusioni è avvenuta principalmente attraverso la spettroscopia Micro-Raman, poiché la dimensione delle inclusioni non ha permesso di ottenere buoni risultati con la diffrazione a raggi x a cristallo singolo.

Inoltre, la spettroscopia ad InfraRosso ci ha permesso di calcolare il contenuto di azoto nei diamanti e il loro stato di aggregazione.

Le principali inclusioni trovate sono anatasio, calcite, dolomite, olivina e inclusioni di fase fluida.

Questa associazione mineralogica solitamente indica un'origine litosferica, ma il ritrovamento di un'unica inclusione di ringwoodite ha aperto la possibilità che questi diamanti si siano formati in condizioni sub-litosferiche, nella parte più profonda della zona di transizione (525-660 km di profondità circa).

Inoltre, il contenuto di azoto e il suo stato di aggregazione non hanno confermato la natura litosferica o sub-litosferica dei campioni.

Studi successivi sono necessari per un'identificazione definitiva dell'inclusione più importante, la ringwoodite.

Contents

Introduction

Diamonds are rare, but very important minerals to give information on Earth's interior, thanks to their formation's depth (from about 120 km to more 800 km).

Diamond is the high-pressure polymorph of the graphite: it has cubic crystal structure and very simple chemical composition, it is composed of carbonium atoms (C) and it can crystallize from 120-150 Km depth, in function of the temperature (graphite-diamond boundary).

Diamonds form by metasomatic process that involves "C-H-O-bearing fluid" or melt at high depth, and this allows to track carbon mobility in the deep Mantle, mantle redox state and to follow the path and history of the carbon from which diamond is composed.

Therefore, diamonds give an important contribution the Earth's carbon cycle (Shirey el al. 2013).

At the Earth's surface, diamonds are present as xenocrystals in kimberlites or lamproites, particular magmatic rocks (primary source), in secondary host sedimentary rocks or in alluvial deposits (secondary sources).

The eruption of kimberlites or lamproites is associated with the stable Archean cratons (old and seismically stable) where the lithospheric mantle extends from about 40 km depth down to perhaps 250-300 km (under the oceans it extends only to 110 km) and for its shape, this part of mantle is called "mantle keel" (figure A).

This is more melt-depleted and deeper than Proterozoic and younger continental keels and its lowermost reaches are in the diamond stability field.

The Archean lithospheric mantle keels are the most diamond-producer regions, and probably their depth facilitates the production of kimberlitic magma, explaining the presence of diamondiferous kimberlite fields associated to the cratons.

The origin of the secondary sources is due to the alteration of the primary host rocks, and following transport and deposition of the diamonds, which are very resistant to the alteration, in different zones.

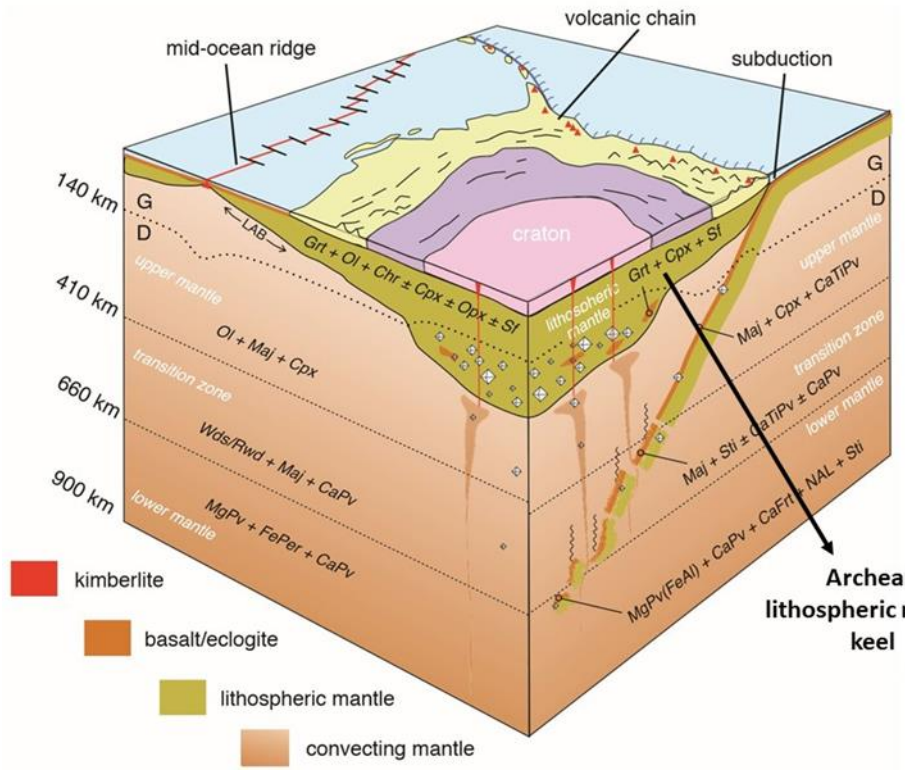

Figure A. Geological scheme of the environment of the diamond formation (modified from Shirey et al. 2013).

Moreover, the study of their inclusions can provide the mineralogy of upper mantle, transition zone and lower mantle.

Diamonds are divided in two groups, in function of their formation's depth; the first one involves the lithospheric diamonds, they crystallize from about 120 km (the boundary graphite/diamond) to 220/230 km, they usually have pseudo- or octahedral shape and the amount of nitrogen is relative high.

Based on their parental rocks, the lithospheric diamonds are divided in P-type (peridotitic paragenesis), E-type (eclogitic paragenesis) and websteritic type.

The P-type diamonds are sub- divided in harzburgitic, lherzolitic and wehrlitic paragenesis, and the main inclusions are olivines, chrome-pyropes, chromites, enstatites, chrome-diopsides and sulphides.

The E-type diamonds, instead, contain garnets, omphacites, sulphides, coesites, ilmenites and kyanites.

The websteritic type diamonds mainly contain pyropes, clino-pyroxenes and sulphides.

The lithospheric diamonds represent the 99% of the worldwide diamond population and they are mainly recovered in West, Central and South Africa, Siberia, North Australia, Canada, Brazil and more rarely in China, India and North Europe (figure B) (Shirey et al. 2013).

The second group involves the sub-lithospheric or superdeep diamonds; they form from about 300 km to more 800 km, they usually have irregular shape and the amount of nitrogen is relative low.

Different divisions are present based on parental rocks; we consider the classification of Kaminsky (2012) and he recognizes three types, juvenile-ultramafic, analogue of eclogitic and carbonatic association.

In the juvenile ultramafic association, the inclusions that we usually find are ferropericlases, MgSi-perovskites, CaTi-perovskites, stishovites, tetragonal almandine-pyrope phase, TAPP (jeffbenite,(Nestola et al. 2016)),olivines, spinels, manganoilmenites, titanites, native nickel, native iron, magnetites, majorites garnets and moissanites.

In the analogue to eclogitic type, the inclusions entrapped in the diamonds are phases “Egg”, (aggregates of euhedral and cubic grains of $AlSiO_3OH$) and stishovites.

In the carbonatic association the main inclusions are calcites, dolomites, nyerereites, nahcolites and halides.

However, these are not the inclusions of the initial mineral assemblage, but they are the result of the retrograde transformations that occur during the rise of the diamond from the depth to the surface.

The superdeep diamonds represent the 1% of the worldwide diamond population and they are mainly found in Brazil (in particular in Juina area, (Kaminsky et al. 2009; Bulanova et al. 2010)), Canada, South Africa and South Australia (figure B).

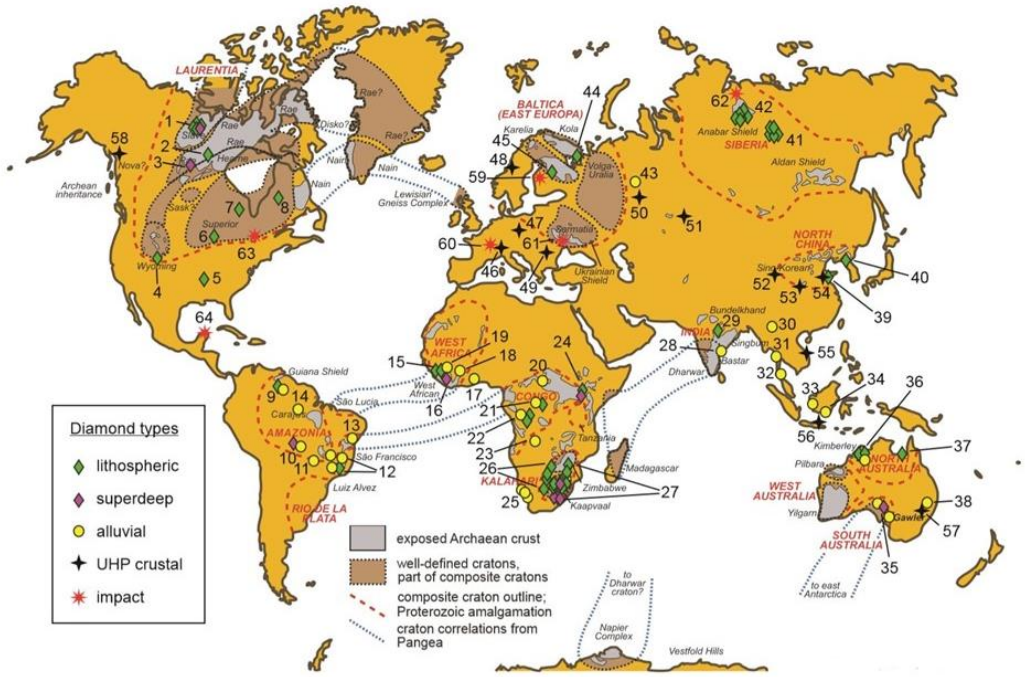

Figure B. Diamond localities in the World, both lithospheric and sub-lithospheric ones (from Shirey et al. 2013).

The identification of the inclusions and the characterization of the diamonds (lithospheric vs. sub-lithospheric) is important to determine the mineralogy, the petrology, the geochemistry and geodynamics of the Earth's Mantle, the fluid circulation at different depth levels during the metasomatic processes, their source and the provenance of the carbon.

The aim of this thesis is to characterize for the first time, a set of diamonds (figure C) coming from secondary alluvial deposits of Ubangy River, natural border between The Democratic Republic of Congo and The Central African Republic; the deposits are far about 150 km to North-East from the capital Bangui (Central African Republic).

Although the alluvial deposits of this country have been studied and explored by the mining company, especially in 50s, to find new diamonds source and to estimate the diamond potential, the diamonds coming from the Central African Republic have never been studied and characterized.

Figure C. The diamonds set coming from Central African Republic, studied in this thesis work.

The only studied materials from this place are the carbonado samples: carbonado is porous aggregates of micrometres-size diamond crystals; they are not rare, but they are never found in kimberlites and they mainly contain typical minerals of Earth's Crust rather than Mantle's ones, and their $\delta_{13}C$ is lower than kimberlite diamonds' one (Ozima et al. 1991).

The hypothesis about their formation are a lot, but at present, a sure theory does not exist.

A common feature of these samples is the presence of noble gases and radiation-damage products: this suggests that the formation environment is uranium-rich crustal one.

A series of microstructural and chemical studies on Brazilian and African samples (Kagi et al. 1994; De et al. 1998) have been conducted to explain this, but the doubts are still a lot.

However, the thesis does not consider this aspect, and we only focus on the diamond samples and the main aim of this work is the characterization of these (lithospheric vs. sub-lithospheric diamonds).

The analytical techniques used to identify the inclusions are the Micro-Raman spectroscopy; the Fourier Transform InfraRed spectroscopy (FTIR) was applied to study the diamond impurities.

1. Geological setting

1.1. Provenance of samples

The diamonds come from secondary alluvial deposits of Ubangy River, natural border between The Democratic Republic of Congo and The Central African Republic; the specific deposits are far about 150 km to the capital Bangui (Central African Republic).

Figure 1.1. The geographic map of Central African Republic (CAR); the red star indicates the possible position of the alluvial deposits, from which the studied diamonds were recovered.

In this country, the discovery of the first diamond-bearing alluvial deposits was in 1931 in the West and South-West of this country; this marked the onset of mining and the geological surveying in these zones.

This created great interest in this area and it led to a detail exploration of the geological formations, to understand the possible provenance of the diamonds.

The result of this work allowed to define the Carnot Formation and the Mouka-Ouadda Formation as host rocks of diamonds.

Subsequently, a detailed geological study was made and undertaken principally for the mining companies, but it was interrupted in the 1960 when the country became independent and the exploitation stopped.

Despite this, in the 80s and 90s new studies were carried out to define the provenance and the processes of emplacement of the detrital material, like diamonds, and the depositional environment of this formation.

In addition, since 2007 the Central African Republic has been a member of the Kimberley Process Certification Scheme (KPCS): it is an international activity whose goal is to prevent trade in conflict diamonds while helping to protect trade through monitoring of the production, exportation and importation of rough diamonds throughout the world.

The Central African Republic, how member of this program, must report its official amount of diamond imports and exports, and the data are then made public to allow a monitoring by the all members of the organization.

So, new studies about diamonds, their possible provenance and their recovering have conducted in the last years.

1.2. Geology of Central African Republic

Before to focus on the diamond-bearing alluvial deposits, the Carnot Formation and the Mouka-Ouadda Formation, it is necessary to explain the geology of Central African Republic.

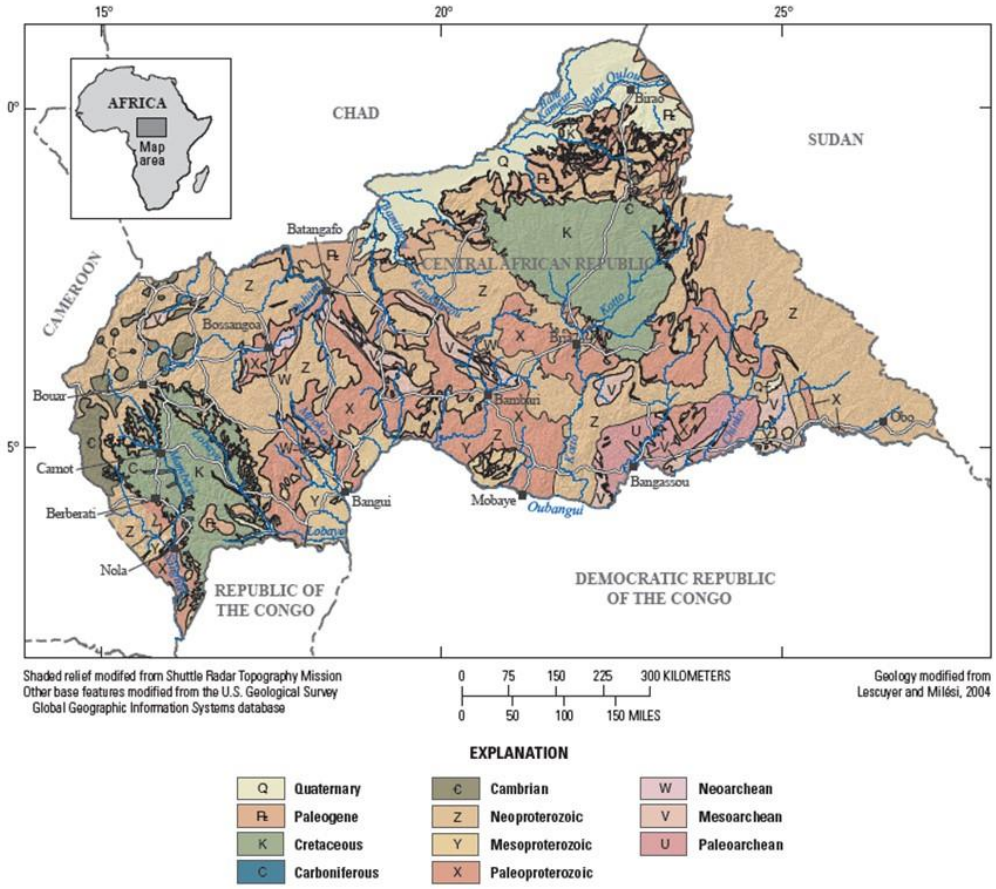

Figure 1.2. The geological map of Central African Republic (from Chirico et al. 2010). The explanation divides the geological formations in function of the geological age.

According to Chirico et al. (2010), the geology of CAR consists mainly of basement rocks of Archean and Proterozoic age, which can be divided into two main geological groups: a granitic-gneissic complex and a schist-quartzitic complex.

The granitic-gneissic complex is probably of Neoarchean age and it is composed of gneissic, granite and amphibolite rocks.

Also included in this group of basement rocks is a series of sedimentary volcanic sequences that are typically referred to as “greenstones”.

Overlying the Archean basement rocks is the schist-quartzitic complex, which is thought to be of Neoproterozoic age and it is composed of quartzitic and schistose rocks that are only weakly metamorphosed and generally folded.

Both these complexes are intruded throughout the country by basic rocks of Neoproterozoic age.

Overlying these older rocks is a sequence of Paleozoic rocks: the two main Paleozoic formations are the Mambéré Formation (located in the western CAR) and the Kombélé Formation (located in the eastern CAR) and both have glacial origin.

The Mambéré Formation is a tillite composed of both basal and flow tills as well as reworked glacial deposits derived from sandstone, conglomeratic sandstone and siltstone that occur in continuous beds, lenses and isolated rocks.

The Kombélé Formation is a conglomeratic sandstone tillite composed of glacial-outwash plain sediments.

Both the Paleozoic formations generally range in thickness from 30 to 50 meters and they are covered by Cretaceous sandstone units lying unconformably above them.

The Mesozoic, probably Cretaceous, fluvial sequences of conglomeratic sandstones concealing the Paleozoic glacial tillites form two distinct plateaus, one in the east and one in the west.

The western plateau is composed of the Carnot Formation and the eastern one by the Mouka-Ouadda Formation (figure 1.3): both are host rocks of diamonds and then they are better explained (see subchapters 1.3 and 1.4).

The two formations extended much farther south and north than today; later erosion of these developed the current plateau landform.

A series Cenozoic rocks occurs in two distinct zones within CAR: the first is a series Paleo-Tchadienne continental terminal sandstones and the second is the Bambio Sandstone.

Recent Pleistocene deposits have filled in the northern basin and generally divided into either Neo-Tchadienne alluvium or recent alluvial deposits.

Quaternary alluvial deposits are also found in the many riverine floodplains throughout the country.

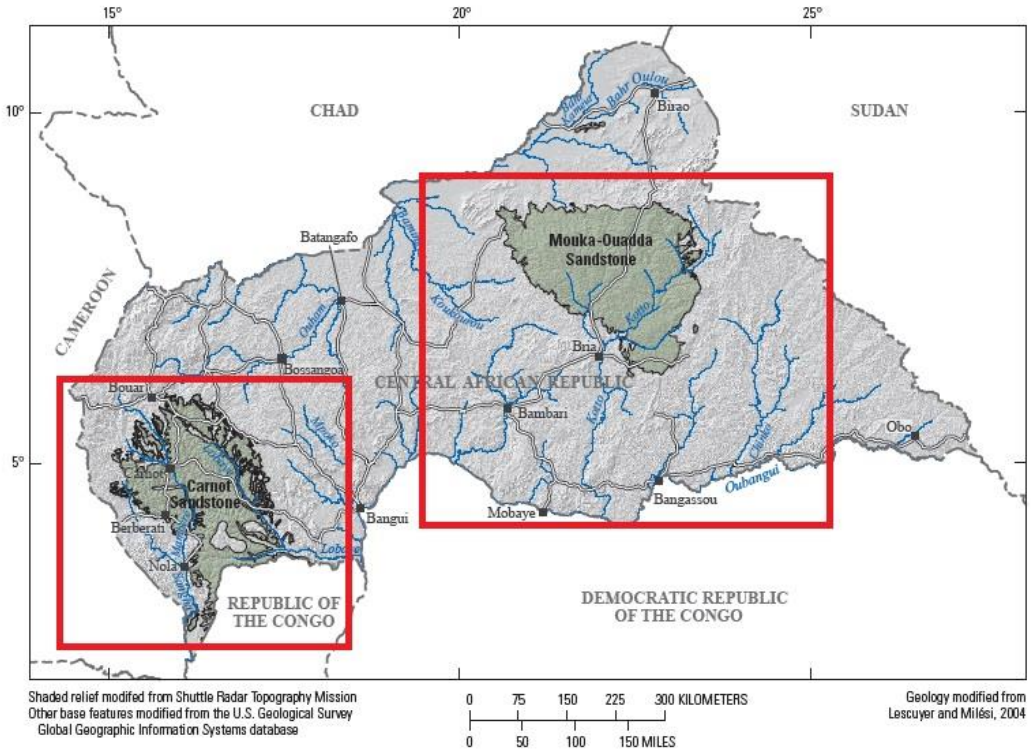

Figure 1.3. The Carnot and the Moukka-Ouadda Formations (modified from Chirico et al. 2010).

1.3. The Carnot Formation

The Carnot Formation is one of the two sandstone formations within Central African Republic that is considered a host rock of diamonds.

It is a sub-horizontal, supposedly Cretaceous, continental sandstone-conglomerate unite, covering an area of 46,000 km² in the southwest of Central African Republic and northernmost of Congo.

It is up to 400 m thick and transgressively overlies the Devonian-Carboniferous Mamberè Glacial Formation and it is discordant with the Precambrian formations of the schist-quartzite complex to the south and the granite-gneiss complex to the north (Censier et al. 1999).

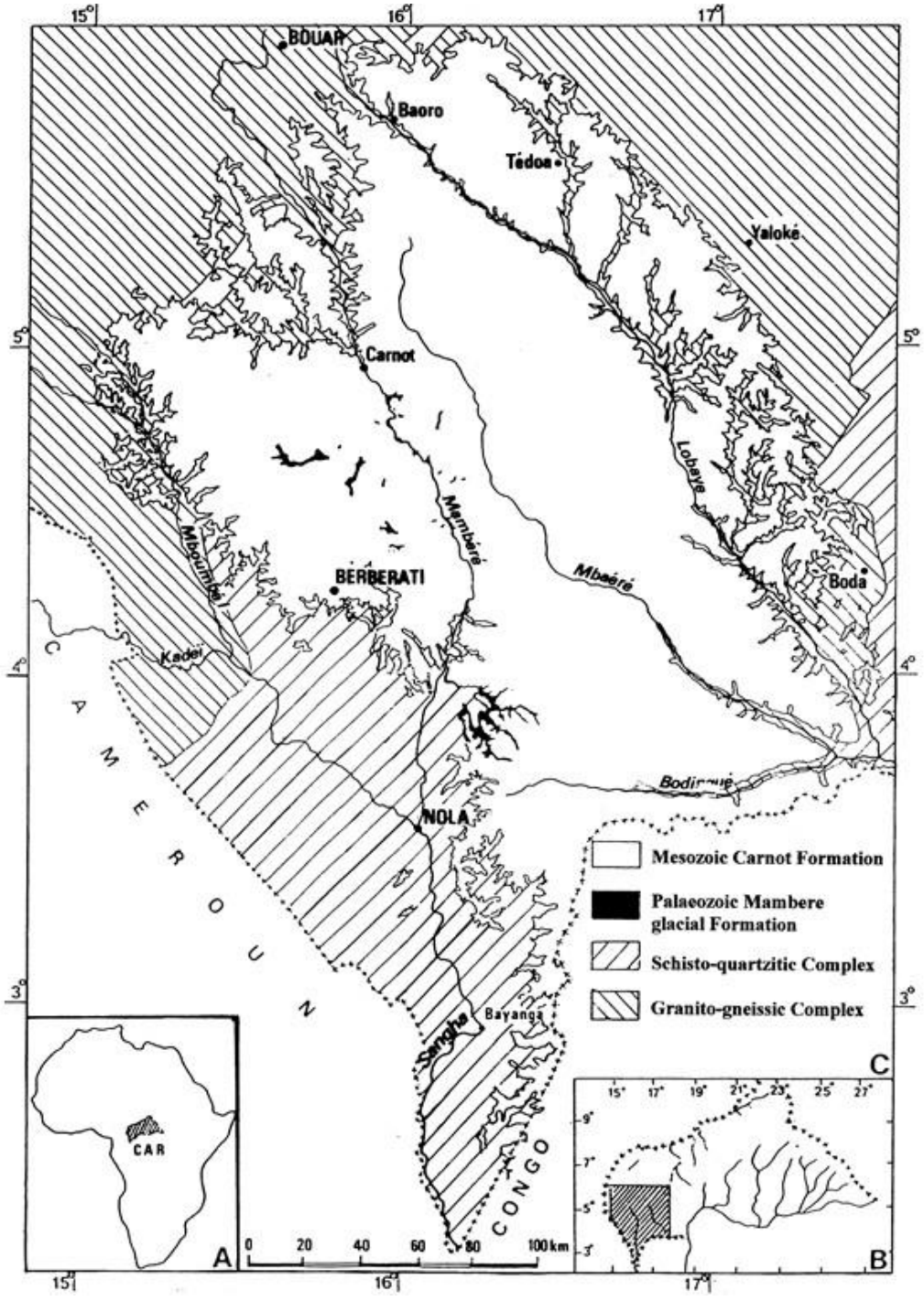

Figure 1.4. Map of the Carnot Formation (from Censier et al. 1999).

According to Censier et al. (1999), the formation exhibits three different facies: conglomerates, sandstones and siltstones.

The conglomerates are divided in three types: the basal, the interbedded and the graded conglomerates.

The first one is composed of quartzite pebbles, quartzite-sandstone and quartz and clay-silt material; it occurs in the northern and north-western part of the formation, and it is less common in the central part and it is not found in southern part.

The second one is composed of sandstone matrix that contains well-rounded quartzite pebbles, quartzite sandstone and oblong to ovoid quartz fragments up to 3 to 4 cm in length.

It is sandwiched between the sandstone horizons, either as horizontal beds, or as lenses formed by channel-fill structure; it is less frequent higher in the formation.

The third one consists of well-worn pebbles of quartz, quartzite-sandstone and quartzite; it is usually micro-conglomerates, forming the base of graded structure.

The sandstones are the most abundant facies within the Carnot Formation; the clastic fraction is composed of a large percentage of monocrystalline quartz (75-99%) and lithic fragments (quartzite, quartzite sandstone and kaolinitic material).

The feldspar is identified only in a few samples; there is a small portion of clay matrix (<15%) and the more-or-less developed cement is siliceous.

More authors gave different names to the lithology of this facies, but they agree that this is a quartz arenite.

The siltstones are limited in extend and form laminated bed succession with alternating arenaceous and clay-silt beds.

The cross-bedding is composed of tabular sets which are either superposed or with intercalated horizontal conglomerates beds; the foreset beds are either asymptotic, gently curved and tangentially based, or planar and angular-based.

They are frequently graded, ranging from micro-conglomerates to medium to fine sandstones.

This cross-bedding resulted from the migration and stacking of subaqueous ripples and dunes under the influence of a moderate hydrodynamic regime.

The conglomerates are arranged either in horizontal beds or as lenticular beds; the thicknesses vary from a few cm to 25-30 cm for the horizontal beds and are less than 4-5 cm for lenticular ones (Censier et al. 1999).

The analysis of the cross-bedding direction within the Carnot Formation shows that the values are distributed uniformly in each area whatever the lithostratigraphic level: the overall direction of flow of the fluvial network which succeeded one another in space and in time was NNW.

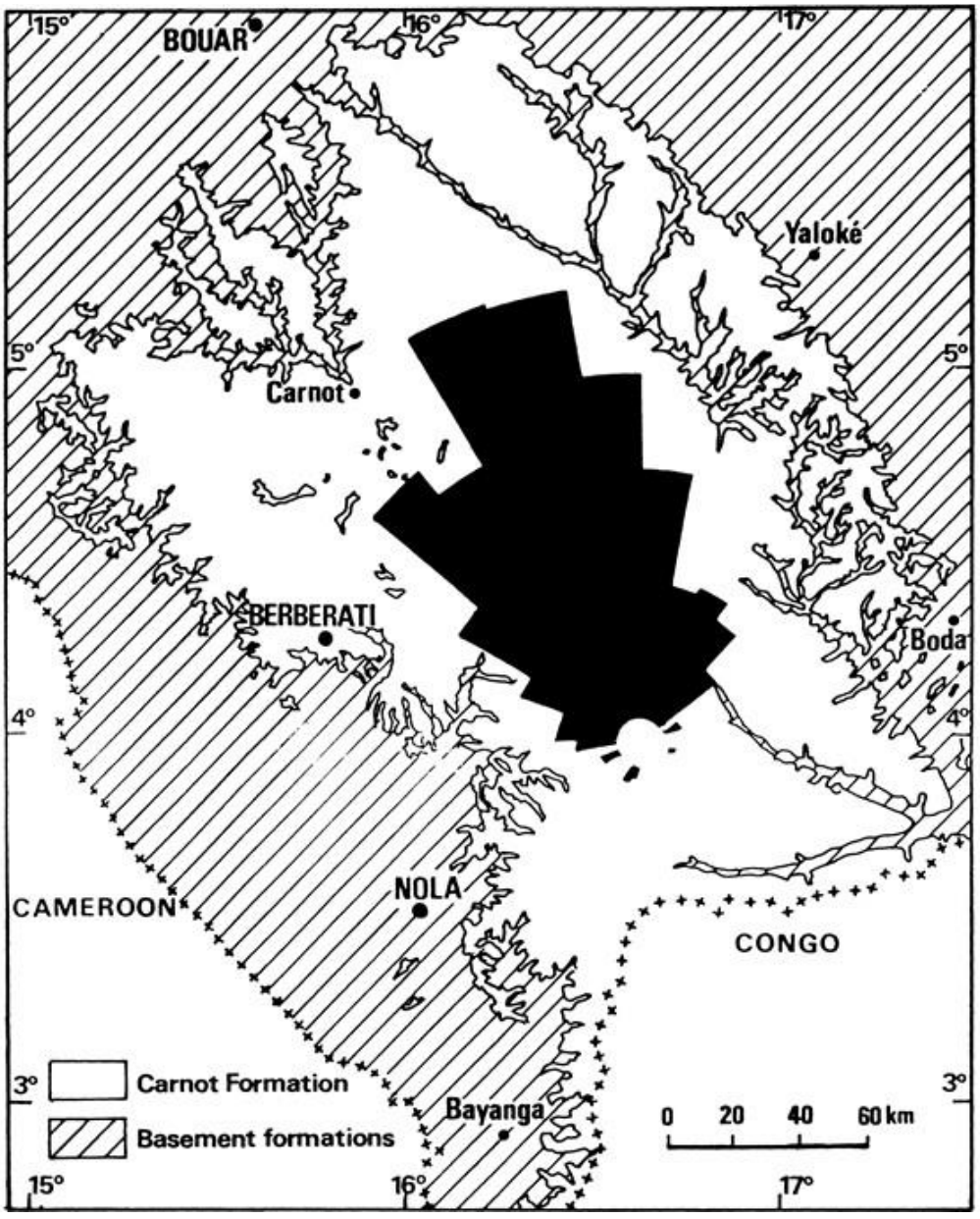

Figure 1.5. General direction of paleocurrents within the Carnot Formation (from Censier el al. 1999).

Another important feature of this formation is the presence of a series of heavy minerals and in decreasing order of importance, these minerals are: zircon, tourmaline, rutile, staurolite, kyanite, titanite and hyacinth zircon.

Their spatial-temporal distribution within the formation and the presence or lack of these minerals in the adjacent formations give us the information about the provenance of these material.

From south to north of the Carnot Formation, the mineralogical suite becomes poorer in minerals which cannot withstand transport and relatively richer in resistant minerals along this direction: this evolution indicates a transport of the detrital material from south to north.

There is a lack of variation within the mineralogical suite from bottom to top of the formation and from east to west: this indicates that all the detrital material was derived as a result of a uniform sedimentary setting.

Moreover, the comparison of the mineralogical suites from the Carnot Formation with those from the underlying formations show that the detrital material is derived from the weathering of the Mambéré Glacial Formation and of the Precambrian schist-quartzite complex (Censier et al. 1999).

The study and the analysis of the lithology and the sedimentary structure of the Carnot Formation allowed to define the depositional environment of this.

The very common cross-bedding within the sandstone facies, the presence of horizontally and lenticular conglomerate beds indicate that the depositional environment is typically fluviatile.

Most of the features of this formation, as the low dispersion of the direction of the paleocurrent flow, the coarseness of the detrital material, etc, suggests that the ancient fluvial system was a braided stream one.

The surface of the original sedimentary basin was much larger than has been interpreted based on the current limits of the formation; the western margin may have extended beyond the CAR and Cameroon border.

In addition, the most important feature of this formation for our studies is that the Carnot Formation is the host rock of the diamonds in the west and southwest of the Central African Republic.

So, considering the geological history of the Carnot Formation related to the geodynamic development of north Central Africa in the Cretaceous, the direction of the drainage system (NNW), the provenance of detrital material, the diamond parental rocks, kimberlites or lamproites, could be located to the SSE of the depositional area of the Carnot Formation (probably in northern Democratic Republic of Congo).

Moreover, a study of the surface of a series of diamonds coming from the western alluvial diamond deposits (probably associated with the Carnot Formation) was carried out to determine the geological history of the diamonds.

The samples were analysed with the scanning electron microscope (SEM) to identify the main features of the diamonds surface, that can be associated to the magmatic phase and transport-sedimentation phase.

The fissures on the faces are considered the main marks of wear: these give a general matt appearance and the edges disappear, but the general aspect of the crystal is preserved.

The presence of a lot of small fissures on the surface can be interpreted as a result of considerable transport and the primary source of diamonds can be located at a great distance (Censier et al. 1995).

So, also this aspect supports the hypothesis of the provenance of the diamonds from the Kimberlites in the Democratic Republic of Congo.

1.4. The Mouka-Ouadda Formation

The Mouka-Ouadda Formation is the second sandstone formation in the Central African Republic, considered a host rock of diamonds.

It is a triangular plateau that covers 40 000 km² and it is located to east and north-east of the CAR.

The thickness of the deposits ranges between 100 and 500 m (if we ignore the erosion) and the formation is placed noncomfomably over the Kombélé Formation, a Paleozoic glacial a periglacial formation, or in angular unconformity over the Precambrian basement formation.

The deposition of the Mouka-Ouadda Formation occurred probably in the Cretaceous and the deposits show many sedimentary structure (Malibangar et al. 2006).

According to Malibangar et al. (2006), the Mouka-Ouadda Formation is mainly composed of two lithofacies: conglomerates and sandstones.

The first occurs both like massive tabular or lenticular structures interbedded in the sandstone facies or like graded conglomerates; the microconglomerates form beds up to 3 m thick with erosional bases and the pebbles are very rounded and there is little amount of silt-sand matrix.

Moreover, generally the southern part is composed of quartzite and quartzite sandstone pebbles (the size is about 5 cm) and the silt-sand matrix is relative abundant (20-25%).

The northern part shows cobbles and quartzite schist and granite-gneiss boulders (the size is between 20 and 30 cm) with very little silt-sand matrix (<10%).

The sandstone is the most abundant facies in the Mouka-Ouadda Formation: in vertical section, the lower part exhibits medium to coarse grain size and the colour of sandstone varies from yellow to beige, whereas the upper part commonly contains fine-grained material.

The quartz grains represent the 70-90% of the components and they are usually sub-angular with straight or undulose extinction and the most of them derives from granites and some have metamorphic origin.

Moreover, in this facies little amount of feldspar is present and also lithic fragments of quartzite, gneiss and quartzite sandstone.

The silt-sand and clay-silt matrix is not abundant (5-10%) and locally a thin siliceous cement has resulted from the syntaxial overgrowth of silica around quartz grains.

In the Mouka-Ouadda Formation, the sandstone facies shows planar cross-bedding and trough cross-bedding; the conglomerates are either massive with slight grading or bedded with either planar or trough cross bedding.

In addition, both in norther and southern part, the vertical and lateral changes of the siliciclastic facies indicate that the sandstone and conglomerate material of the formation evolved in a typically fluviatile environment (figure 1.6).
The analysis of the sedimentary structures suggests deposition in a proximal to distal, braided-stream environment with mixed loads (Malibangar et al. 2006).

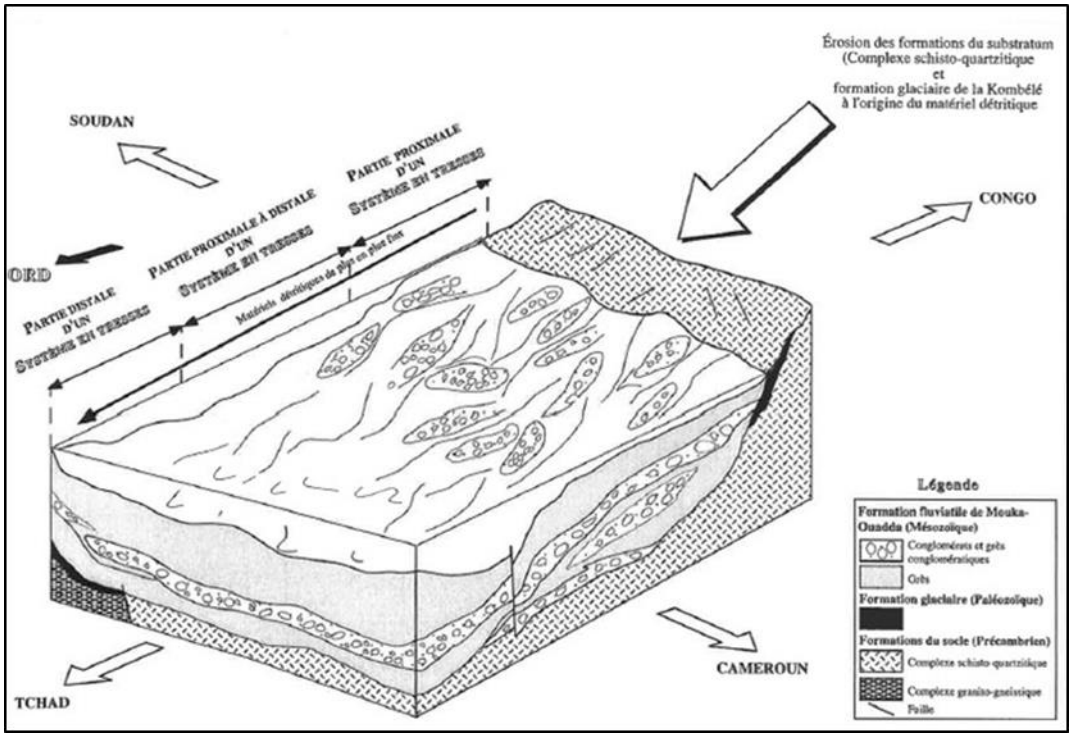

Figure 1.6. Paleogeographic evolution of the Mouka-Ouadda Formation (fluviatile environment) (from Malibangar et al. 2001).

The direction of the paleocurrents was obtained by the analysis the sedimentary structure, in particular planar cross-bedding, the trough cross-bedding and the current ripples; the results exhibit NW-NNE dispersion, providing an initial indication of the provenance of the detrital material (figure 1.7) (Malibangar et al. 2006).

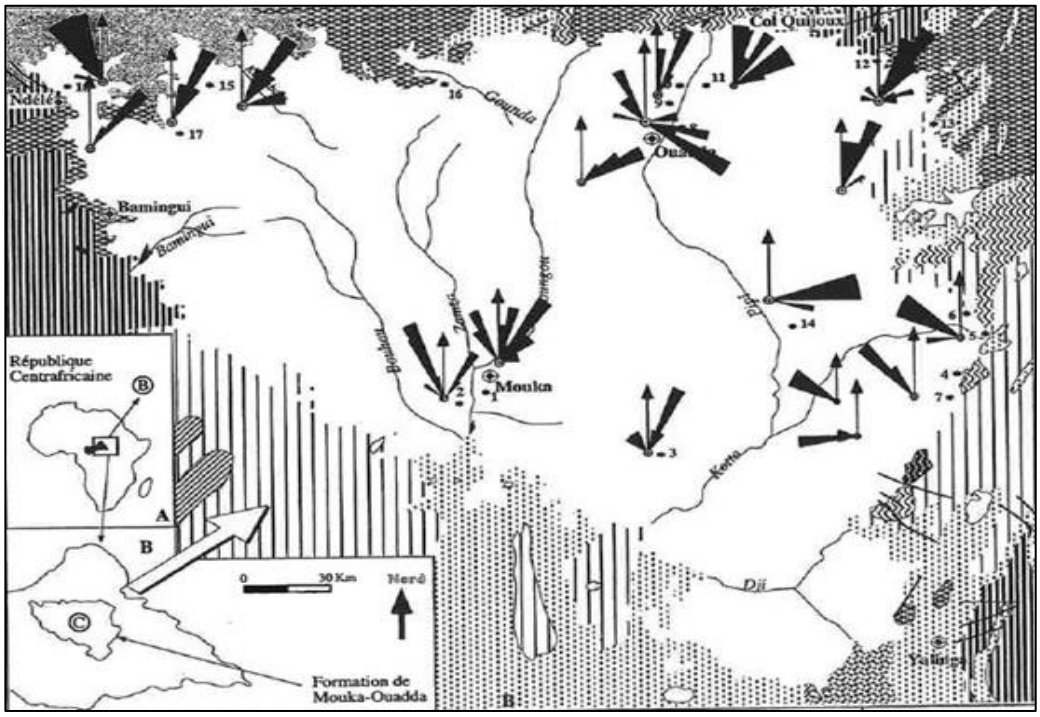

Figure 1.7. Paleocurrents recorded in the Mouka-Ouadda Formation (from Malibangar et al. 2001).

Also, in Mouka-Ouadda Formation heavy minerals are present and they are divided in three groups: the firsts are moderately abundant and in decreasing order we can find zircon, tourmaline, rutile, staurolite and hyacinth zircon.

The seconds are rare accessory heavy minerals and they are epidote, kyanite, hornblende, garnet, apatite and titanite.

The third group is composed of sillimanite, monazite and brookite; these minerals are found only in few samples.

The anatase found both in the Kombélé and Mouka-Ouadda Formations has neo-genetic origin.

Considering the type of heavy minerals found in the Mouka-Ouadda Formation, the detrital material derives from the glacial Kombélé Formation and the schist-quartzite complex units; the granite-gneiss complex units are not an essential source of detrital material for the formation: the only heavy minerals come from these units are the apatite and monazite, but they are very rare in the formation.

In addition, the amount of zircon, tourmaline and rutile of the samples from every zone of the formation, is about constant, but the values increase from the norther part.

This may be related to mechanical and chemical resistance of these heavy minerals in the contest of transportation from their source region in the south to the north (this hypothesis is also supported by the paleocurrents).

Moreover, a topographic study of the ante-fluviatile surface between the Mouka-Ouadda Formation and the other formations was conducted: the results exhibit the presence of a SW-NE slope of the surface and probably when the deposits were emplaced, the surface was not fully planed.

So, this confirms that the detrital material was derived from source area to the south (Malibangar et al. 2006).

The Mouka-Ouadda Formation is a secondary source rock of diamonds and considering the direction of the paleocurrents (NNE-NW), the provenance of the detrital material and the topography of the ante-fluviatile surface, the primary of diamonds could be located to south of this formation, and probably in northern Democratic Republic of Congo, like in the case of Carnot Formation (Malibangar et al. 2001).

1.5. Alluvial deposits

In the Central African Republic another important resource of diamonds is the alluvial deposits.

The geological exploration allowed to establish the Carnot Formation and the Mouka-Ouadda Formation like host rock of diamonds and they are considered secondary source rocks.

However, diamonds were found also in areas next to these formations and, since the extension of these was much larger in the past, probably diamonds are the remnants of the erosion of the sandstones.

So, the liberated diamonds are washed downstream and deposited in recent Quarternary alluvium and terrace deposits along the river courses.

In these areas, three types of alluvial placer deposits are recognized: alluvial flat and channel deposits, low terrace deposits and high terrace deposits.

The formation and development of these require two fundamental elements: the first is the presence of primary diamond sources nearby (in this case they are undiscovered, but the kimberlites located in northern Democratic Republic of Congo are a possible source), and the second is the tectonic setting that uplift the Cretaceous sandstone, considered the secondary sources of diamonds, reversing the flow direction of the river systems and eroding them.

This allowed the liberation of diamonds and the subsequent deposition in alluvial deposits in the river valleys.

Another important factor for the development of these deposits is the climate conditions occurred in the geological time; the climate influences the flow regimes in the river system and consequently the erosion, the transport and the deposition of the sediments.

In the CAR the alluvial deposits are associated with the Carnot and Mouka-Ouadda Formation and for this reason they are divided in two diamantiferous areas:

the first in the west and occurs in the Kadéi-Mambéré-Sangha region, and second in the east in the Haute-Kotto region (Chirico et al. 2010).

1.6. Possible primary sources of diamonds discovered in Central African Republic

In the Central African Republic primary sources of diamonds, as kimberlites o lamproites, are not present; the Carnot and the Mouka-Ouadda Formations are considered secondary source rocks, and diamonds in the alluvial deposits probably come from the erosion of these formations and their subsequent transport and deposition.

According to Censier et al. (1999) and Malibangar et al. (2006), considering the paleo-flow of the drainage system that was present in the Carnot Formation (NNW) and in Mouka-Ouadda Formation (NNE) and the provenance of the others heavy

minerals and sediments, probably the primary sources are located at South of the formations, in the northern Democratic Republic of Congo (DRC).

In this country the exploration for diamonds started in 1900, when the King Leopold-II gave to the Company Tanganyika Concessions Limited (TCL) the exclusive prospecting right in the southern part of the country (de Wit et al. 2015).

The first country's diamond was discovered by the company in 1903 in the Mutendele stream in Katanga Province.

So, the continuous research conducted by the company led to the discovery of the first kimberlite field on the Kundelungu plateau in DRC, in 1908.

Subsequently, other alluvial diamond deposits were found in Kasai region and Bakwanga Town (Mbuji Mayi).

From 1946 the Bakwanga cluster kimberlites and the Tshibua cluster kimberlites (Tshibwe) were discovered.

In the following years, De Beers started the exploration and the Bas-Congo kimberlites (South of Kinshasa) and clusters near Kabinda were found by the company (de Wit et al. 2015).

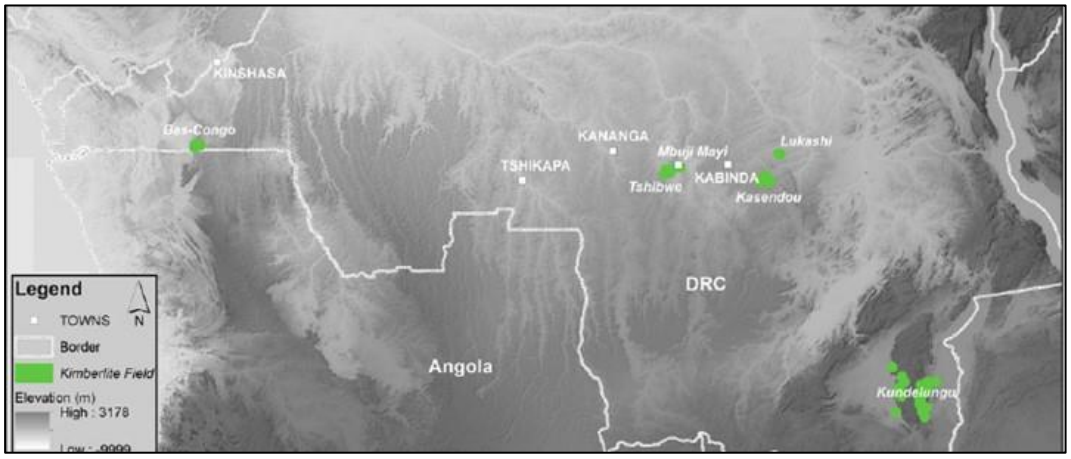

Figure 1.8. The kimberlite fields in the Democratic Republic of Congo (from de Wit et al. 2015).

The more northern Kimberlite field is the Bas-Congo Kimpangu one; the kimberlite dykes are located to South of Kinshasa close to the border with Angola and intruded into Neoproterozoic sediments of the West Congolian Group; the dykes are up to 3 m wide and trend north- northeast.

This was discovered by De Beers in 1974.

Considering Censier et al. (1999) and Malibangar et al. (2006), the diamonds discovered in the secondary diamond rocks and consequently in the alluvial deposits come from a primary source located in the northern DCR and this kimberlite field is the best candidate.

Moreover, most of the kimberlite field is located to the central regions of DRC: the first is the Kasai Oriental Kabinda Kimberlite Field, discovered by De Beers and Bugeco S.A.

The Kimberlites include crater-facies volcaniclastic, resedimented volcaniclastic and coherent magmatic varieties and were emplaced through Neoproterozoic dolomitic limestones of the Mbuji Mayi Supergroup with dolerite sills, and overlying Mesozoic siliciclastic sediments (Walker 2011).

In some kimberlites, both micro- and macro-diamonds have been recovered.

The second central kimberlite field is the Kasai Oriental Mbuji Mayi Kimberlite Field, which is divided in Mbuji Mayi and Tshibwe Clusters.

The kimberlite pipes of the Mbuji Mayi Cluster are located to the south of Mbuji Mayi town and they are primarily aligned along an E-W trend; they are emplaced through Archean basement and siliciclastic sediments and stromatolic, dolomitic limestones of Neoproterozoic age of the Mbuji Mayi Supergroup (Delpomdor et al. 2013), which are overlain by arenaceous sediments of Cretaceous age.

The upper parts of the kimberlites show crater facies litho-types, including resedimented volcaniclastic kimberlites and pyroclastic kimberlites.

The emplacement age is estimated at ca. 70 Ma (Schärer et al. 1997).

The Tshibwe kimberlite Cluster is composed of Tshibwe, Tshinyama, Kakongo, Tshambila, Ndaye and Tshinkasa pipes.

The most important is the Tshibwe pipe and it is located within a broadly east-west orientated valley surrounded by low hills.

Its facies are dominated by volcaniclastic kimberlite, including sandstone-rich, monolithic and heterolithic breccia types, as well as the more competent, green-grey, massive volcaniclastic and transitional kimberlite types (de Wit et al. 2015).

The studied diamonds coming from the pipes of the Kasai Oriental Mbuji Mayi Kimberlite Field and related alluvial deposits have lithospheric origin and the inclusions entrapped in these are mainly olivine, garnet, clino-pyroxene and ortho-pyroxene (both eclogitic and peridotitic paragenesis), but also kyanite, rutile, zircon and magnesian ilmenite are present (Ntanda et al. 1982; Kosman et al. 2016).

In the southern DRC the Kundelungu kimberlites occur as two separate groups on the Kundelungu Plateau in Katanga Province.

The kimberlite field comprises an eastern and a western group consisting of 16 and 17 kimberlites, respectively.

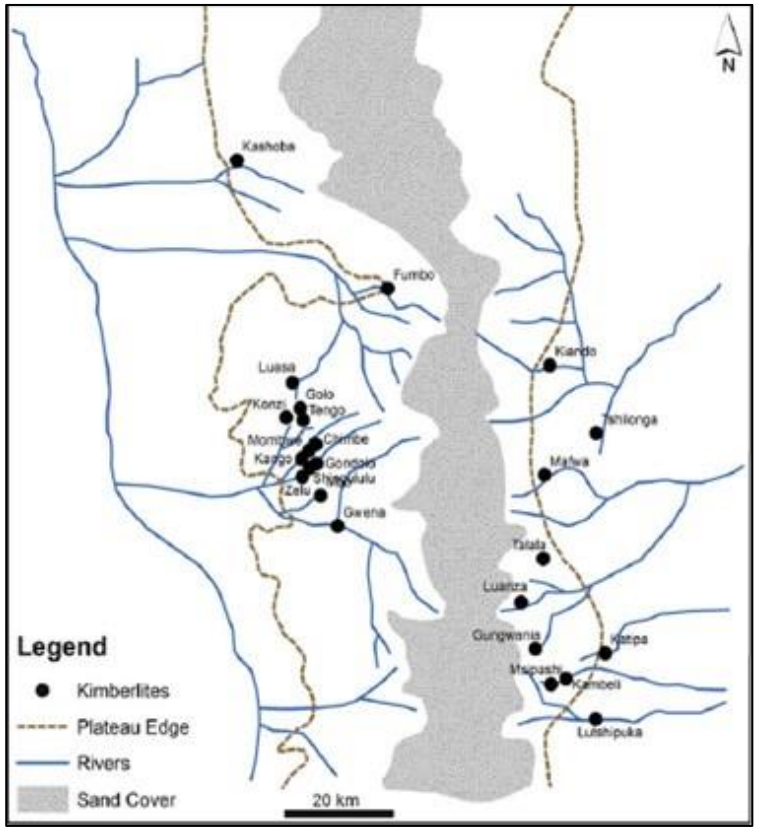

Figure 1.9. The Kundelungu kimberlites fields (from de Wit et al. 2015).

The uppermost rock types comprise both magmatic and volcaniclastic kimberlites suggesting hypabyssal and crater/diatreme facies preserved, respectively.

The kimberlites have intruded undeformed mudrocks, sandstones and limestones of the Neoproterozoic Biano Subgroup of the upper part of the Katanga Supergroup (Kampunzu and Cailteux 1999).

A recent dating of groundmass of peroskite of two pipes in the southern end of the eastern group, has provided an age of 32±2 Ma (Batumike et al. 2008).

2. Materials and methods

2.1. Samples

The studied set is composed by twelve diamonds: the average size is about one cm along the longest direction, the shape is from pseudo-octahedral to irregular and the colour is variable from grey to yellow, sometimes vivid (figure 2.1 a-n).

Every diamond has a big number of inclusions, clearly visible with the optical microscopy: most of them have a dark colour, others are transparent; the size of the inclusions is variable.

For this study, the diamonds are identified with the name *Centr_01, Centr_02, ..., Centr_12*; the related inclusions are named *Centr_01_01, Centr_01_02, ..., Centr_01_n*, etc.

Despite the big number of inclusions within the diamonds, at first the Micro-Raman analysis of these did not give any results and so, to improve the quality of these, three diamonds were polished: they maintain their original shape, but the surface is composed by a series of facets.

The polishing of diamonds is a delicate and long work and, in our samples, it is made by Franco Salvadego, a diamond cutter from Turin.

These samples are recognized with the name *Centr_01_tg, Centr_02_tg, Centr_03_tg*.

In this thesis work we focused on the study of the sample *Centr_01_tg* and *Centr_02_tg*, since also after the polishing, in the sample *Centr_03_tg*, the analyses were not satisfying.

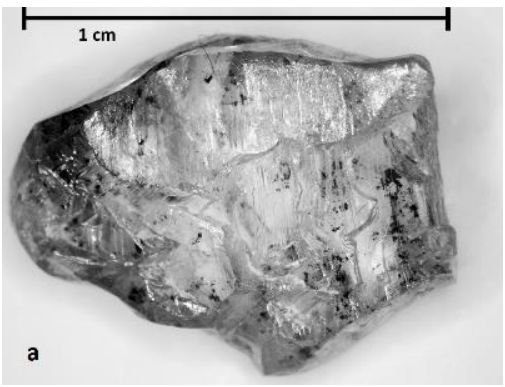

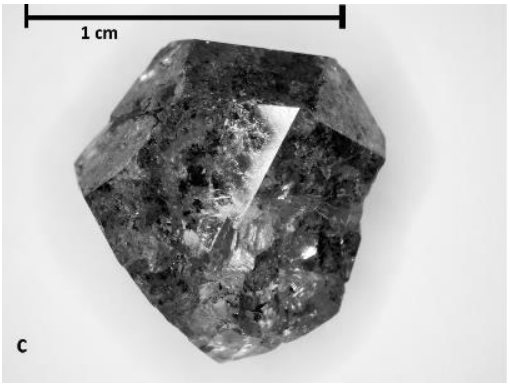
1 cm
c

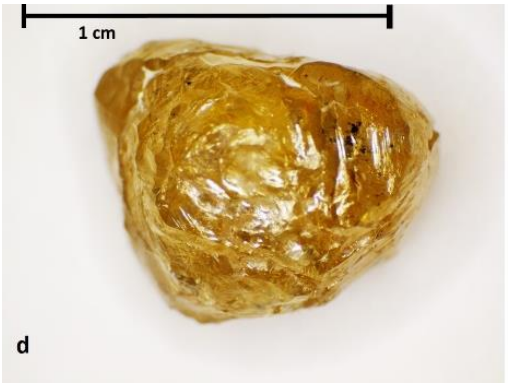
1 cm
d

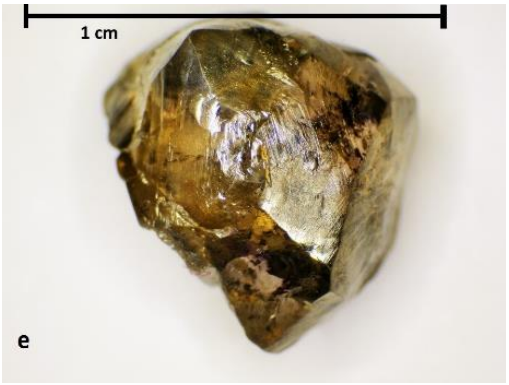
1 cm
e


1 cm
f

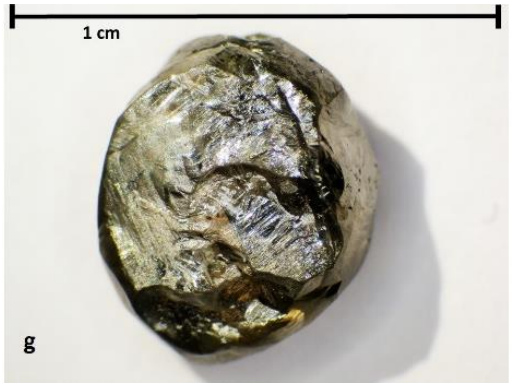
1 cm
g

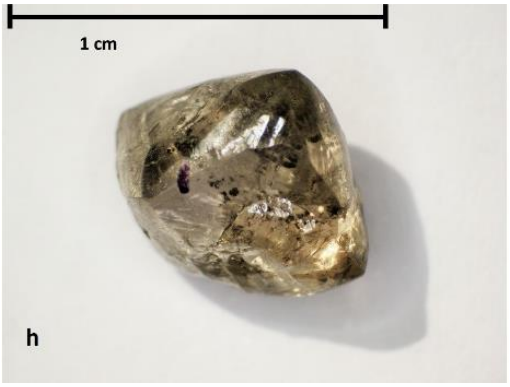
1 cm
h


1 cm
i

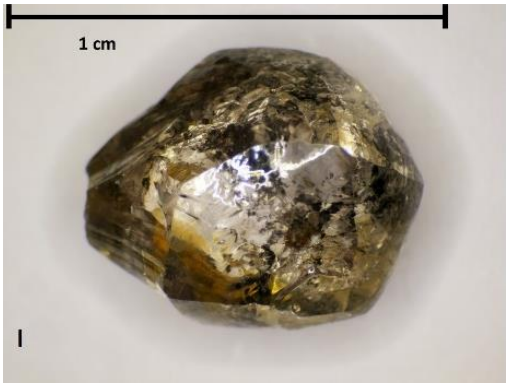
1 cm
l

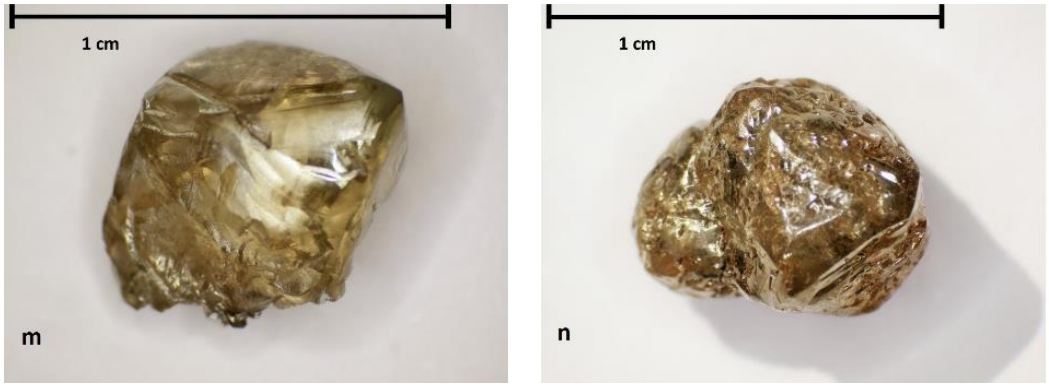

Figure 2.1. The diamonds samples studied in this work; **a.** Centr_01 (before the polishing); **b.** Centr_02 (before the polishing); **c.** Centr_03 (after the polishing); **d.** Centr_04; **e.** Centr_05; **f.** Centr_06; **g.** Centr_07; **h.** Centr_08; **i.** Centr_09; **l.** Centr_10; **m.** Centr_11; **n.** Centr_12.

2.2. Micro-Raman spectroscopy

The analytical technique used to identify the diamond inclusions was the Micro-Raman spectroscopy; this allowed us to recognize the smaller and the fluid inclusions (it is not always possible with the single-crystal x-ray diffraction).

This method is based on the "Raman effect", a not elastic scattering that produces a wavelength variation caused by the interaction between a laser and the molecular vibrations; this allows to analyse both mineral and fluid phases.

The result of the analysis is a "Raman spectrum" and it is reported in a graph that shows the Raman shift (the difference in wavenumbers between the observed and incident radiation) on the x-axis, and the intensity of radiation on the y-axis.

The spectrum is composed by a series of peaks and their position is defined by the Stock Lines, in function of the chemistry and the vibrational mode of molecules that compose the analysed material.

So, every material has a characteristic Raman spectrum and the identification is possible by a comparison with a database.

In this work the Raman spectra of the inclusions were collected with a Thermo Scientific DXR MicroRaman (figure 2.2), located at "Dipartimento di Scienze Chimiche" (DISC), University of Padua.

Figure 2.2. The Micro-Raman spectrometer (Thermo Scientific DXR MicroRaman) located at DISC, University of Padua.

It is equipped with 10x and 50x-LWD objectives; the spectra were recorded between 100 and 3500 cm^{-1} with a spectral resolution between 2.7 and 4.2 cm^{-1} and 1.1 µm spatial resolution, using a 532 nm (green) excitation laser at a power between 5 and 10 mW.

The Raman system was set with 900 lines/mm and a 25 µm pinhole.

The collect exposure time was between 10 and 60 s and the sample exposure was between 2 and 8 times; the background was not collected and during the acquisition a fluorescence correction was applied.

The database used to compare the collected spectra is RUFF Raman Minerals; the elaboration of the data was carried out using the Thermo-Scientific OMNIC for Dispersive Raman software.

2.3. Fourier Transform InfraRed (FTIR) spectroscopy

The Fourier Transform InfraRed spectroscopy is an analytical technique based on the same physical principle of the Micro-Raman one (both are sensitive to the vibrational modes of the molecules), but the IR is more sensitive to the anti-symmetric vibrations; the result of the analysis is an adsorption spectrum.

In the diamond studies, this technique is used to recognize the diamond impurities: in the diamond structure, the carbonium can be substituted by more than 60% of the elements in the periodic table, but the most common are nitrogen, hydrogen, silicon, nickel and boron (Field 1992).

These substitutions are important both in gemmology and geology: in the first case, different types of these give diamonds different shades of colour and in the second case lithospheric diamonds are characterized by a bigger amount of nitrogen than the sub-lithospheric ones (e.g. Stachel et al. 2002).

Moreover, the aggregation state of the nitrogen is sensitive to the temperature and it is a good geo-thermometer (Taylor et al. 1990) indeed, this rises with the temperature and the time of residence in the mantle (Evans et al. 1982).

The classification of the diamonds in function of their impurities is (Breeding et al. 2009):

- Type I (N impurities; N > 20 ppm):
    - Type Ia (aggregated N impurities):
        - Type IaA (A-aggregated N pairs)
        - Type IaB (B-aggregated 4N+V)
    - Type Ib (isolated single N impurities):
- Type II (no N impurities; N< 20 ppm):
    - Type IIa (no N or boron impurities)
    - Type IIb (boron impurities).

The FTIR spectrum shows different absorptions in function of the chemical elements, that produce the impurities, and the type of defect and aggregation-state of the nitrogen (Type IaA, IaB or Ib).

The analyses of this with the software DiaMap (Howell et al. 2012) allows the calculation of the total nitrogen amount, the nitrogen concentration in the form of

A centres, the nitrogen concentration in the form of B centres and the percentage of B centres; we used this software to elaborate our data.

In this work the spectra were collected with a FT-IR interfaced with gas analysis and optical microscope (Nicolet) at “Dipartimento di Ingegneria Industriale” (DII), University of Padua.

The acquisition was in transmission mode for 60 s at a spectral resolution of 0.5 cm−1. Background spectra were collected for 120 s before the analysis and were subtracted from each measured absorbance spectrum.

3. Results

3.1. Micro-Raman spectroscopy

The Single-crystal X-ray Diffraction analysis did not give satisfying results about the inclusions within the diamonds, probably for the size of these, so the Micro-Raman spectroscopy was used to study the mineral and fluid inclusions.

The Raman spectra collected from our samples were compared with the spectra of RRUFF Raman Minerals database; the results are shown in the Table 3.1 (sample *Centr_01_tg*) and in the Table 3.1 (sample *Centr_02_tg*).

Centr_01_tg:

Inclusions	**Type of mineral o fluid phase**
Centr_01_tg_01	Anatase
Centr_01_tg_02	Anatase
Centr_01_tg_03	Anatase
Centr_01_tg_04	Anatase
Centr_01_tg_05	Anatase
Centr_01_tg_06	Anatase
Centr_01_tg_07	Calcite
Centr_01_tg_08	Anatase
Centr_01_tg_09	Calcite + Anatase
Centr_01_tg_10	Ringwoodite + ?
Centr_01_tg_11	Fluid phase (Nimis et al. 2016)
Centr_01_tg_12	Fluid phase (Nimis et al. 2016)
Centr_01_tg_13	Fluid phase (Nimis et al. 2016)

Table 3.1. The mineral and fluid inclusions within the diamond *Centr_01_tg* identified with Micro-Raman spectroscopy.

Centr_02_tg:

Inclusions	Type of mineral and fluid phase
Centr_02_tg_01	Olivine
Centr_02_tg_02	Olivine
Centr_02_tg_03	Olivine
Centr_02_tg_04	Olivine
Centr_02_tg_05	Olivine
Centr_02_tg_06	Fluid phase
Centr_02_tg_07	Anatase
Centr_02_tg_08	Olivine
Centr_02_tg_09	Fluid phase
Centr_02_tg_10	Olivine
Centr_02_tg_11	Fluid phase
Centr_02_tg_12	Fluid phase
Centr_02_tg_13	Olivine
Centr_02_tg_14	Anatase
Centr_02_tg_15	Olivine
Centr_02_tg_16	Olivine
Centr_02_tg_17	Olivine
Centr_02_tg_18	Fluid phase
Centr_02_tg_19	Fluid phase
Centr_02_tg_20	Fluid phase
Centr_02_tg_21	Fluid phase
Centr_02_tg_22	Olivine
Centr_02_tg_23	Fluid phase
Centr_02_tg_24	Olivine
Centr_02_tg_25	Olivine
Centr_02_tg_26	Olivine
Centr_02_tg_27	Fluid phase

Centr_02_tg_28	Olivine
Centr_02_tg_29	Fluid phase
Centr_02_tg_30	Olivine
Centr_02_tg_31	Olivine
Centr_02_tg_32	Dolomite

Table 3.2. The mineral and fluid inclusions within the diamond *Centr_02_tg* identified with the Micro-Raman spectroscopy.

The main inclusions found in the sample *Centr_01_tg* are anatase (figure 3.1), calcite (figure 3.2) and the fluid phase (Nimis et al. 2016) (figure 3.3).
Moreover, only one inclusion of ringwoodite is found in this sample; the spectrum in addition to the ringwoodite peaks (about 796 and 830 cm-1) shows three more peaks at 328, 530 and 731 cm-1 (figure 3.4).
Probably these peaks are produced by another phase, that we have not been able to identify; this could be a new mineral.

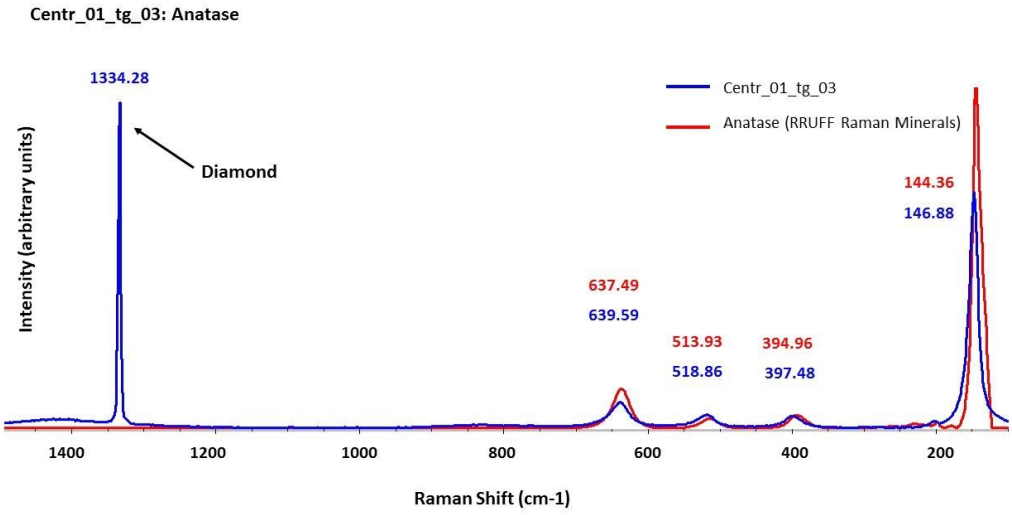

Figure 3.1. The Raman spectrum of an inclusion of anatase (*Centr_01_tg_03*) in the sample *Centr_01_tg*, in which the characteristic peaks are well defined.

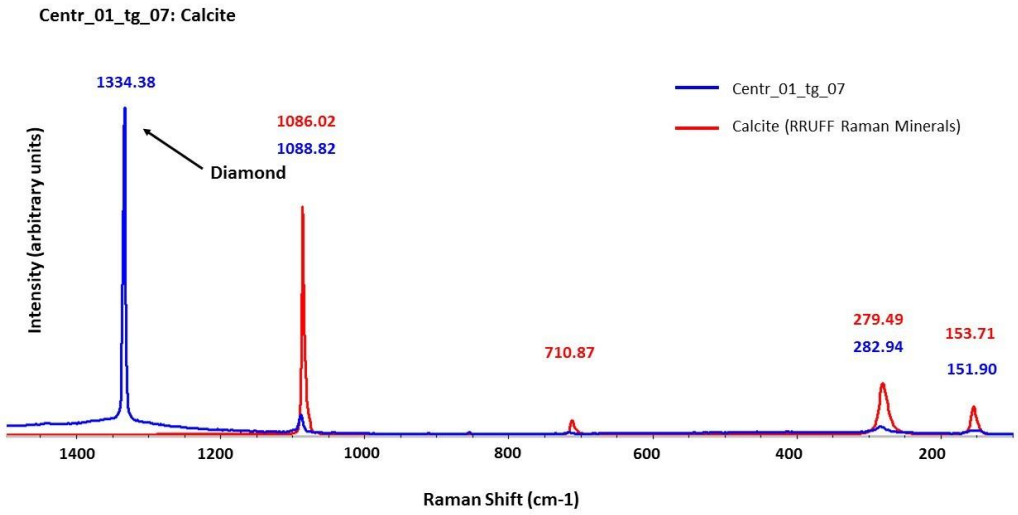

Figure 3.2. The Raman spectrum of an inclusion of calcite (*Centr_01_tg_07*) in the sample *Centr_01_tg*.

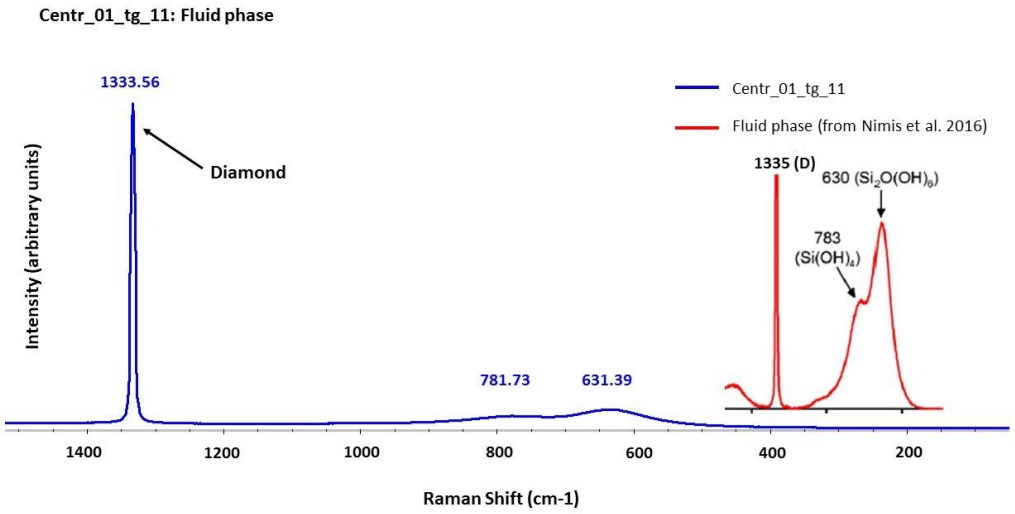

Figure 3.3. The Raman spectrum of an inclusion of fluid phase (*Centr_01_tg_11*) in the sample *Centr_01_tg*.

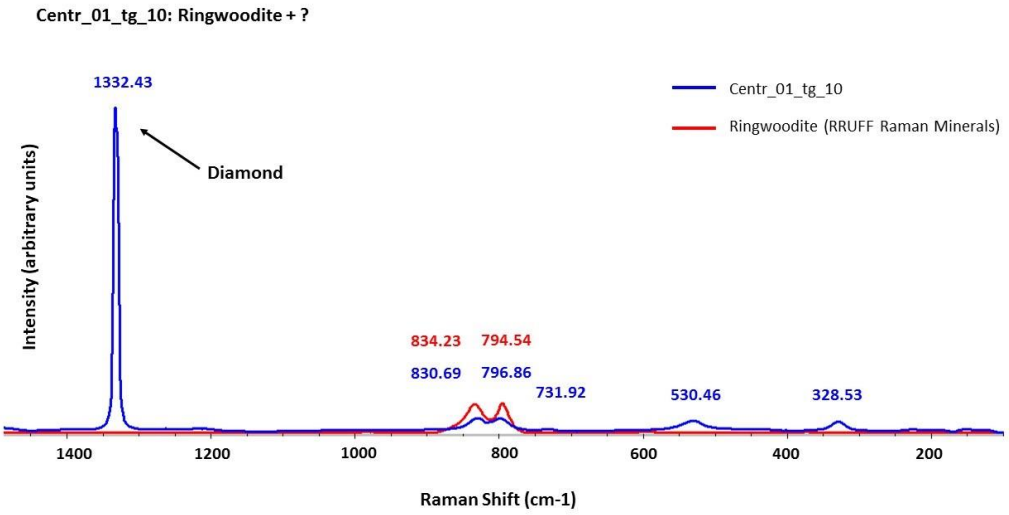

Figure 3.4. The Raman spectrum of the ringwoodite inclusion (*Centr_01_tg_10*) in the sample *Centr_01_tg;* the peaks at 328, 530 and 731 cm-1 are probably produced by a non-identified phase.

In the sample *Centr_02_tg* the main inclusions are olivine (figure 3.5), anatase (figure 3.6), fluid phase (Nimis et al. 2016) (figure 3.7) and dolomite (only one inclusion) (figure 3.8).

The dolomite spectrum also shows two peaks (144 and 662 cm-1); probably these peaks are produced by a non-identified phase, that could be a new mineral.

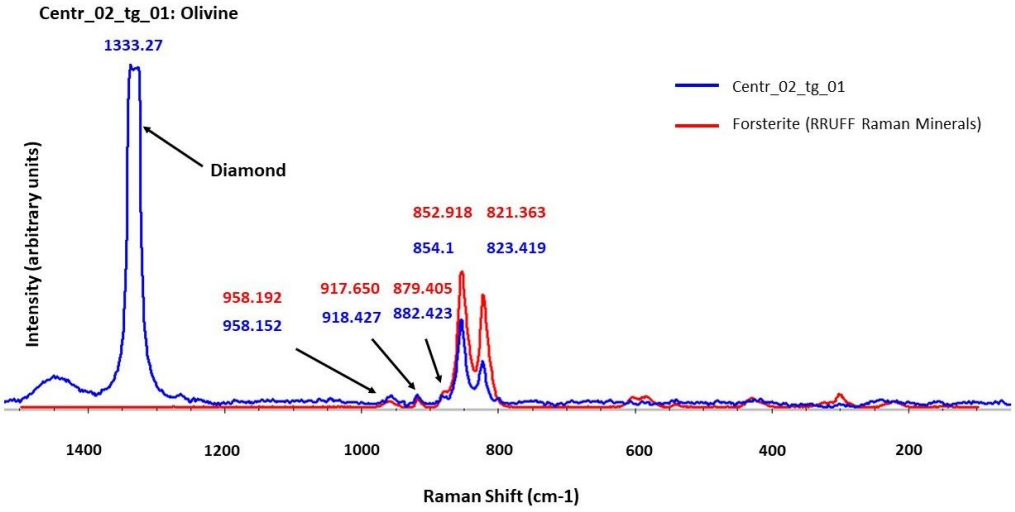

Figure 3.5. The Raman spectrum of an inclusion of olivine (*Centr_02_tg_01*) in the sample *Centr_02_tg*, in which the peaks are well defined.

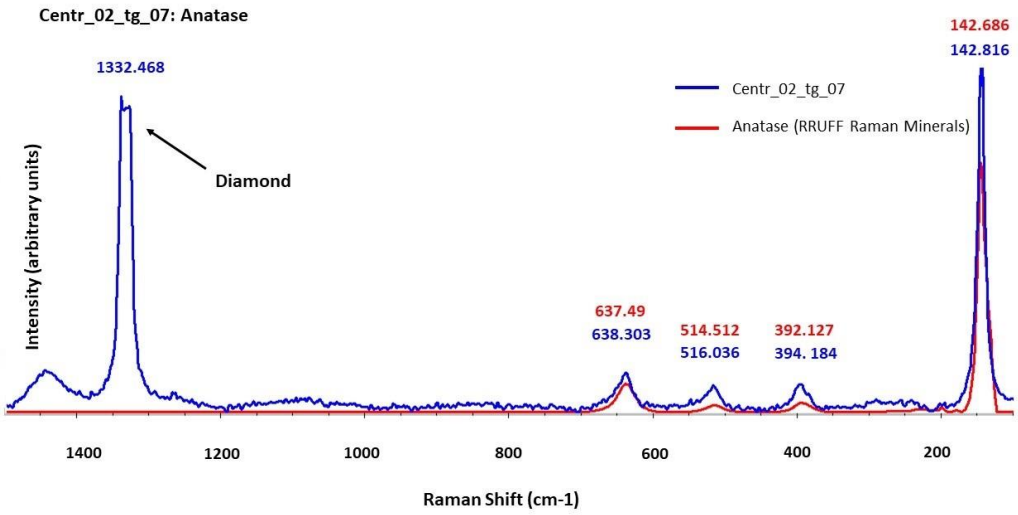

Figure 3.6. The Raman spectrum of an inclusion of anatase (*Centr_02_tg_07*) in the sample *Centr_02_tg*, in which the peaks are well defined.

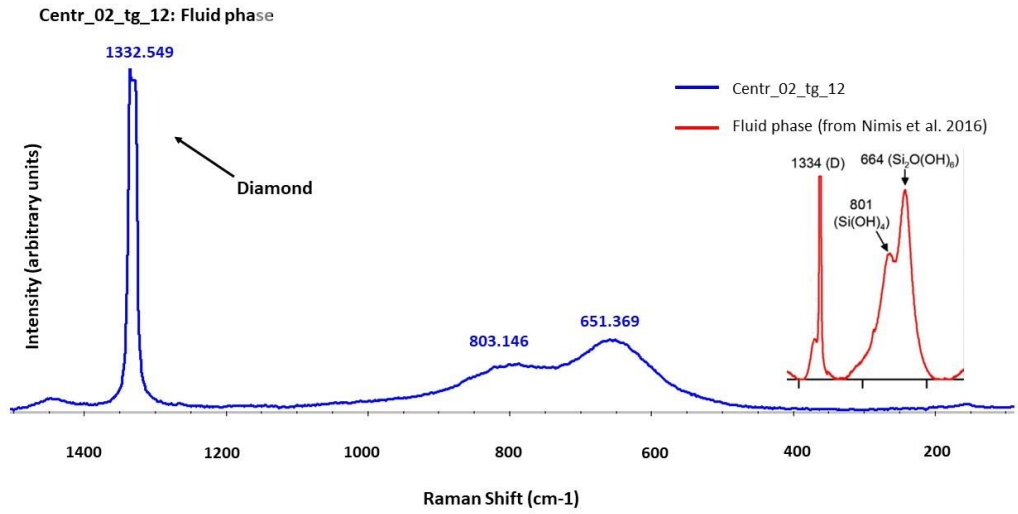

Figure 3.7. The Raman spectrum of an inclusion of fluid phase (*Centr_02_tg_12*) (Nimis et al. 2016) in the sample *Centr_02_tg*, in which the peaks are well defined.

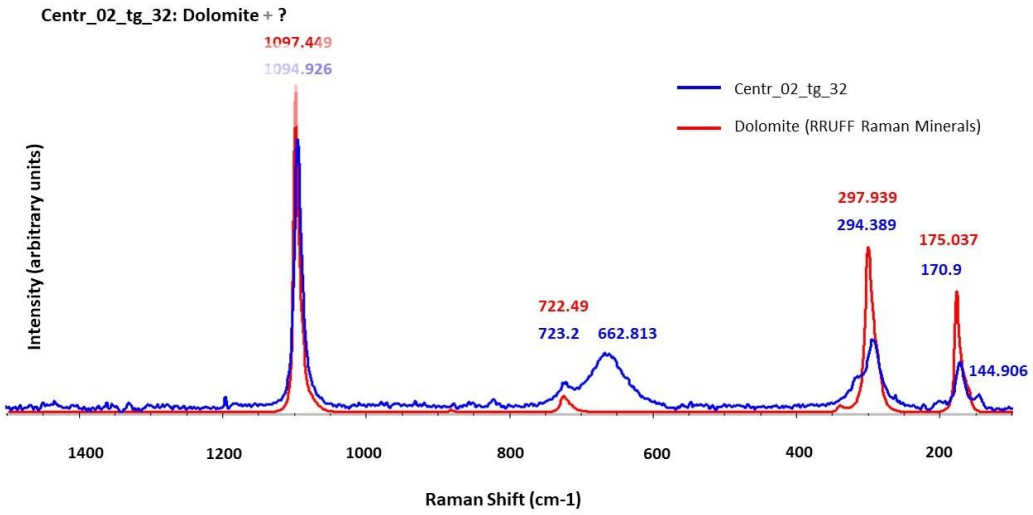

Figure 3.8. The Raman spectrum of the inclusion of dolomite (*Centr_02_tg_32*) in the sample *Centr_02_tg;* the spectrum also shows two peaks (144 and 662 cm-1), that are probably produced by a non-identified phase.

The spectra of all inclusions collected from the samples *Centr_01_tg* and *Centr_02_tg* and related photos are reported in Appendix A and Appendix B, respectively.

3.1.1. Olivine

The olivine is the main inclusion found within the studied diamonds and their identification was mainly performed by the Micro-Raman spectroscopy (see subchapter 3.1.).

The Raman spectrum of the olivine shows two main peaks: the first between 808-825 cm-1 (Si-O symmetric stretching band) and the second between 837-858 cm-1 (Si-O asymmetric stretching band) (Mouri et al. 2008).

Their shift is related to their chemical composition (solid solution between forsterite Mg_2SiO_4 and fayalite Fe_2SiO_4), and pressure and temperature conditions.

The position of the Stockes Lines in the case of olivine entrapped in the diamonds, can give us information about their chemical composition (Chopelas 1991; Mouri et al. 2008) and residual pressure exerted by the host (Chopelas 1990).

Increasing the Mg# (Mg#=100 x Mg/ (Mg + Fe)) and the pressure, the Raman peaks shift linearly toward smaller values (Yasuzuka et al. 2009).

In this thesis work, we calculated the medium composition of the olivines within the sample *Centr_02_tg* (the sample that contains the major number of olivine inclusions), using the model calibrated by Yasuzuka et al. (2009).

First of all, we obtained the equation to determine the composition, using the data of position of the peak 1 (825 cm-1) acquired by Yasuzuka et al. (2009), for olivines with different composition at 0 GPa pressure.

Mg# (%)	**Peak 1**
100	824.71
92.7	823.4
90.1	822.93
89.5	822.5
87.5	822.56
84.6	821.28
82.3	821.8
76.7	820.36
73.7	819.64
70.7	819.46

Table 3.3. Values of olivine composition and related peak position, obtained by Yasuzuka et al. (2009).

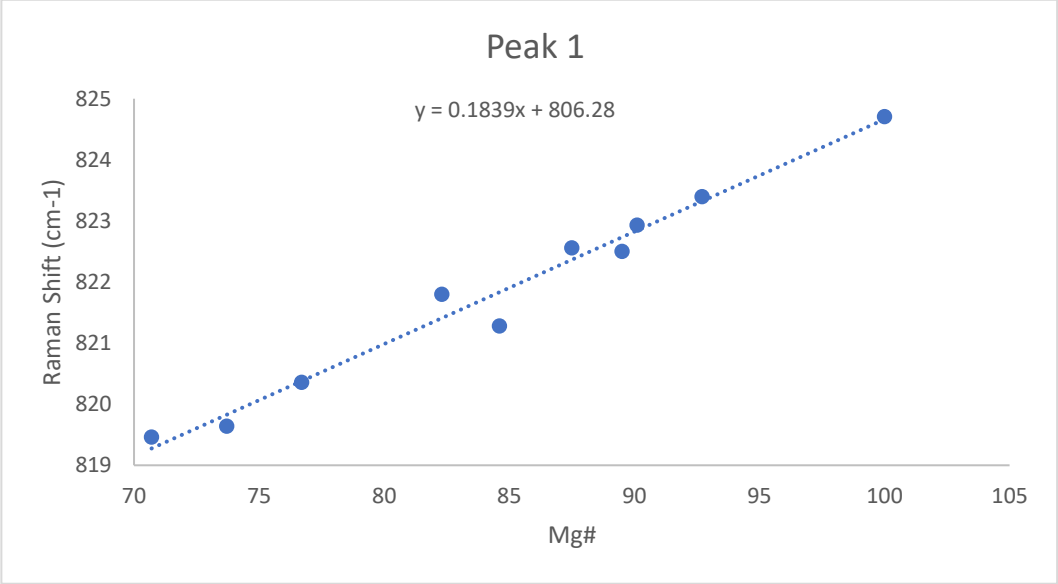

Figure 3.9. Data obtained by Yasuzuka et al. (2009), plotted in a graph Mg# (%) vs. Raman Shift (cm-1); fitting this values, we determined the equation to calculate the composition of the olivines within the sample *Centr_02_tg*.

Subsequently, we determined the precise peak positions of the our olivines, their composition using the equation y=0.1839x+806.28 and then we calculated the average composition (medium).

We used the position of peak 1 (825 cm-1) because it is the peak more sensitive to the pressure.

Olivine	**Peak 1 (cm-1)**	**Mg# (%)**
Olivine_01	823.419	93.19738989
Olivine_02	822.858	90.14681892
Olivine_03	823.054	91.21261555
Olivine_04	822.605	88.77107123
Olivine_05	822.548	88.46112017
Olivine_06	823.266	92.36541599
Olivine_07	822.876	90.24469821
Olivine_08	823.383	93.00163132
Olivine_09	822.465	88.00978793

Olivine_10	823.135	91.65307232
Olivine_11	822.773	89.6846112
Olivine_12	822.743	89.52147906
	Medium	90.52247598
	Deviation Standard	1.758223347

Table 3.4. The peak positions and related composition of the olivines within the sample *Centr_02_tg* and average composition obtained by these data.

The average composition is about 90.52 % Mg#; in the lithospheric diamonds, the composition of harzburgitic olivines usually has a range in Mg# between 90.2 and 95.4 and lherzolitic olivines between 90.1 and 93.6 (peridotitic paragenesis) (Stachel and Harris 2008).

If we consider the olivines found in the sub-lithospheric diamonds (retrograde transformations of wadsleyite of ringwoodite), the composition falls in a range of Mg# between 88 and 97 (Kaminsky 2012).

The value that we calculate, falls in the range in both case; so, we can consider in this case that the effect of the pressure, if it is present, is negligible and this value like average composition of olivines.

3.1.2. Possible temperature of formation of diamonds.

In the sample *Centr_02_tg*, the Micro-Raman spectroscopy allowed to collect three Raman spectrum of graphite inclusions, in which the G peak is well defined.

Basing on a study in which the possible temperature of formation of the urelite Almahata Sitta was calculated in function of the Full Width Half Maximum (FWHM) of the G-band Raman peak of the graphite associated to the meteorite (Ross et al. 2011), we tried to apply this model to our diamonds.

The Raman spectrum of disordered graphite is composed of two mainly peaks: the G peak around 1580-1600 cm-1 and the D peak around 1350 cm-1 (Ferrari et al. 2000).

In the paper of Ross et al. (2011), a study to determine the possible theory for the diamond formation in the Almahata Sitta urelite was conducted by the Micro-Raman analysis of graphite and diamond in the meteorite.

To define the temperature of formation it was used an expression (3.1) based on the Full Width Half Maximum of the G peak of Raman spectrum of graphite.

The expression is:

$$T_{max}(°C) = 1594.4 - 20.4\tau_G - 5.8 \times 10^{-2}\tau_G^2 \quad (3.1)$$

where τ_G is the Full Width Half Maximum of the G peak.

This approach has never been tested in the kimberlitic or terrestrial diamonds, but we tried to use this for our samples, to obtain a possible temperature of formation.

In particular, it was applied in the sample *Centr_02_tg*, in which three inclusions were found and were produced a well-defined G peak (figure 3.10 a, b, c).

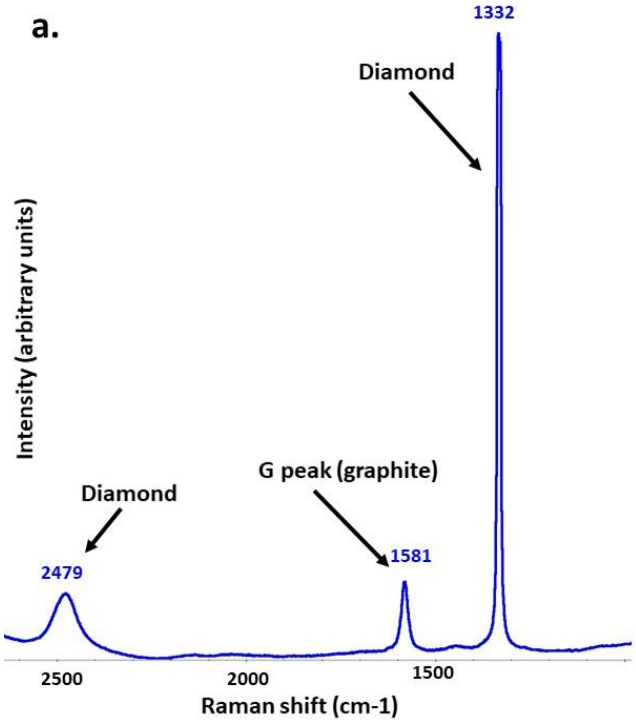

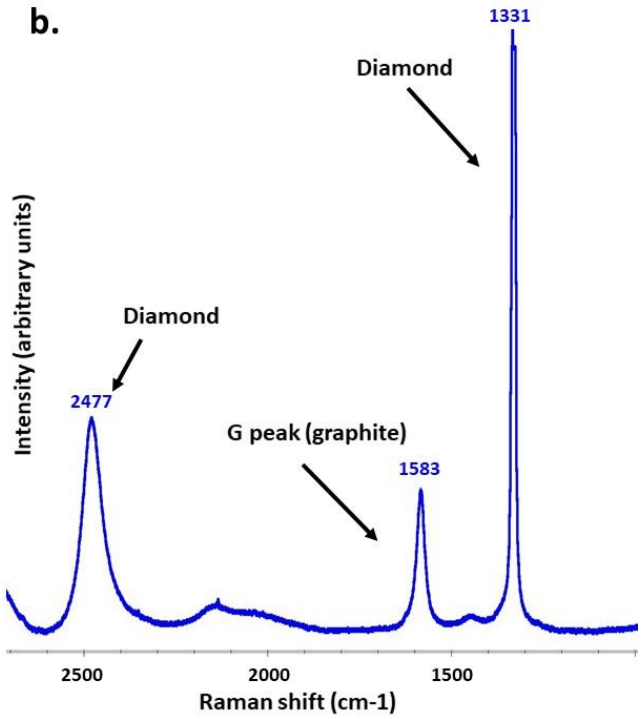

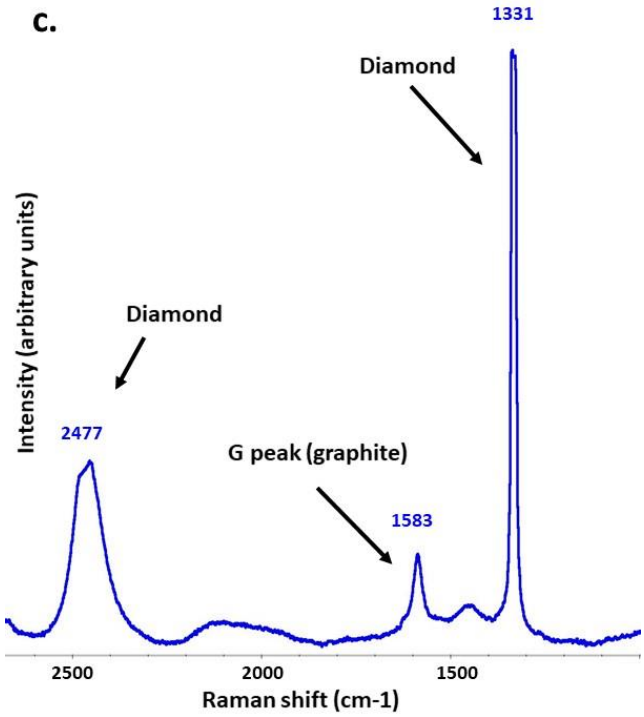

Figure 3.10 a, b, c. The Raman spectra of the three inclusions of graphite within the sample *Centr_02_tg*.

The Full Width Half Maximum of the G peaks are obtained by the software OMNIC for Dispersive Raman, and inserting this value in the expression 3.1, we calculated a possible medium temperature of formation of the diamond (table 3.5).

Inclusion	**FWHM (cm-1)**	**Temperature (°C)**
Graphite_a	21	1399
Graphite_b	27	1348
Graphite_c	35	1273
	Medium	1340
	Deviation Standard	52

Table 3.5. The FWHM of the graphite inclusions and the formation temperature, obtained by the expression 3.1.

The calculated possible formation temperature is about 1340 °C (±52°C) and if this approach gives a real estimate of the formation temperature, this is relative high and suggests a diamond crystallization in particular conditions.

3.2. Fourier Transform InfraRed (FTIR) spectroscopy

The Fourier Transform Infrared spectroscopy in the diamond study allows to identify the impurities of the diamonds, to classify them in function of this and to determine the state of aggregation of nitrogen and basing on this, the residence time of the diamonds in the Mantle and temperature (see subchapter 2.4.).

In this thesis work, we collected the FTIR spectrum of the sample *Centr_01_tg* and we calculated the nitrogen amount, the type and the aggregation state with the software DiaMap (Howell et al. 2012).

We only analysed the sample *Centr_01_tg* because it is the unique diamond of the set with a thickness that allows the acquisition of the FTIR spectrum (figure 3.11).

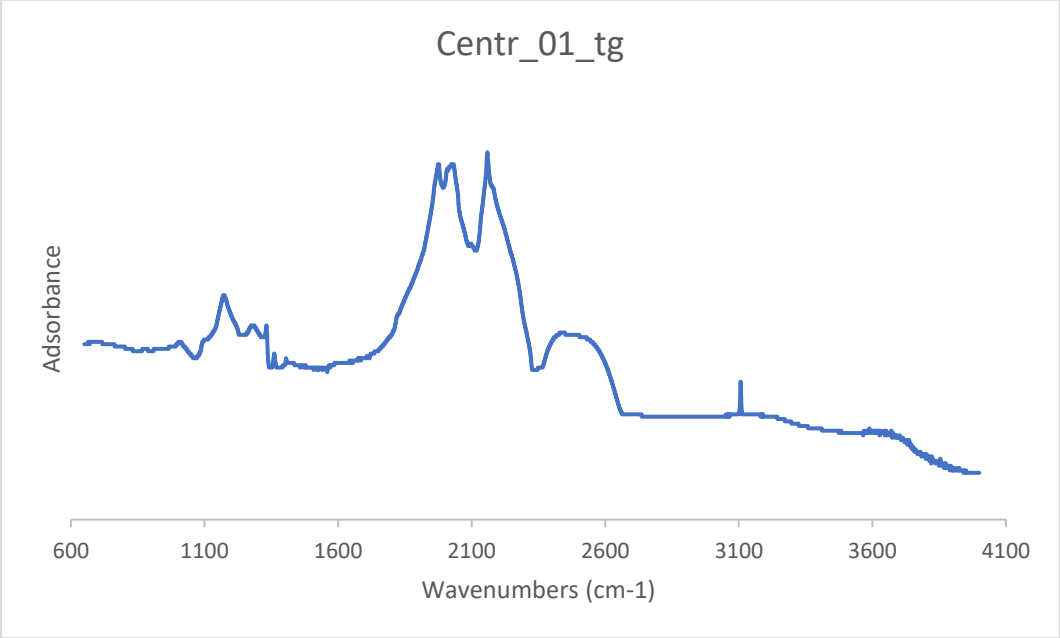

Figure 3.11. FTIR spectrum of sample *Centr_01_tg* collected at "Dipartimento di Ingegneria Industriale" (DII), University of Padua.

The FTIR spectrum of the diamond shows different areas of adsorption, in function of the impurities and their state of aggregation; the intrinsic diamond feature in the spectrum occurs between 1800 and 2700 cm-1.

The features related to the nitrogen adsorption are mainly two and they occur between 1000 and 1400 cm-1; they are distinguished in B' band, that is the result platelets, extended planar defects that containing aggregates of nitrogen (1358-1378 cm-1), D component, an additional feature that the platelets create as a result of their lattice vibrational mode (1140-1340 cm-1).

The third feature is related to the vibrations of hydrogen and it occurs at about 3107 cm-1 (Howell et al. 2012).

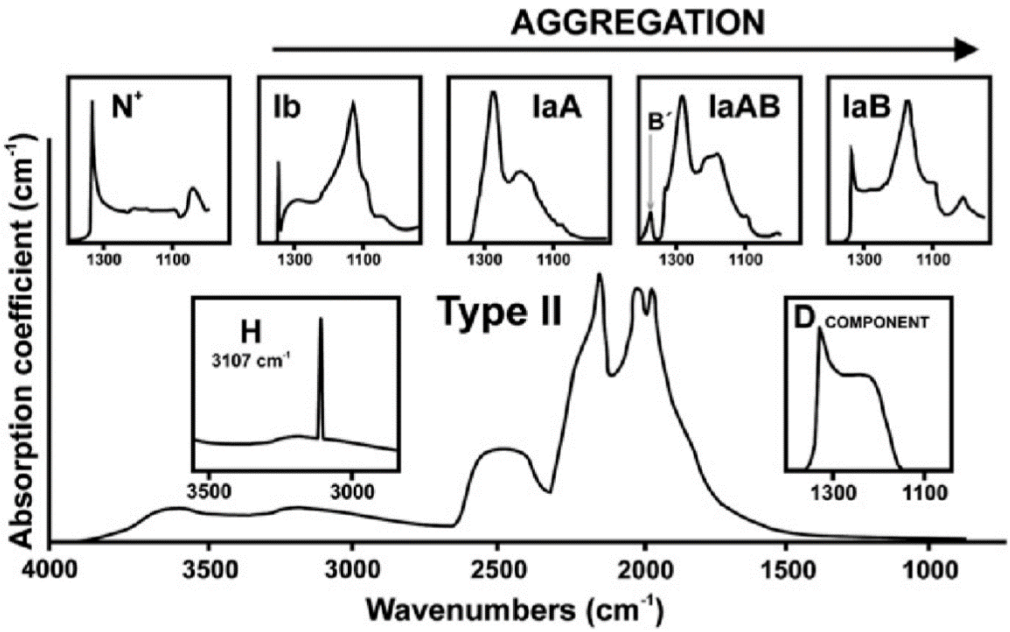

Figure 3.12. The FTIR spectrum of diamond and related features, due to the nitrogen and hydrogen adsorption (from Howell et al. 2012).

The DiaMap software uses a least-squares-fitting approach to the deconvolution to obtain the nitrogen-related data of our spectra: it involves scaling and combining between one and three reference spectra to fit the raw data.

This software does not require the spectra to be baseline- corrected or normalized and the fit of individual nitrogen components is only carried out between 1000 and 1350 cm-1, instead of up to 1400 cm-1, to prevent any large B' band influencing the fitting process (Howell et al. 2012).

Moreover, it provides data about the presence of both hydrogen and platelets.

The DiaMap software has been written in the PERL programming language, that uses downhill minimization function to find the best fit in our normalization and deconvolution process.

The reference spectra are contained within the script and the raw data are interpolated so that they have the same single wavenumber spacing as the reference spectra.

To obtain the nitrogen-related data the spectrum is normalized and this requires conversion of the y-data component from absorbance to absorption coefficient.

This occurs through the fit of interpolated raw data and the Type IIa reference spectrum and when the fit is achieved, the conversion factor to transform the absorbance values in units of absorption coefficient is calculated.

Finally, the individual nitrogen components are fitted to the raw data in the range of 1001-1350 cm-1; it is performed using a least-squares fit combined with a new linear correction of the raw data; the quality of the fit is measured by providing a value for the sum of squares (Howell et al. 2012).

DiaMap provides information about the nitrogen concentration in the form of A centers (Na), the nitrogen concentration in the form of B centers (Nb), the contribution of the D component (Nd), the total nitrogen concentration (N_total), the percentage of B centers (Nb/N_total x 100), the sum of the squares from the nitrogen deconvolution fit (sum_squares), the height of the hydrogen band at 3017 cm-1 (H), the area of the B' band (area), the peak position of the B' band (corresponding wavenumber), the height of the B' band (biggest in the 1351-1380 range) and the height of the hydrogen band at 1405 cm-1 (1405 peak).

The error of the nitrogen concentration, determined by this method, is about ± 10% (Howell et al. 2012).

The analysis of the spectrum of sample *Centr_01_tg* (see figure 3.11) through this method has given these results (figure 3.13):

NITROGEN						HYDROGEN		Platelets		
Na (ppm)	Nb (ppm)	d	N total (ppm)	% IaB	Fit	H @3107 (cm-1)	H @1405 (cm-1)	Area I(B') (cm-2)	Peak Position (cm-1)	Peak Height (cm-1)
13.9	107.5	0.589	121.4	88.5	9.6641	1.7	0.3	5.7	1361	0.8

Figure 3.13. The results about the nitrogen concentration and the presence of both hydrogen and platelets of the sample *Centr_01_tg*, obtained with the DiaMap elaboration.

The fit of the spectrum (figure 3.14) gives us a total amount of nitrogen of 121.4 ppm, of which 13.9 ppm in the form of A centers and 107.5 ppm in the form of B centers; the percentage of B centers is 88.5 %.

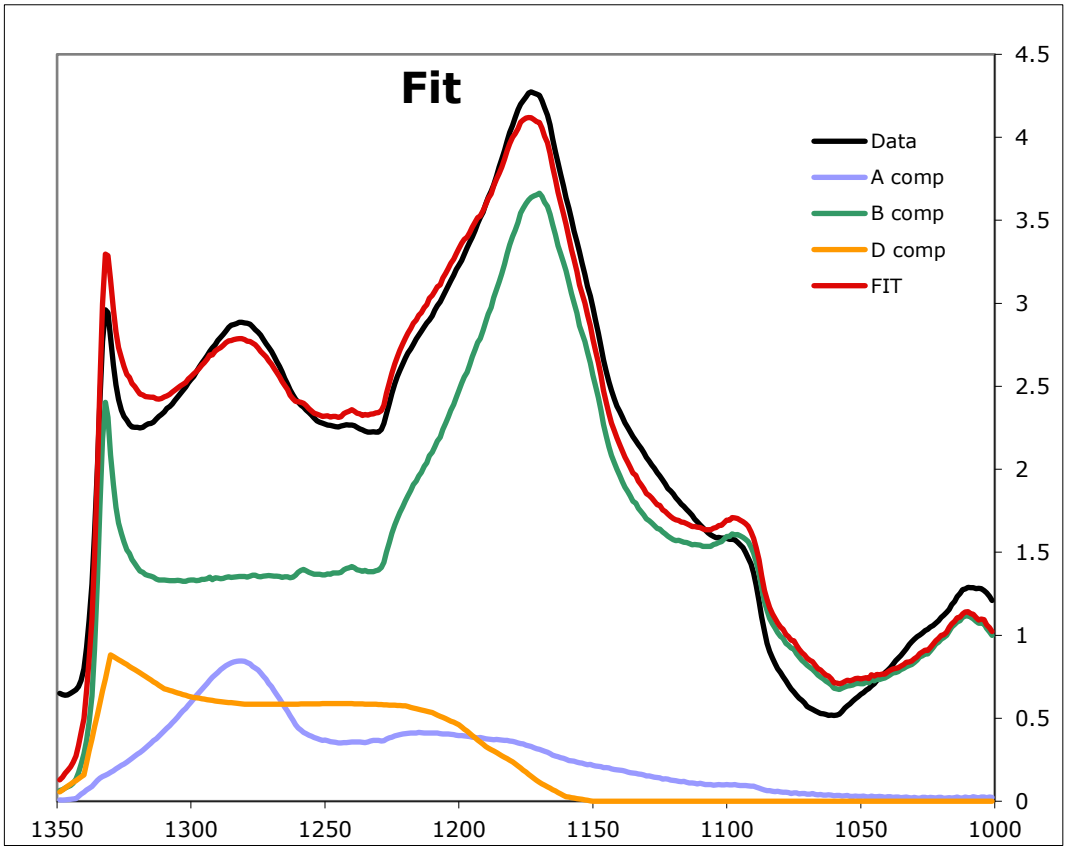

Figure 3.14. The fit of the spectrum of the sample *Centr_01_tg* in a range between 1000 and 1350 cm-1, to determine the nitrogen concentration; the black line corresponds to the raw data, the red one to the fit data, the blue one to the nitrogen concentration in the form of A centers, the green one to the nitrogen concentration in the form of B centers and the yellow one to the contribution of the D component.

Moreover, the presence of both hydrogen and platelets was determined (peak position of hydrogen both at 3107 and 1405 cm-1 and the peak position of the B' band at 1362 cm-1).

According to the classification of the diamonds in function of their impurities (Breeding et al. 2009), the sample *Centr_01_tg* is a Type I diamond (presence of nitrogen) and the 88.5 % of nitrogen is in form of B centers (B-aggregated 4N + V).

So, it is a Type IaAB diamond and the most of nitrogen is aggregated in form of B centers, and only a small concentration in the form of A centers (A-aggregated N pairs).

The high percentage of B centers indicates a high aggregation state of nitrogen and this suggests that the diamond suffered relative high temperature (Taylor et al. 1990) and had a relative long residence in the mantle (Evans et al. 1982).

A model to determine the temperature of the formation in function of the residence time in the mantle, it was calculated by Dr. Samantha Perrit (De Beers), that collaborated with us to this thesis project.

In her elaboration she used a nitrogen content of 126 ppm and an aggregation state of 84 % of nitrogen in form of B centers; considering the error in the estimate of these value, we can relate her model (table 3.6) with our results.

t(Ga)	**T(Ma)**	**T(°C)**	**Total N**	**%N as B**
3	3000	1206	126	84
2	2000	1217	126	84
1	1000	1236	126	84
0.5	500	1256	126	84
0.1	100	1304	126	84
0.005	50	1326	126	84
0.001	10	1378	126	84
0.0005	5	1402	126	84
0.0001	1	1549	126	84

Table 3.6. Temperature of formation of diamonds at different time residence in the mantle, in function of the amount of nitrogen and its aggregation state; these data were calculated by Dr. Samantha Perrit (De Beers) using the variable from: LEAHY K, TAYLOR W R (1997) The influence of the Glennie Domain deep structure on the diamonds in Saskatchewan kimberlites. Russian Geology and Geophysics, 38, 481-491.

Considering a residence time in the mantle between 1 and 3 Ga, the temperature varies between 1206 and 1236 °C (difference of only 30 °C) and this can indicate an origin in the deeper lithosphere.

However, applying the method used to calculate the temperature formation of the meteorites by the FWHM of the G peak of the graphite (see section 3.1.2), we obtained an average temperature of 1340 °C.

Considering the error, if this temperature is right, the residence time in the mantle could be between 10 and 50 Ma.

Even if for sub-lithospheric diamonds the residence time in the mantle is lower than for the lithospheric ones (Shirey et al. 2013), this is very low and probably this value is unrealistic.

Moreover, the approach of Ross et al. (2011) has never been tested in the natural diamonds and this estimate could not be right.

4. Discussion: lithospheric or sub-lithospheric nature of the diamonds coming from the Central African Republic

In this thesis work, the identification of diamond inclusions was mainly performed by the Micro-Raman spectrometry, since the size of inclusions did not allow to obtain good results with the Single-crystal x-ray diffraction.

In both samples *Centr_01_tg* and *Centr_02_tg*, the Micro-Raman analysis permitted the recognition of fluid phase inclusions, found for the first time in gem-quality diamonds by Nimis et al. (2016).

The Raman spectrum of this fluid phase is mainly characterized by two broad peaks at 617-671 cm-1 and 761-825 cm-1and these are at least five times broader than those of mineral inclusions.

This indicates that the peaks are produced by a non-crystalline material and they can be assigned to $Si_2O(OH)_6$ dimers and $Si(OH)_4$ monomers in an aqueous fluid (Nimis et al. 2016).

These main peaks can be accompanied by a shoulder near the upper end of the measured spectral range (3400-3570 cm-1), considered to be the 3600 cm-1 O-H stretching band of water and by a weak broad band at about 1650 cm-1, which is attributed to H2O bending in a fluid system.

In our spectra only the two main peaks are well visible (figure 4.1).

This fluid phase is usually located at the interface between the diamond host and the mineral inclusions; in the case of our inclusions, we were not able to define the type of mineral phases, since inclusions with similar appearance do not give Raman signal, if not those of fluid phase, and with the Single-crystal x-ray diffraction analysis we did not obtain any results (figure 4.2).

In the paper of Nimis et al. (2016), the fluid phase was found both around silicate and non-silicate inclusions, and the composition is always hydrous silicic; this means that the fluid is not a result of post-entrapment reactions between an aqueous fluid and the included minerals.

So, these fluids are the vestiges of the original fluids which were in contact with the diamonds during their formation (Nimis et al. 2016).

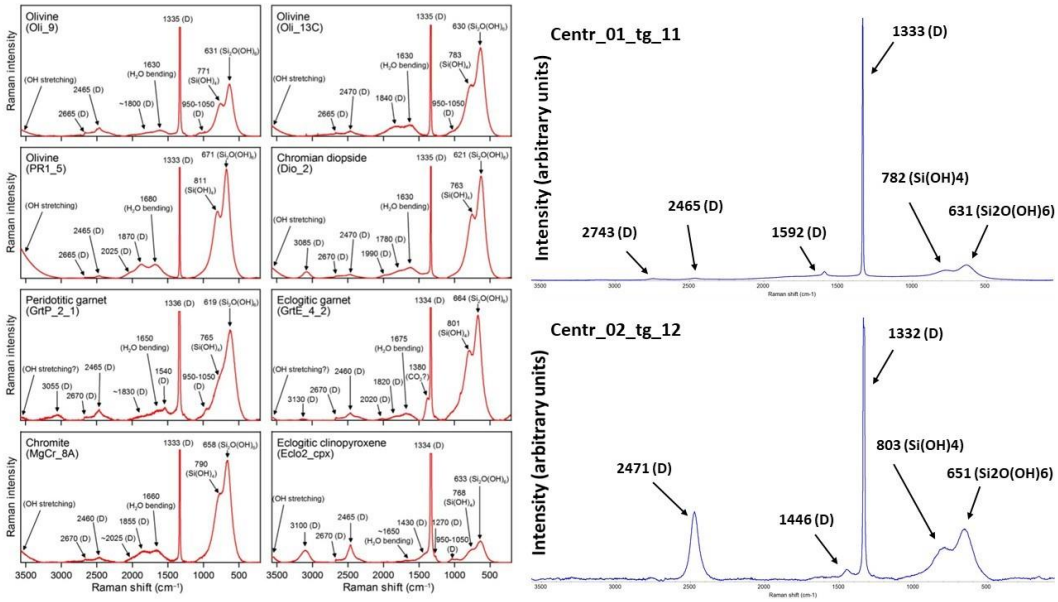

Figure 4.1. In the left, the spectra of hydrous silicic fluid are shown (from Nimis et al. 2016); in the right a spectrum of fluid from sample *Centr_01_tg* and one spectrum of fluid from sample *Centr_02_tg*, are shown: in these spectra only the two main peaks are well visible (related to the Si2O(OH)6 dimers and Si(OH)4 monomers).

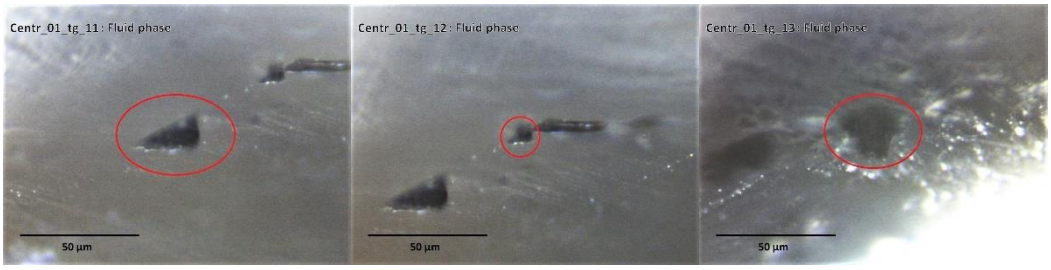

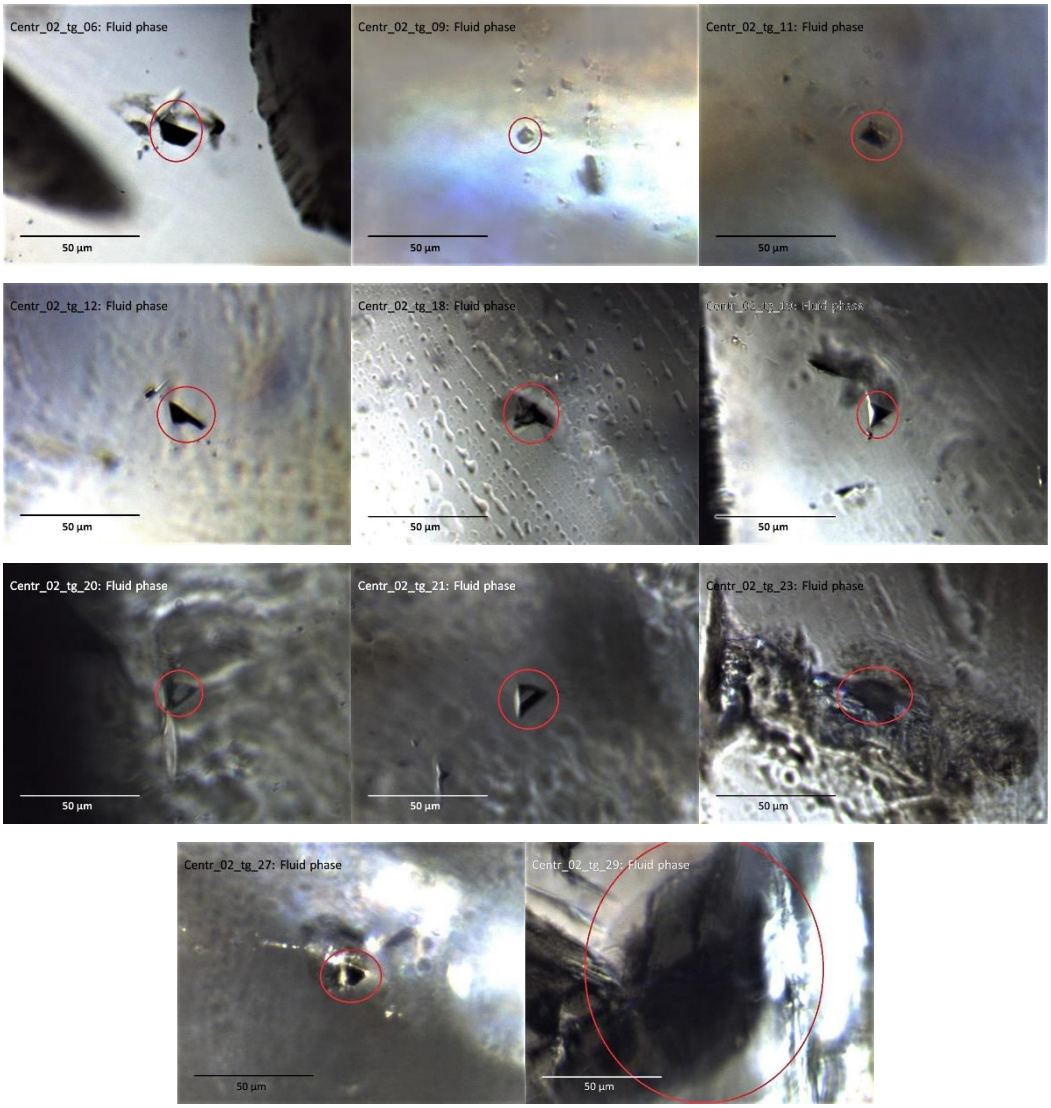

Figure 4.2. The photos of inclusions that the Micro-Raman analysis provides the Raman spectrum of hydrous silicic fluid; probably the fluid is located at the interface between the diamond host and the mineral inclusions.

The identification of the mineral phases was not possible, but some inclusions have similar appearance of olivines within the same samples.

This indicates that this fluid is either a major diamond-forming medium or a typical residue remaining from diamond forming metasomatic reactions.

However, in the lithospheric Mantle diamonds can precipitate from both oxidized (H_2O-rich) and reduced (CH_4-rich) C-H-O fluids or carbonatic melts during their isochemical ascent, isobaric cooling and reactions with mantle rocks, but all these

processes lead to a H_2O-rich composition of the fluids during the precipitation of the diamonds.

So, we cannot determine the oxidized or reduced nature of the parental fluids, basing on only these data.

Moreover, the presence of a fluid phase at the interface between the host and inclusion can have other important implications: for example, in the determination of the residual pressure of the inclusions, in the diamond-imposed shape of inclusions and in the formation of graphite around the inclusions in gem-quality diamonds during the heating experiments.

So far, this hydrous silicic fluid has found only in the lithospheric diamonds.

Another important inclusion found both in sample *Centr_01_tg* and *Centr_02_tg* is the anatase.

The anatase is the relative low-temperature and low-pressure polymorph of the rutile; this mineral phase is stable at temperature below the 600 °C and pressure below the 0.2 GPa (Dachille et al. 1968).

The rutile is the TiO_2 polymorph that we usually find within the lithospheric diamonds, both in the peridotitic paragenesis (especially in lherzolite one) and in the eclogitic paragenesis (Shirey et al. 2013).

However, the anatase has found within the diamonds yet; the first discovery of this inclusion as primary was in a diamond coming from Finsch kimberlite pipe in South Africa (Wang et al. 1996).

The inclusions within this diamond, in addition to anatase, are olivine, magnesite and graphite; it was classified as a lithospheric diamond with peridotitic paragenesis.

Considering the stability field of anatase (relative low pressure and temperature), the formation of this inclusion is not compatible with the P-T condition in the upper mantle.

Moreover, the reactions that transform the anatase in rutile with the temperature increase and in TiO_2(II) with the pressure increase are irreversible and the anatase

cannot be considered the retrograde product of the rutile, during the cooling and the pressure release.

In the diamond studied by Wang et al. (1996), the anatase grains are aligned in the edge of the magnesite inclusion and this suggests that the presence of anatase is related to topotactical relations.

The crystal structure of the anatase provides a better match with the crystal structure of the magnesite than those of rutile along a specific crystallographic plane and so, the topotaxy can be the reason of the crystallization of metastable anatase rather than the rutile.

In our samples, the identification of the anatase inclusions was performed by the Micro-Raman spectroscopy and only in one case the anatase was found in association with the calcite (figure 4.3).

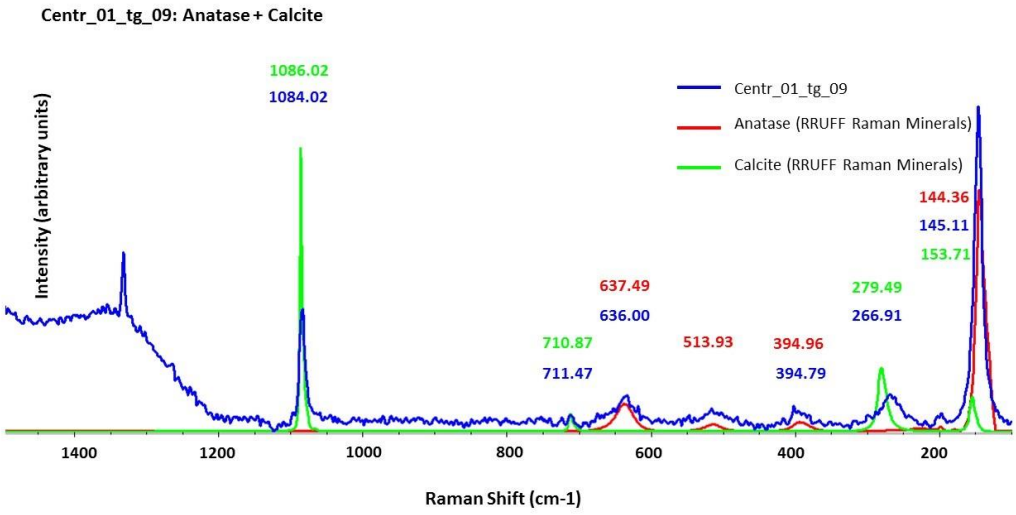

Figure 4.3. The Raman spectrum of the inclusion *Centr_01_tg_09;* this spectrum shows the presence of anatase and calcite in assemblage.

At present, we cannot determine if our anatase inclusions are primary or epigenetic and we cannot explain its association with the calcite.

The anatase inclusions were found in other diamonds (Barron et al. 2008), but they are present within the cracks and considered epigenetic inclusions.

In the sample *Centr_01_tg* two inclusions of calcite were found (one of this in association with the anatase) and in the sample *Centr_02_tg* only one inclusion of dolomite probably associated with an unknown phase (see figure 3.8).

The calcite within the studied lithospheric diamonds is always considered as an epigenetic inclusion (Meyer et al. 1986), instead the dolomite as primary inclusion (Stachel et al. 1998); both these carbonates were found in sub-lithospheric diamonds coming from Juina Area, Brazil (Brenker et al. 2007; Bulanova et al. 2010; Kaminsky 2012).

The first occurrence of dolomite in a lithospheric diamond coming from Mwadui kimberlite in Tanzania was explained with the possible, high and localised influx of CO_2 in the formation environment of diamonds, where the extent of the carbonation reactions carries out to eliminate the clinopyroxene by the reaction $2Mg_2SiO_4 + CaMgSi_2O_6 + 2CO_2 = CaMg(CO_3)_2 + 4MgSiO_3$ (Stachel et al. 1998).

However, calcite and dolomite phases were found within diamonds coming from alluvial deposits in Juina area (Brazil): these carbonates have negative shape and they are present as single crystal, this suggest their primary nature and they are in association with $CaSiO_3$-walstromites and olivines inclusions (Brenker et al. 2007).

The presence of $CaSiO_3$-walstromite-olivine association within the same diamonds can be explained as the retrograde phases of the original paragenesis ringwoodite (γMg_2SiO_4) + CaSi-perovskite, that is stable only within the lower part of the Transition Zone (580-670 km), or periclase (MgO) + MgSi-perovskite + CaSi-perovskite, stable in the Lower Mantle (>670 km); this confirmed the super-deep nature of these diamonds.

The coexistence of these mineral phases with the carbonates, considered as primary inclusions, suggests the provenance of calcite and dolomite in the transition zone or lower mantle.

The origin of these carbonates is related to the CO_2- enriched crustal or lithospheric material transported at high depth via subduction processes.

The subducting slabs are composed of several type of carbonate lithologies and in the case of the mineral assemblage within the diamonds studied by Brenker et al.

(2007), the ophicarbonate (Ca-metasomatism of the peridotitic lithospheric Mantle) is the more probable precursor lithology.
The high-pressure phase equilibria calculated for the ophicarbonates suggests that the original carbonate is retained during the subduction of the oceanic lithospheric slab to depth exceeding 200 km.
Considering also the decarbonation of aragonite as an experimentally well know mechanism for diamond formation in the lower part of the upper mantle, the connection between the subducted calcareous material and the diamond formation can be supported (Brenker et al. 2007).
In our samples, the calcite is found in association with the anatase, ringwoodite and the hydrous silicic fluid, whereas the dolomite with the anatase, olivine and hydrous silicic fluid.

In the sample *Centr_02_tg*, the olivine is the main inclusion and it is in association with the anatase, dolomite and hydrous silicic fluid.
In the diamonds this mineral phase usually indicates lithospheric origin and peridotitic paragenesis; it can be found with Cr-pyropes, chromites and sulphides (dunite-harzburgitic mineral paragenesis) and with pyropes, enstatites, Cr-diopsides and sulphides (lherzolitic mineral paragenesis) (Shirey et al. 2013).
The olivines within the lithospheric diamonds are generally colourless (figure 4.4) and high in forsterite content (consistent with an origin from peridotitic sources); the Mg # (%) less than 88 and major than 96 is very rare, the harzburgitic olivines usually fall in a range between 90.2 and 95.4 and the lherzolitic ones between 90.1 e 93.6 (Stachel et al. 2008).

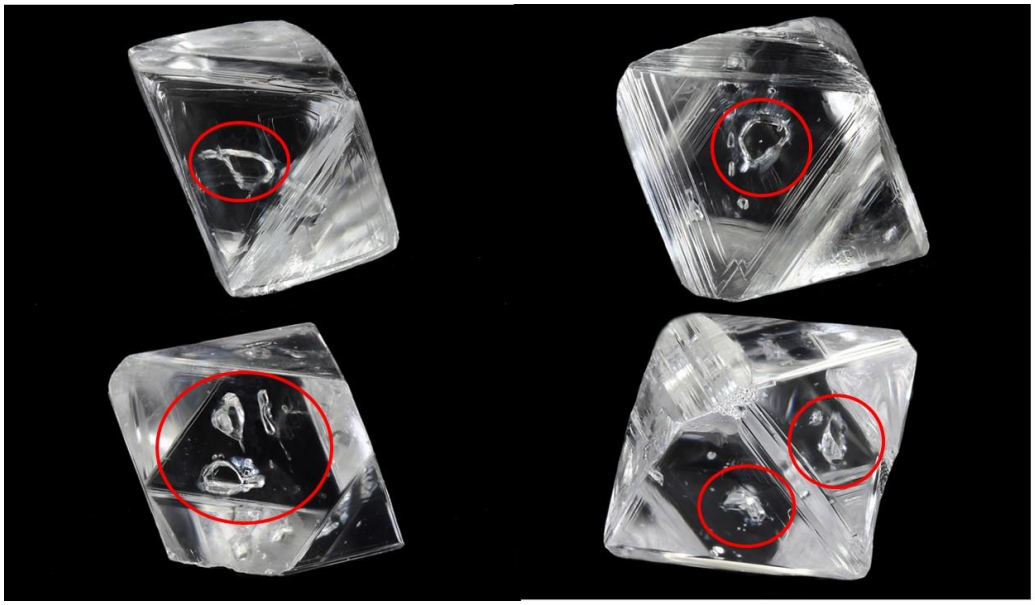

Figure 4.4. The colourless olivine inclusions in lithospheric diamonds; the inclusions are within the red circles.

The study of olivine inclusions can give several types of information about the lithospheric diamonds, for example the determination of the crystal-structure through the single-crystal x-ray diffraction provides information about the distribution of Mg^{2+} and Fe^{2+} cations in the crystallographic sites (composition of olivine) and the residual pressure of the inclusions, from which the calculation of formation pressure is possible through the elastic methods (Nestola et al. 2011).

Moreover, the determination of crystallographic orientation of the olivine inclusions respect to the diamond host, using the single-crystal x-ray diffraction, has allowed to give a possible explanation about the syngenetic or protogenetic relation between the inclusions and their host (Nestola et al. 2014; Bruno et al. 2016; Milani et al. 2016).

In addition, the position of the Raman peaks of olivine inclusions provides information about their composition and residual pressure (Yasuzuka et al. 2009).

However, the olivine inclusions can be found in the sub-lithospheric diamonds and they usually are in association with garnet and clinopyroxene, garnet, clinopyroxene and $CaSiO_3$-walstromite, and enstatite, ferropericlase and $CaSiO_3$-walstromite (Shirey et al. 2013).

The mineral phases within the sub-lithospheric diamonds, are usually the products of retrograde reactions that occur during the ascent of diamond toward the surface and probably the olivine is the retrograde product of wadsleyite or ringwoodite, that are considered two of the main mineral phases in the transition zone and predicted by several models.

The olivines within the sub-lithospheric diamonds are usually colourless and fall in a range of Mg# between 88 and 97, including low-Mg varieties and they are characterized by low concentration of Ni, that is a different aspect from the olivines found in the lithospheric diamonds (Kaminsky 2012).

In the sample *Centr_02_tg*, the olivine is the main inclusions within the diamonds: the calculation of their composition through the position of the Raman peak 1 (about 823 cm-1) (Yasuzuka et al. 2009) provides an average value of Mg# of 90.52 (±1.75).

This composition can be compatible both we consider the lithospheric or sub-lithospheric nature of our sample.

However, the appearance of these olivine inclusions is very different from the usual olivine found in the lithospheric diamonds (figure 4.5); their size is less than 50 µm and they are never completely colourless, but they have blueish shades, and in some cases, they are dark with brownish shades.

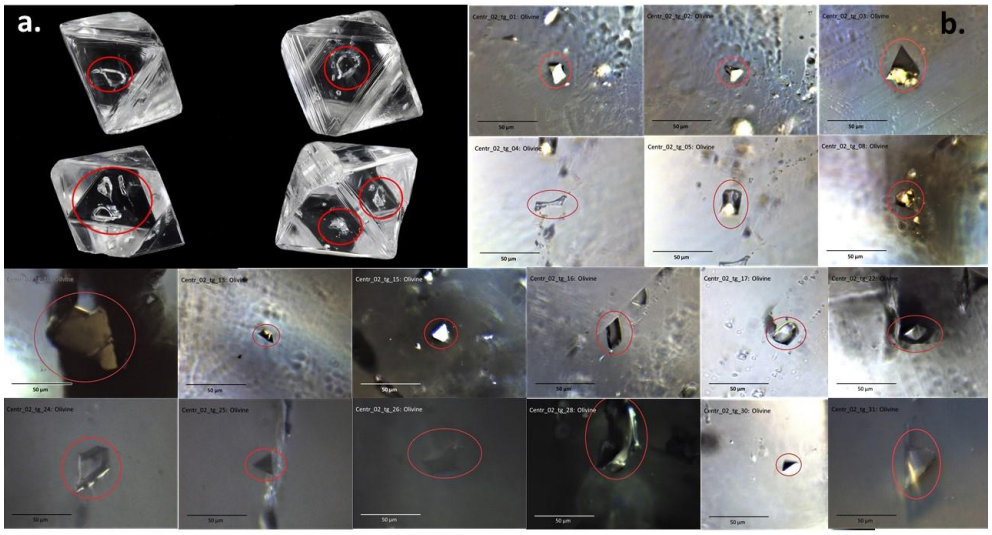

Figure 4.5. The olivine inclusions within lithospheric diamonds (a.) vs. the olivine inclusions within the sample *Centr_02_tg* (b.).

Despite the strange appearance of the olivine inclusions and the irregular form of the diamonds, probably the presence of hydrous silicic fluid inclusions associated with the olivines could lead us almost surely to classify the diamonds samples coming from Central African Republic as lithospheric diamonds (as the diamonds coming from the Kimberlites of Democratic Republic of Congo).
However, the occurrence of only one inclusion of ringwoodite, probably associated with an unknown phase, in the sample *Centr_01_tg* has provided the possibility that these diamonds could be sub-lithospheric ones.

The ringwoodite and the wadsleyite are the hydrous and high-pressure polymorph of the olivine; theoretical and experimental models have demonstrated that the Earth's transition zone (410-660 km depth) could be a major repository for water and the presence of a seismic discontinuity at about 410 km depth could be due to the transformation of the olivine in the wadsleyite (Chen et al. 2002; Smyth et al. 2003).
Despite the capacity of water storage of olivines in the upper mantle is very low (Novella et al. 2015), it is experimentally estimated that the wadsleyite and the ringwoodite, stable olivine polymorphs at these depth, could host on their crystal structure up to 3.3 and 2.5 per cent in weight of H_2O, respectively.
In the diamonds that we consider sub-lithospheric, which crystallization occurred in the transition zone or in the lower mantle, the olivine inclusions are found; it is supposed that they are the retrograde products of wadsleyite or ringwoodite and it is explained to a probable very high velocity of back-transformation of these high-pressure polymorph of the olivine (at present this velocity and the kinetics of transformation of these phases in olivine are unknown, (Nestola 2017)).
However, the finding of a not back-transformed ringwoodite inclusion in a diamond coming from the alluvial deposits in Juina area (Brazil) has confirmed the existence of the sub-lithospheric diamond, the presence of the ringwoodite in the transition zone and has given the possibility to calculate the water amount in its crystal

structure and in the part of transition zone in which this phase crystallized (525-660 km depth) (Pearson et al. 2014; Nestola et al. 2016).

In the work of Pearson et al. (2014), the identification of the ringwoodite inclusion was carried out by the Single-crystal X-ray Diffraction and the Micro-Raman spectroscopy.

The Micro-Raman analysis provided the presence of $CaSiO_3$-walstromite associated to the ringwoodite (figure 4.6).

The Raman spectrum of the ringwoodite differs from those of olivine for the spacing between the two main peaks, since in the ringwoodite spectrum (peaks at 796 and 844 cm-1) is 30% wider than olivine one (peaks at 823 and 854 cm-1).

The ringwoodite spectrum collected in the Juina diamond the main peaks are shifted to higher wavenumbers, due to the influence of compressive stress developed around the inclusion.

Moreover, the broader peaks are probably due to the increased disordering resulting from the tendency of ringwoodite to revert in olivine at lower pressure.

The amount of water was calculated by integrating the peaks at about 3150 and 3680 cm-1 of the FTIR spectrum of this inclusion (that correspond to the OH stretching vibration) and it was obtained a minimum estimate of 1.4-1.5 wt%; this value is affected by a large uncertainty, caused by the difficulty to constrain the thickness of sample during the FTIR analysis (Pearson et al. 2014).

So, both this inclusion is syngenetic or protogenetic, its water amount is representative of the water concentration of its formation environment.

If it does not represent a localized water enrichment, this result allowed to recalculate the amount of H2O in the transition zone and the entire reservoir of terrestrial H2O (Nestola et al. 2016), opening a possible new scenario in the global Earth's water cycle.

First of this finding, the amount of water in the transition zone was calculated considering a water concentration of 2000 ppm in the ringwoodite, this value represents only 1/15th of the maximum solubility of ringwoodite (it was experimentally estimated between 2.5 and 3%).

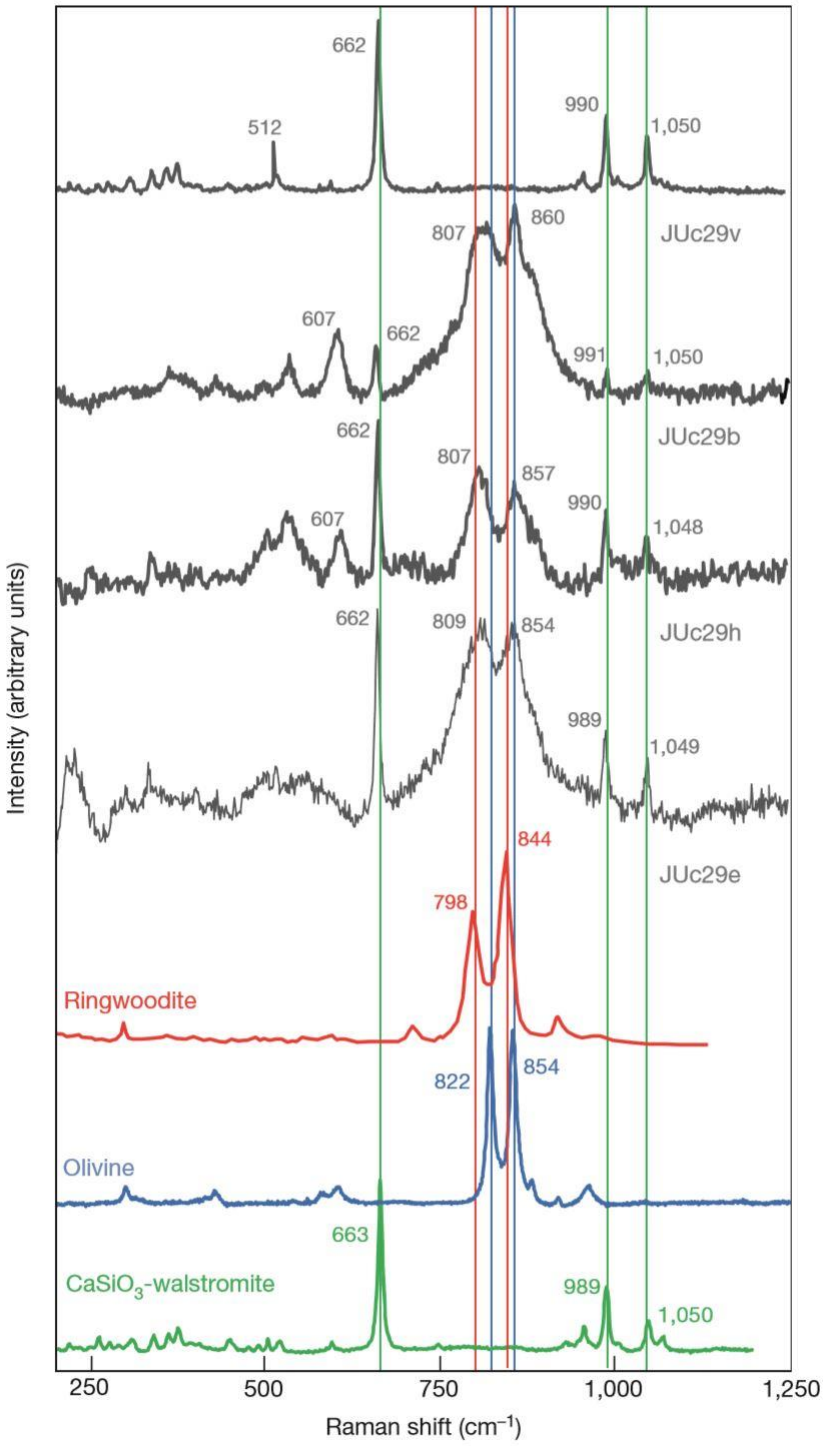

Figure 4.6. The Raman spectrum of the ringwoodite inclusion, associated to the CaSiO3-walstromite, in the diamond from the alluvial deposits of Juina area (Brazil) studied by Pearson et al. (2014) (from Pearson et al. 2014).

Moreover, the total amount of water must be determined, considering the water solubility of other hydrous mineral phases in the transition zone, as wadsleyite, majoritic garnet, diopside and $CaSiO_3$-perovskite.

The ringwoodite inclusion studied by Pearson et al. (2014) contains about the 1.4 wt% in H_2O (14000 ppm) and this value is higher than that used by the models reported in literature and represent the 50% of the maximum water solubility of this phase.

If it is considered the same water solubility for the other hydrous mineral phases that compose the transition zone, a new estimate of the water content of the transition zone can be calculated and the result is 4.5 times of the previous content (Nestola et al. 2016).

However, this concentration can be realistic, if the water amount in the ringwoodite inclusion of the Brazilian diamond does not represent a localized water-enrichment in the transition zone.

In every case, this finding has opened a new scenario in the global Earth's water cycle and new possibilities for the role of water in the geological evolution of our planet.

In the sample *Centr_01_tg*, the possible ringwoodite inclusion was identified by the Micro-Raman spectroscopy: its size is less than 10 μm (figure 4.7) and probably it is associated to a new/unknown mineral phase.

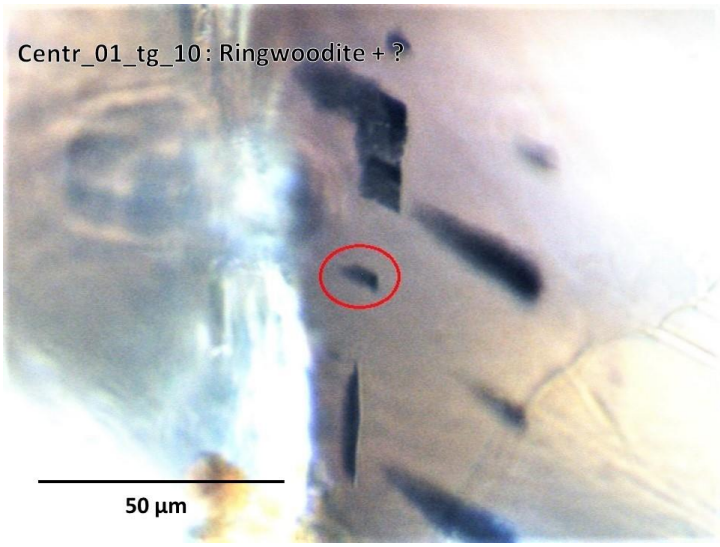

Figure 4.7. The possible ringwoodite inclusion in the sample *Centr_01_tg.*

The collected Raman spectrum shows the main two peaks of the ringwoodite at about 796 and 830 cm-1(very similar to the ringwoodite spectrum from the RRUFF Raman Minerals), but near the peak at 796 cm-1, a small shoulder is present at about 812 cm-1 (figure 4.8).

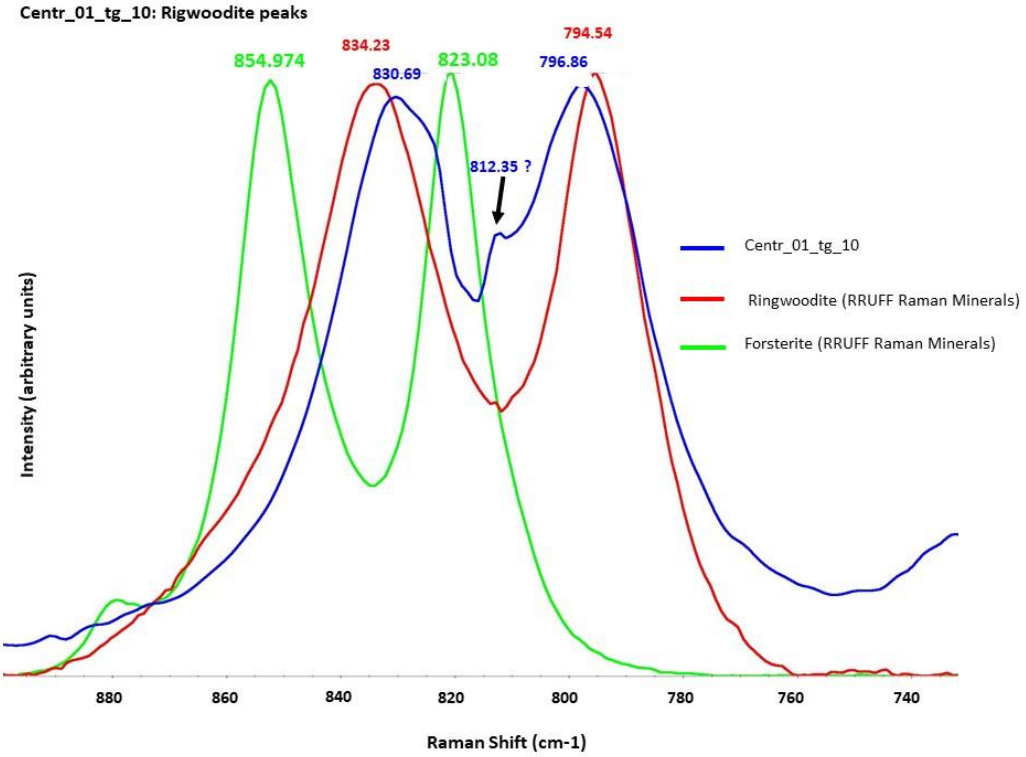

Figure 4.8. The Raman spectrum of inclusion *Centr_01_tg_10*, with focus on the two main peaks of ringwoodite.

The same Raman spectrum shows also 3 peaks at about 328, 530 and 731 cm-1 and, since we are not able to recognize a possible mineral phase that can produce these peaks, we suppose that these belong to a new/unknown phase (figure 4.9).

In this way, the small shoulder at 812 cm-1, if it is really a peak, could be produced by the same new phase, but we do not affirm this until more detailed analyses will carry out.

Moreover, if we compare the Raman spectrum of our ringwoodite to those of the ringwoodite by Pearson et al. (2014), the two main peaks are not shifted to higher

values of wavenumber; probably the effect of the compressive stress around the inclusion is negligible.

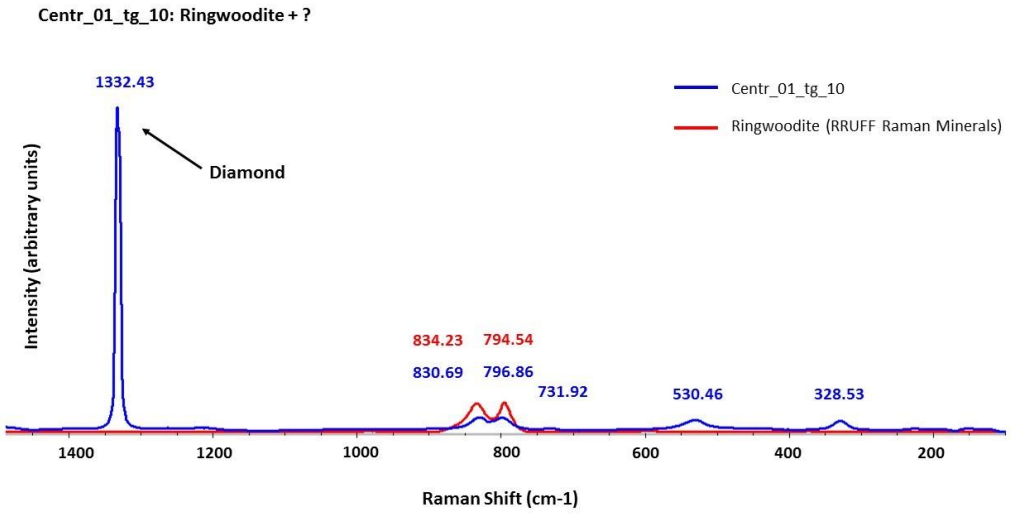

Figure 4.9. The Raman spectrum of inclusion *Centr_01_tg_10*, in which are present the diagnostic peaks of ringwoodite and 3 peaks that probably belong to a new mineral phase.

In the sample Centr_01_tg, the possible ringwoodite coexists with the anatase, calcite and the hydrous silicic fluid; none olivines were found in this diamond.
If this inclusion is really ringwoodite, we could affirm the sub-lithospheric nature of this diamond and their formation in the transition zone, between 525 and 660 km depth.
Moreover, if we consider that the all diamonds had the same origin, the olivines in the sample *Centr_02_tg* could be the back-transformation of the ringwoodite.

In addition, the finding of three inclusions of graphite in the sample *Centr_02_tg* by the Micro-Raman spectroscopy, which Raman spectra show a well-define G peak, allowed us to calculate a possible formation temperature of this diamonds.
This was obtained using a method based on the FWHM of the G peak of graphite and applied to calculate the temperature of formation of the Almahata Sitta urelite (see subchapter 3.1.2.) (Ross et al. 2011).

Despite this approach has never been tested in terrestrial diamonds, we tried to apply it to our sample, obtaining an average temperature of 1340 °C (±50 °C).

In the lithospheric diamonds the estimated temperature of formation, using thermometers based on the chemical equilibria between the mineral phases at different P-T conditions, is around 1150-1200 °C (Stachel et al. 2008).
However, the range of P-T conditions of diamonds formation is wide and in particular situations the temperature can be between 1250-1400 °C for peridotitic diamonds formed in the deep lithosphere or major than 1400 °C for diamonds formed in the ascending mantle plume (Shirey et al. 2013).
Moreover, in sub-lithospheric diamonds the temperature can be higher, reflecting the P-T conditions of the deeper formation environment.
So, if the calculated temperature is realistic, this diamond formed at particular conditions in the lithosphere or in sub-lithospheric conditions.
However, the temperature-model calculated in function of the nitrogen amount and the residence time in the mantle by Samantha Perrit shows that if this temperature is real, the residence time is between 10 and 50 Ma.
This value is unusual, since even if for sub-lithospheric diamonds the residence time is less long than lithospheric ones, it is similar or less than the average emplacement time of the kimberlites.
If we consider a residence time between 1 and 3 Ga, instead, the temperature is about 1230 °C and this indicates a probable formation temperature in the deep lithosphere.

Finally, to conclude our study with the intention to determine lithospheric or sub-lithospheric nature of diamonds coming from Central African Republic, we analysed the impurities of these diamonds, with focus on the nitrogen content.
From the analysis of the FTIR spectrum of the diamond *Centr_01_tg* through the software DiaMap, it is obtained that the diamond is a type IaAB, the nitrogen amount is about 121 ppm and the 88% of the nitrogen is aggregated in form of B centers and subsequently it has a high state of aggregation (see sub-chapter 3.3.).

In general, the lithospheric diamonds are characterized by a relative high nitrogen amount, whereas the sub-lithospheric ones by relative low nitrogen amount, but with a very high state of aggregation, reflecting the high-temperature environment of formation and residence of the diamonds.

At present, a precise threshold value of nitrogen amount to distinguish lithospheric and sub-lithospheric diamonds does not exist.

However, in a work of Stachel et al. (2002), the nitrogen content of diamonds coming from alluvial deposits of Kankan area (Guinea) was calculated.

These diamonds formed at different levels of depth, in the lithosphere, asthenosphere, transition zone and lower mantle and the results of the analyses have shown how the nitrogen amount changes in function of formation depth.

From this study it was obtained that for the lithospheric Kankan diamonds the nitrogen content is high and very variable, between 20 and 1313 ppm for eclogitic type ones, and between 17 and 648 ppm for the peridotitic type ones.

For the diamonds with majorite inclusions, that the authors have considered with formation in the upper part of the transition zone, the nitrogen concentration is between 0 and 126 ppm, and the lower mantle diamonds are Type II (nitrogen below the detection); the state of aggregation of nitrogen is variable.

Others studies of nitrogen amount carried out in the sub-lithospheric diamond coming from Juina area, Brazil (Kaminsky et al. 2009; Bulanova et al. 2010).

The results showed variable concentration of nitrogen and, even if the most of diamonds is the type II (nitrogen content < 20 ppm), some sample have nitrogen amount up to 170 ppm and some are zoned (different N-amount between the core and the rims) with values between about 70 ppm at the core and 570 ppm at the rims (Bulanova et al. 2010).

This feature is not common in the lithospheric diamonds, where the higher concentrations usually are at the core of the diamonds.

Moreover, the most of diamonds with detectable nitrogen amount, is the type IaB, showing a high state aggregation; this suggests a long residence time in the mantle at relative high temperature.

Considering the data obtained to the sample *Centr_01_tg,* the nitrogen amount (121 ppm) could suggest the lithospheric nature of the diamond.

However, in some sub-lithospheric diamonds coming from Juina area, Brazil, the nitrogen concentration has values up to 170 ppm (Bulanova et al. 2010).

Moreover, the high concentration of the nitrogen in form of B centers shows a long residence time in the Mantle in a high temperature environment; this could be characteristic of a sub-lithospheric origin.

In conclusion, the FTIR results cannot be diagnostic to determine the lithospheric or sub-lithospheric nature of our samples.

5. Conclusions

The main aim of this thesis work has been the characterization (lithospheric vs. sub-lithospheric) of a set of alluvial diamonds coming from Central African Republic, for the first time.

In the Central African Republic, there are not kimberlites, and diamonds are found in secondary deposits (the Carnot Formation and the Mouka-Ouadda Formation) that are mainly composed of sandstone and their deposition occurred in the Cretaceous and in alluvial deposits.

The analyses of the paleo-currents recorded in the Carnot Formation and in the Mouka-Ouadda Formation suggest that the primary sources of the diamonds are located at South of these formations, probably in the northern part of the Democratic Republic of Congo (Censier et al. 1999; Malibangar et al. 2001).

Previous studies of diamonds coming from different kimberlites in DRC do not show any finding of sub-lithospheric diamonds (Ntanda et al. 1982; Kosman et al. 2016) in these zones.

In our samples, the identification of the inclusions was performed by the Micro-Raman spectroscopy and our results can resume as follows:

- The sample *Centr_01_tg* shows the coexistence between anatases, calcites and hydrous silicic fluid phase inclusions and the finding of possible only one ringwoodite, associated to a new/unknown phase;
- The sample *Centr_02_tg* show the coexistence between olivines, anatases, hydrous silicic fluid phase inclusions and a dolomite.

At present, the anatase, even if it is very rare as primary inclusion in the diamond, and the hydrous silicic fluid phase are found only in the lithospheric diamond (Wang et al. 1996; Nimis et al. 2016).

The calcite and dolomite are rare inclusions and both are identified in the sub-lithospheric diamonds as primary inclusions (Kaminsky 2012), whereas only the dolomite in the lithospheric diamonds (Stachel et al. 1998).

Olivines are the typical inclusion of the lithospheric diamonds with peridotitic paragenesis and they have a lot of implications in the diamond study (Nestola et al.

2011; Nestola et al. 2014; Milani et al. 2016; Yasuzuka et al. 2009; Novella et al. 2015).

However, olivines are found also in sub-lithospheric diamonds and they are considered the back-transformations of wadsleyites or ringwoodites (high pressure polymorphs of olivines in the transition zone, between 410 and 660 km depth).

The analysis of the composition of the olivine through the position of Raman peaks (Yasuzuka et al. 2009), provides an average composition of 90.5 Mg# (%); this value falls both in the possible ranges to lithospheric or sub-lithospheric olivines.

However, the olivines within the sample *Centr_02_tg* have unusual appearance, different to the olivines found in the lithospheric diamonds (see figure 4.5).

The data about the nitrogen content cannot be diagnostic to characterization of diamonds, since, even if the most of sub-lithospheric diamonds are nitrogen-free (Stachel et al. 2002), some samples from Juina area contain up to 170 ppm of nitrogen (Bulanova et al. 2010); moreover, the high state of aggregation could be in agree with a high temperature environment of formation.

In addition, the possible temperature of formation of the diamonds is relative high (considering both the Ross et al. (2011) approach and the model of Samantha Perrit) and suggests a particular conditions formation in the lithosphere or sub-lithospheric conditions.

Considering only these aspects, probably we could classify this diamond set as lithospheric diamonds, since the unique feature that could belong to the sub-lithospheric diamond is the irregular shapes and the possible high temperature of formation.

The finding of a possible ringwoodite associated to an unknown phase in the sample *Centr_01_tg*, has opened the possibility that these diamonds have sub-lithospheric origin in the transition zone between 525-660 km depth.

If the nature of ringwoodite will be confirmed, we could affirm that the studied diamonds coming from the Central African Republic are sub-lithospheric, and if all diamonds had the same origin, the olivines within the sample *Centr_02_tg* could be considered the back-transformation of the ringwoodite at lower pressure.

Moreover, for the first time the hydrous silicic fluid phase could be found in the sub-lithospheric diamonds.

In conclusion, the morphology, the colour and the appearance of the diamonds are not typical of lithospheric diamonds, and obviously if the ringwoodite will be definitive confirm, we can confirm the real nature of the diamonds.

References

Barron, L. M., B. J. Barron, T. P. Mernagh, and W. D. Birch. 2008. "Ultrahigh Pressure Macro Diamonds from Copeton (New South Wales, Australia), Based on Raman Spectroscopy of Inclusions." *Ore Geology Reviews* 34 (1–2): 76–86.

Batumike, J. M., W. L. Griffin, E. A. Belousova, N. J. Pearson, Suzanne Y. O'Reilly, and S. R. Shee. 2008. "LAM-ICPMS U-Pb Dating of Kimberlitic Perovskite: Eocene-Oligocene Kimberlites from the Kundelungu Plateau, D.R. Congo." *Earth and Planetary Science Letters* 267 (3–4): 609–19.

Breeding, Christopher M., and James E. Shigley. 2009. "The 'Type' Classification System of Diamonds and Its Importance in Gemology." *Gems & Gemology* 45 (2): 96–111.

Brenker, Frank E., Christian Vollmer, Laszlo Vincze, Bart Vekemans, Anja Szymanski, Koen Janssens, Imre Szaloki, Lutz Nasdala, Werner Joswig, and Felix Kaminsky. 2007. "Carbonates from the Lower Part of Transition Zone or Even the Lower Mantle." *Earth and Planetary Science Letters* 260 (1–2): 1–9.

Bruno, M., M. Rubbo, D. Aquilano, F. R. Massaro, and F. Nestola. 2016. "Diamond and Its Olivine Inclusions: A Strange Relation Revealed by Ab Initio Simulations." *Earth and Planetary Science Letters* 435: 31–35.

Bulanova, Galina P., Michael J. Walter, Chris B. Smith, Simon C. Kohn, Lora S. Armstrong, Jon Blundy, and Luiz Gobbo. 2010. "Mineral Inclusions in Sublithospheric Diamonds from Collier 4 Kimberlite Pipe, Juina, Brazil: Subducted Protoliths, Carbonated Melts and Primary Kimberlite Magmatism." *Contributions to Mineralogy and Petrology* 160 (4): 489–510.

Censier, C., and J. Tourenq. 1995. "Crystal Forms and Surface Textures of Alluvial Diamonds from the Western Region of the Central African Republic." *Mineralium Deposita* 30 (3–4): 314–22.

Censier, Claude, and Jacques Lang. 1999. "Sedimentary Processes in the Carnot Formation (Central African Republic) Related to the Palaeogeographic

Framework of Central Africa." *Sedimentary Geology* 127 (1–2): 47–64.

Chen, Jiuhua, Toru Inoue, H. Yurimoto, and Donald J. Weidner. 2002. "Effect of Water on Olivine-Wadsleyite Phase Boundary in the (Mg, Fe) $_2$ SiO $_4$ System." *Geophysical Research Letters* 29 (18): 22-1-22–24.

Chirico, Peter G., Francis Barthélémy, and François a. Ngbokoto. 2010. "Alluvial Diamond Resource Potential and Production Capacity Assessment of Guinea." *Scientific Investigations Report 2012 – 5256*, 1–29.

Chopelas, A. 1990. "Thermal Properties of Forsterite at Mantle Pressures Derived from Vibrational Spectroscopy." *Physics and Chemistry of Minerals* 17 (2): 149–56.

Chopelas, A. 1991. "Single Crystal Raman Spectra of Forsterite, Fayalite, and Monticellite." *American Mineralogist* 76 (7–8): 1101–9.

Dachille, Frank, Simons, P.Y., Roy, Rustum. 1968. "Pressure-Temperature Studies of Anatase, Brookite Rutile, and TiO_2(II). a Discussion." *American Mineralogist* 53 (9–10): 1929–39.

De, Subarnarekha, Peter J. Heaney, Robert B. Hargraves, Edward P. Vicenzi, and Patrick T. Taylor. 1998. "Microstructural Observations of Polycrystalline Diamond: A Contribution to the Carbonado Conundrum." *Earth and Planetary Science Letters* 164 (3–4): 421–33.

Delpomdor, Franck, Ulf Linnemann, Ariel Boven, Andreas Gärtner, Aleksey Travin, Christian Blanpied, Aurélien Virgone, Hielke Jelsma, and Alain Préat. 2013. "Depositional Age, Provenance, and Tectonic and Paleoclimatic Settings of the Late Mesoproterozoic-Middle Neoproterozoic Mbuji-Mayi Supergroup, Democratic Republic of Congo." *Palaeogeography, Palaeoclimatology, Palaeoecology* 389: 4–34.

Ferrari, A C, and J Robertson. 2000. "Interpretation of Raman Spectra of Disordered and Amorphous Carbon" 61 (20): 95–107.

Howell, D., C. J. O'Neill, K. J. Grant, W. L. Griffin, N. J. Pearson, and S. Y. O'Reilly. 2012. "μ-FTIR Mapping: Distribution of Impurities in Different Types of Diamond Growth." *Diamond and Related Materials* 29: 29–36.

Kagi, Hiroyuki, Kazuya Takahashi, Hiroshi Hidaka, and Akimasa Masuda. 1994.

"Chemical Properties of Central African Carbonado and Its Genetic Implications." *Geochimica et Cosmochimica Acta* 58 (12): 2629–38.

Kaminsky, Felix. 2012. "Mineralogy of the Lower Mantle: A Review of 'super-Deep' Mineral Inclusions in Diamond." *Earth-Science Reviews* 110 (1–4): 127–47.

Kaminsky, Felix V., Galina K. Khachatryan, Paulo Andreazza, Debora Araujo, and William L. Griffin. 2009. "Super-Deep Diamonds from Kimberlites in the Juina Area, Mato Grosso State, Brazil." *Lithos* 112: 833–42.

Kampunzu, A. B., and J. Cailteux. 1999. "Tectonic Evolution of the Lufilian Arc (Central Africa Copper Belt) during Neoproterozoic Pan African Orogenesis." *Gondwana Research* 2 (3): 401–21.

Kosman, Charles W., Maya G. Kopylova, Richard A. Stern, James W. Hagadorn, and James F. Hurlbut. 2016. "Cretaceous Mantle of the Congo Craton: Evidence from Mineral and Fluid Inclusions in Kasai Alluvial Diamonds." *Lithos* 265: 42–56.

Leahy, K, Taylor W R. 1997. "The influence of the Glennie Domain deep structure on the diamonds in Saskatchewan kimberlites". *Russian Geology and Geophysics* 38: 481-491.

Milani, S., F. Nestola, R. J. Angel, P. Nimis, and J. W. Harris. 2016. "Crystallographic Orientations of Olivine Inclusions in Diamonds." *Lithos* 265: 312–16.

Mouri, Takashi; Enami, Masaki. 2008. "Raman Spectroscopic Study of Olivine-Group Minerals." *Journal of Mineralogical and Petrological Sciences* 103 (2): 100–104.

Mvuemba Ntanda, F., J. Moreau, and H. O. A. Meyer. 1982. "Particularites Des Inclusions Cristallines Primaires Des Diamants Du Kasai , Zaire." *Canadian Mineralogist* 20: 217–30.

Nestola, F., P. Nimis, R. J. Angel, S. Milani, M. Bruno, M. Prencipe, and J. W. Harris. 2014. "Olivine with Diamond-Imposed Morphology Included in Diamonds. Syngenesis or Protogenesis?" *International Geology Review* 56 (13): 1658–67.

Nestola, Fabrizio. 2017. “Inclusions in Super-Deep Diamonds: Windows on the Very Deep Earth.” *Rendiconti Lincei* 28 (4): 595–604.

Nestola, Fabrizio, Antony D. Burnham, Luca Peruzzo, Leonardo Tauro, Matteo Alvaro, Michael J. Walter, Mickey Gunter, Chiara Anzolini, and Simon C. Kohn. 2016. “Tetragonal Almandine-Pyrope Phase, TAPP: Finally a Name for It, the New Mineral Jeffbenite.” *Mineralogical Magazine* 80 (7): 1219–32.

Nestola, Fabrizio, Paolo Nimis, Luca Ziberna, Micaela Longo, Andrea Marzoli, Jeff W. Harris, Murli H. Manghnani, and Yana Fedortchouk. 2011. “First Crystal-Structure Determination of Olivine in Diamond: Composition and Implications for Provenance in the Earth’s Mantle.” *Earth and Planetary Science Letters* 305 (1–2): 249–55.

Nestola, Fabrizio, and Joseph R. Smyth. 2016. “Diamonds and Water in the Deep Earth: A New Scenario.” *International Geology Review* 58 (3): 263–76.

Nimis, Paolo, Matteo Alvaro, Fabrizio Nestola, Ross J. Angel, Katharina Marquardt, Greta Rustioni, Jeff W. Harris, and Federica Marone. 2016. “First Evidence of Hydrous Silicic Fluid Films around Solid Inclusions in Gem-Quality Diamonds.” *Lithos* 260: 384–89. h

Novella, Davide, Nathalie Bolfan-Casanova, Fabrizio Nestola, and Jeffrey W. Harris. 2015. “H2O in Olivine and Garnet Inclusions Still Trapped in Diamonds from the Siberian Craton: Implications for the Water Content of Cratonic Lithosphere Peridotites.” *Lithos* 230: 180–83.

Ovenstone, J., J. O. Romani, D. Davies, and J. Silver. 2003. “Topotactic Crystallisation of Calcite under Hydrothermal Conditions.” *Journal of Materials Science* 38 (12): 2743–46.

Pearson, D. G., F. E. Brenker, F. Nestola, J. McNeill, L. Nasdala, M. T. Hutchison, S. Matveev, et al. 2014. “Hydrous Mantle Transition Zone Indicated by Ringwoodite Included within Diamond.” *Nature* 507 (7491): 221–24.

Ross, Aidan J., Andrew Steele, Marc D. Fries, Lukas Kater, Hilary Downes, Adrian P. Jones, Caroline L. Smith, Peter M. Jenniskens, Michael E.

Zolensky, and Muawia H. Shaddad. 2011. “MicroRaman Spectroscopy of Diamond and Graphite in Almahata Sitta and Comparison with Other Ureilites.” *Meteoritics and Planetary Science* 46 (3): 364–78.

Schärer, Urs, Fernando Corfu, and Daniel Demaiffe. 1997. “U-Pb and Lu-Hf Isotopes in Baddeleyite and Zircon Megacrysts from the Mbuji-Mayi Kimberlite: Constraints on the Subcontinental Mantle.” *Chemical Geology* 143 (1–2): 1–16.

Smyth, Joseph R., Christopher M. Holl, Daniel J. Frost, Steven D. Jacobsen, Falko Langenhorst, and Catherine A. Mccammon. 2003. “Structural Systematics of Hydrous Ringwoodite and Water in Earth’s Interior.” *American Mineralogist* 88 (10): 1402–7.

Stachel, T., and J. W. Harris. 2008. “The Origin of Cratonic Diamonds - Constraints from Mineral Inclusions.” *Ore Geology Reviews* 34 (1–2): 5–32.

Stachel, Thomas, Jeff W. Harris, and Gerhard P. Brey. 1998. “Rare and Unusual Mineral Inclusions in Diamonds from Mwadui, Tanzania.” *Contributions to Mineralogy and Petrology* 132 (1): 34–47.

Taylor, W. R., A. L. Jaques, and M. Ridd. 1990. “Nitrogen-Defect Aggregation Characteristics of Some Australasian Diamonds: Time-Temperature Constraints on the Source Regions of Pipe and Alluvial Diamonds.” *American Mineralogist* 75 (11–12): 1290–1310.

Wang, Alian, Jill D. Pasteris, Henry O.a. Meyer, and Marie L. Dele-Duboi. 1996. “Magnesite-Bearing Inclusion Assemblage in Natural Diamond.” *Earth and Planetary Science Letters* 141 (1–4): 293–306.

Wit, Maarten J. De, François Guillocheau, and Michiel C.J. De Wit. 2015. “Geology and Resource Potential of the Congo Basin.” *Geology and Resource Potential of the Congo Basin*, no. January: 1–417.

Yasuzuka, Takaharu, Hidemi Ishibashi, Masashi Arakawa, Junji Yamamoto, and Hiroyuki Kagi. 2009. “Simultaneous Determination of Mg# and Residual Pressure in Olivine Using Micro-Raman Spectroscopy.” *Journal of Mineralogical and Petrological Sciences* 104 (6): 395–400.

Appendix A

The spectra of inclusions within the sample *Centr_01_tg*:

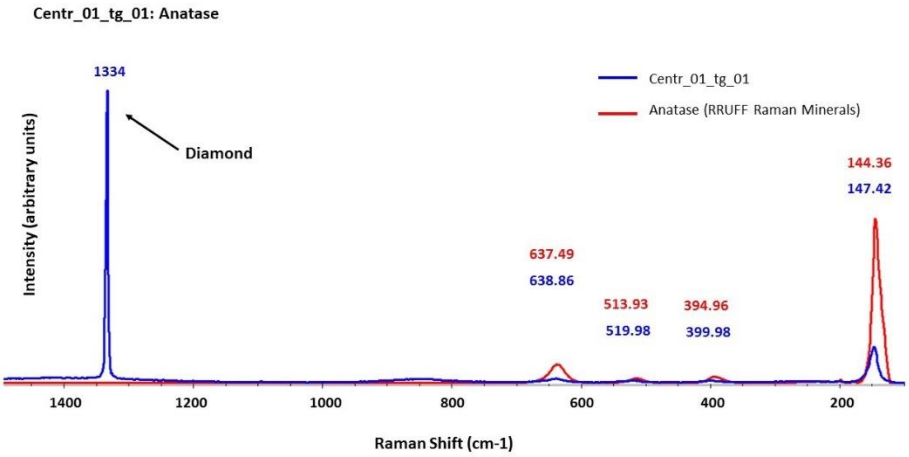

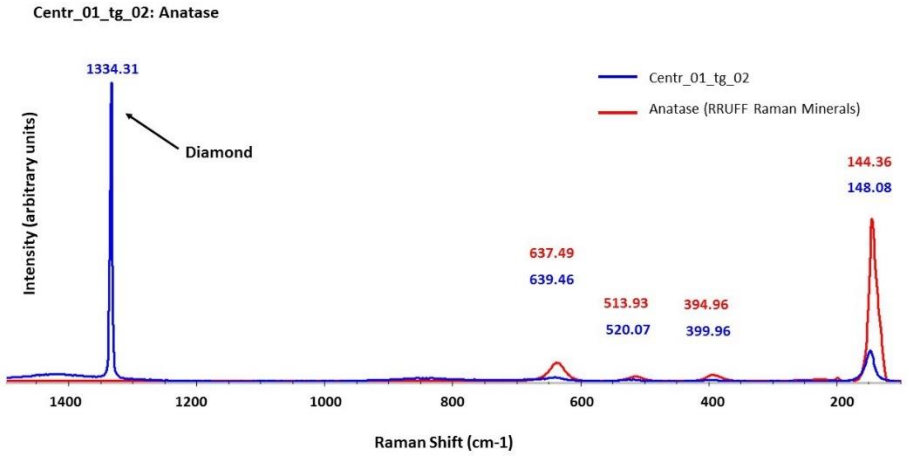

Centr_01_tg_03: Anatase

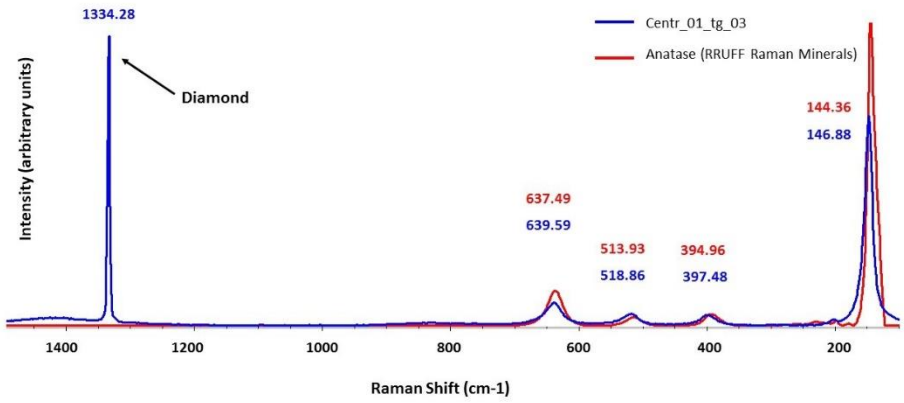

Centr_01_tg_04: Anatase

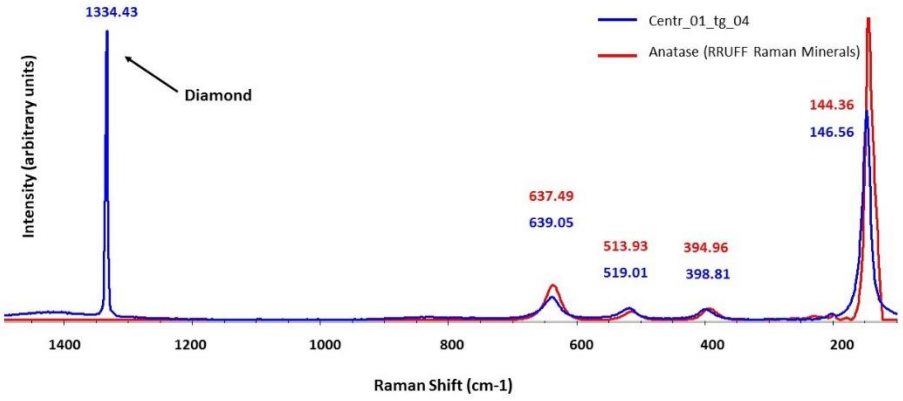

Centr_01_tg_05: Anatase

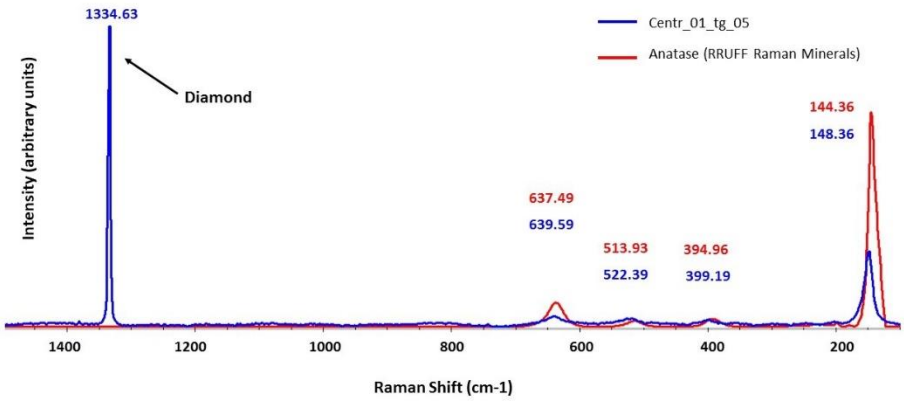

Centr_01_tg_06: Anatase

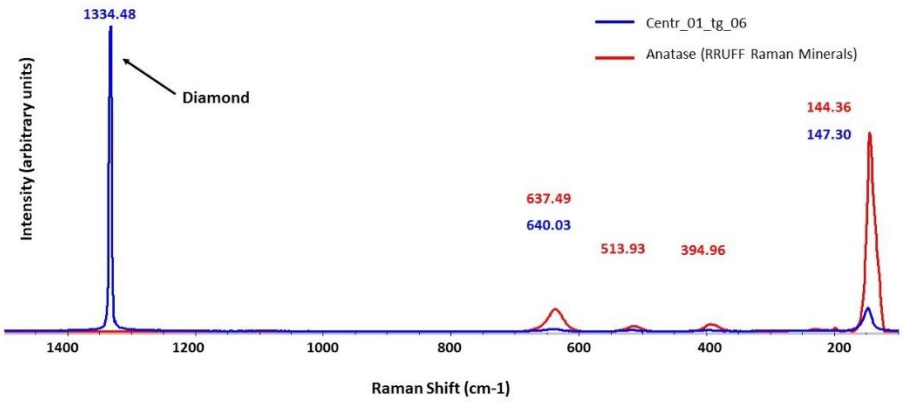

Centr_01_tg_07: Calcite

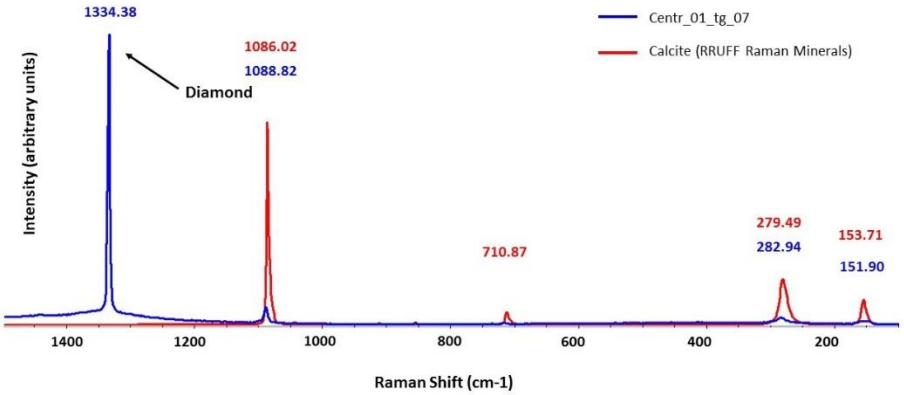

Centr_01_tg_08: Anatase

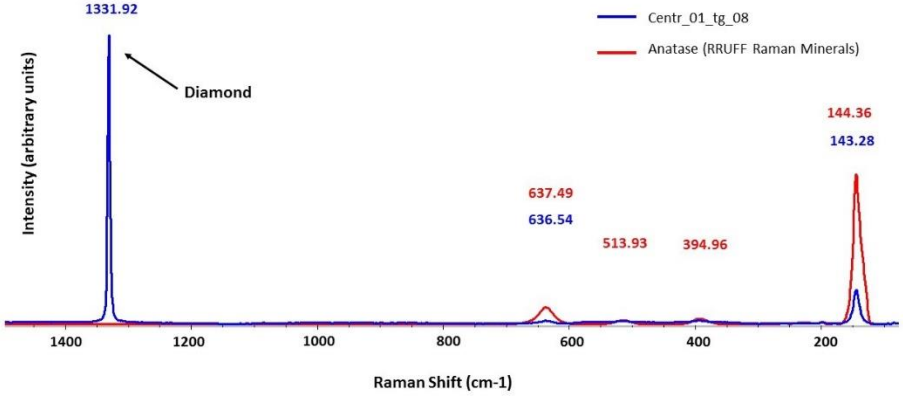

Centr_01_tg_09: Anatase + Calcite

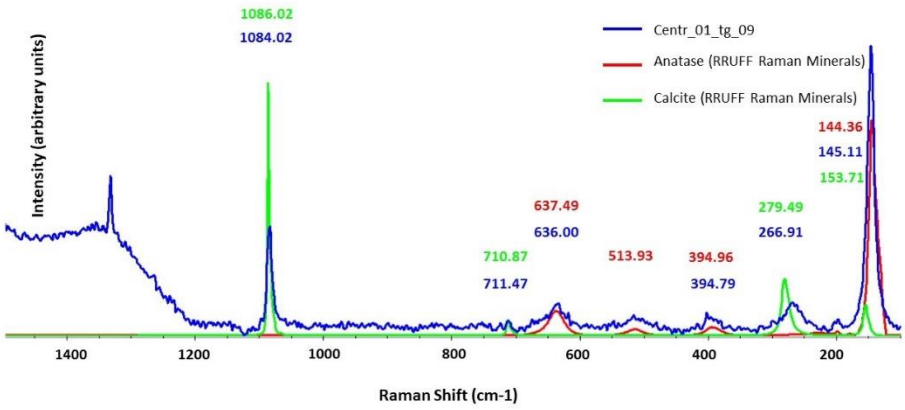

Centr_01_tg_10: Ringwoodite + ?

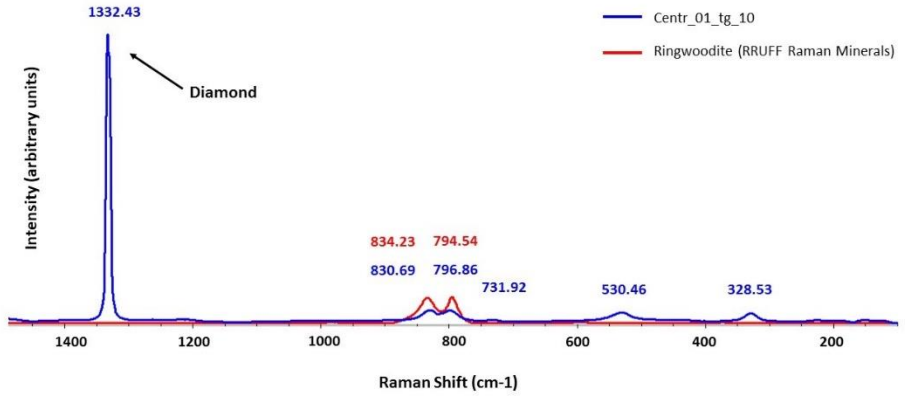

Centr_01_tg_11: Fluid phase

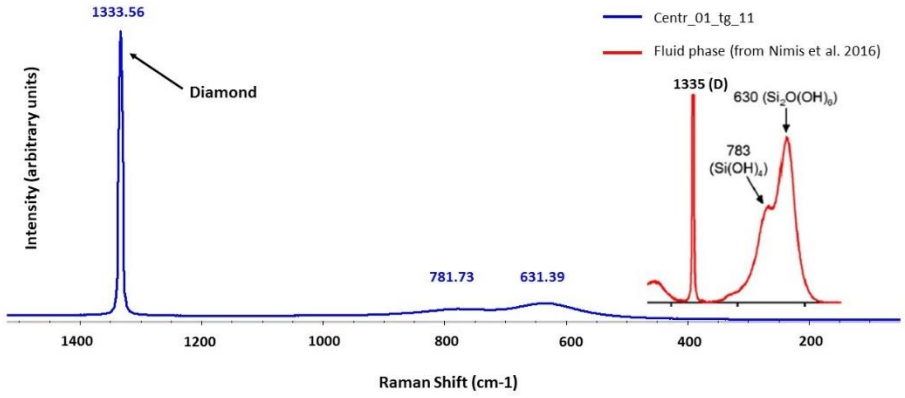

Centr_01_tg_12: Fluid phase

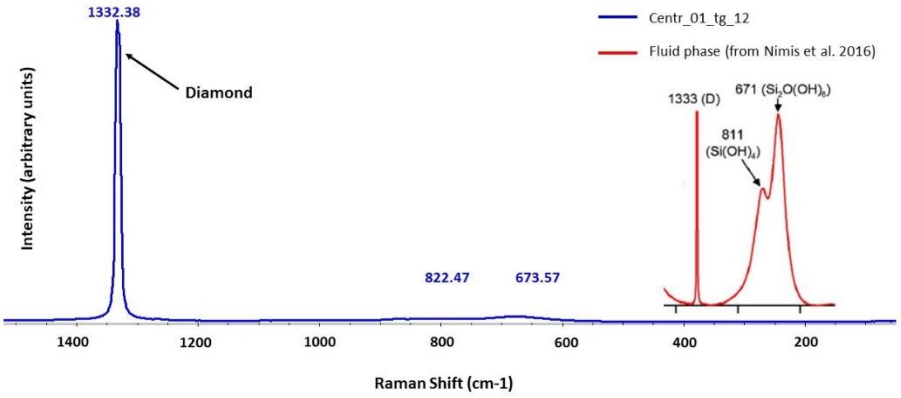

Centr_01_tg_13: Fluid phase

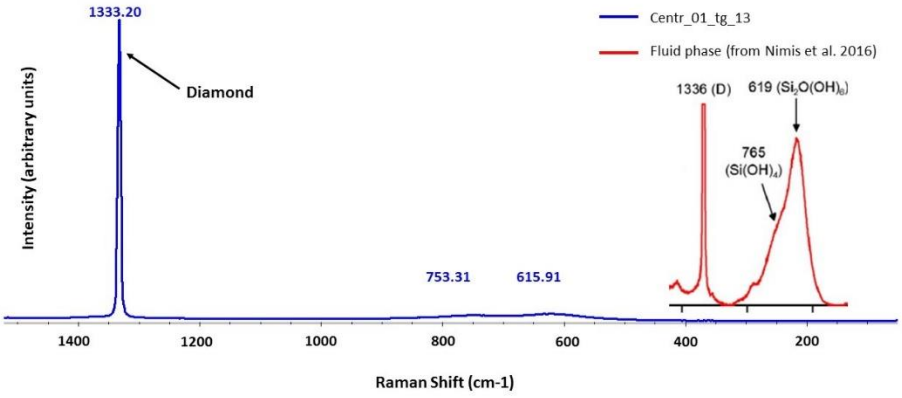

The photos of the inclusions within the sample *Centr_01_tg* (the inclusions are within the red circle):

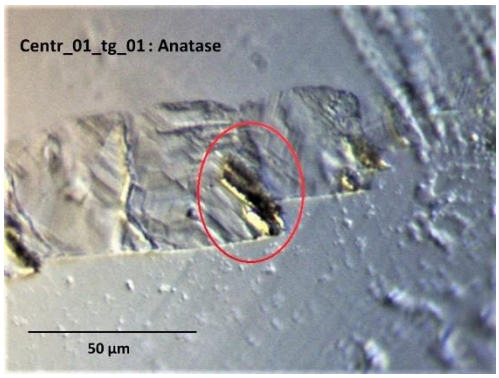

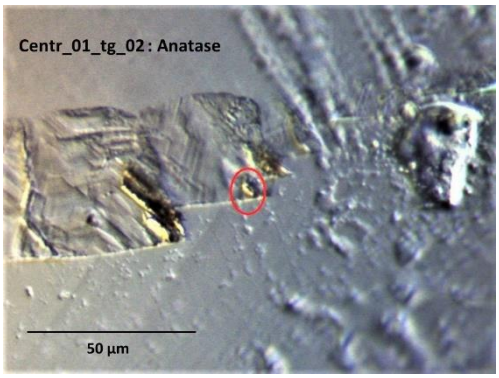

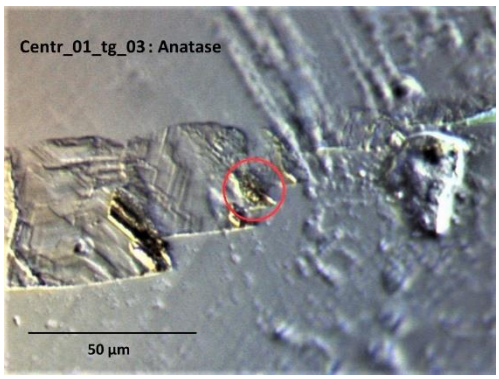

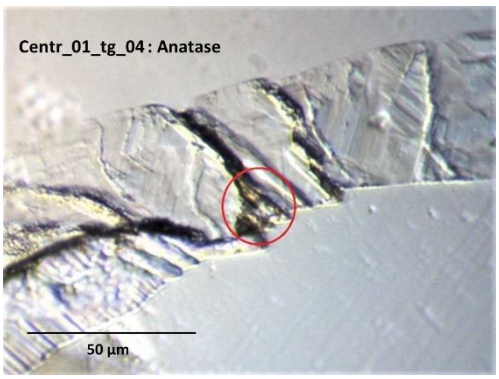

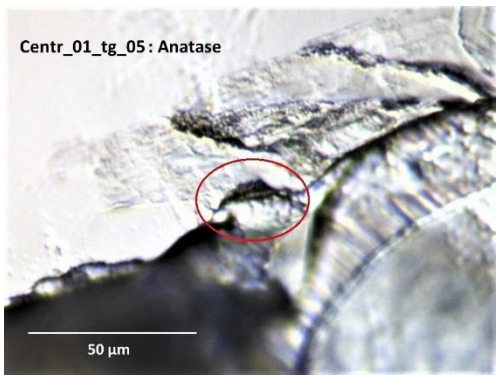

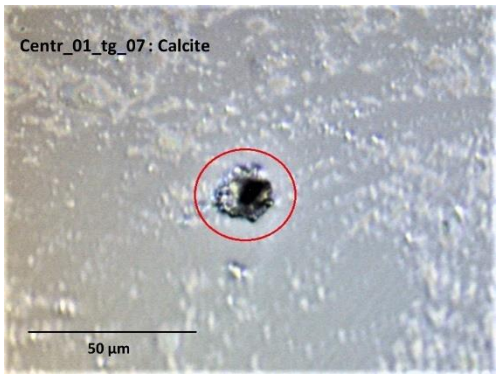

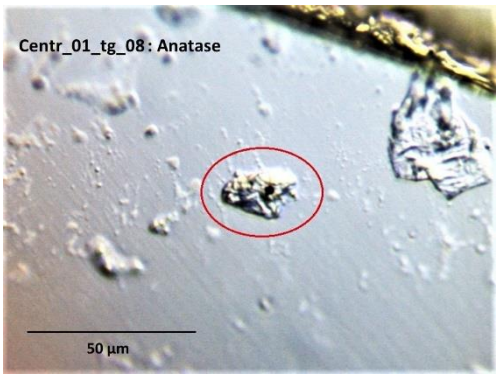

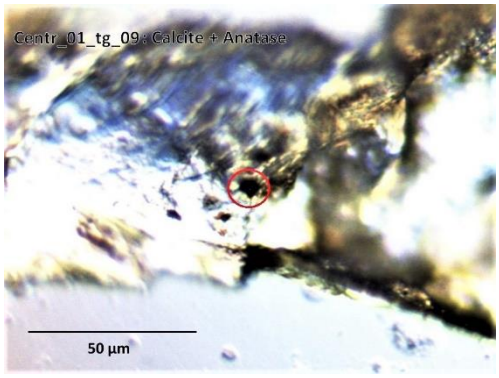
Centr_01_tg_09 : Calcite + Anatase
50 µm

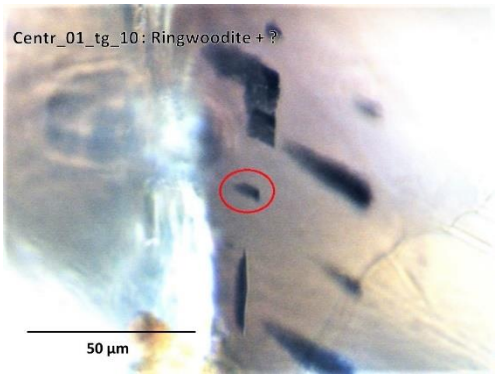
Centr_01_tg_10 : Ringwoodite + ?
50 µm

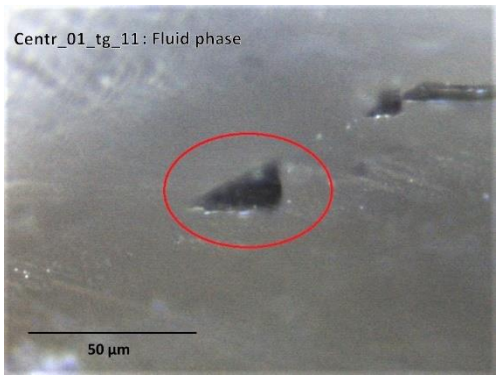
Centr_01_tg_11 : Fluid phase
50 µm

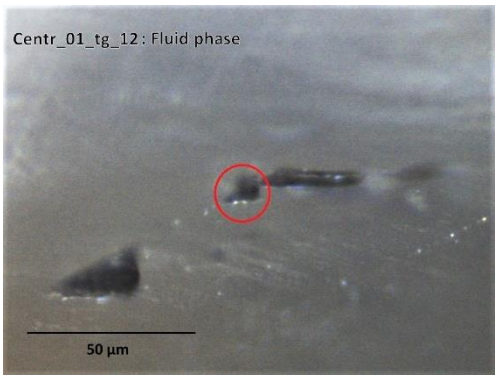
Centr_01_tg_12 : Fluid phase
50 µm


Centr_01_tg_13 : Fluid phase
50 µm

Appendix B

The spectra of inclusions within the sample *Centr_02_tg*:

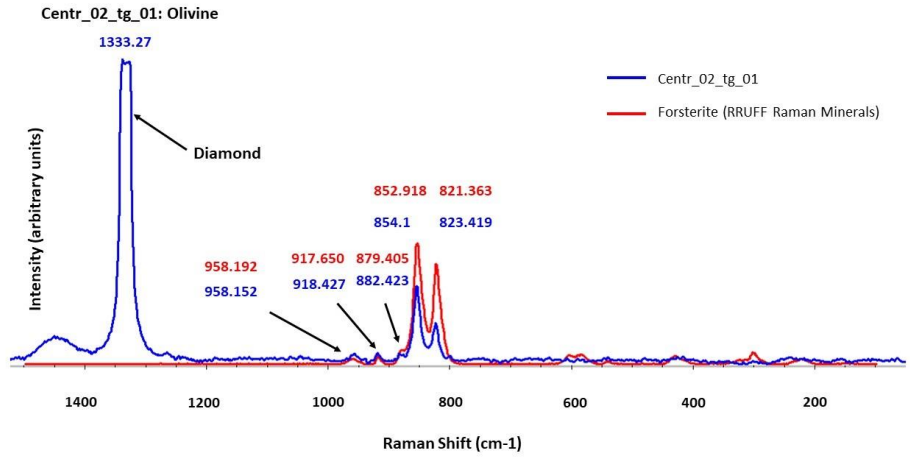

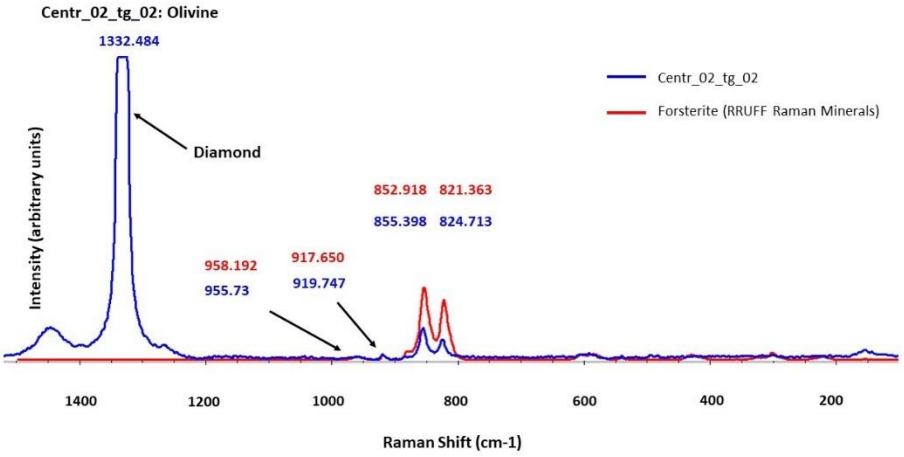

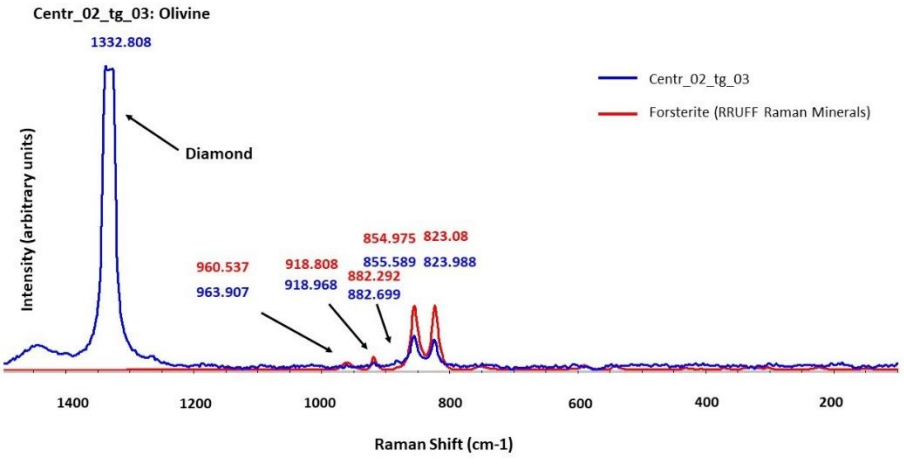
Centr_02_tg_03: Olivine
1332.808
Centr_02_tg_03
Forsterite (RRUFF Raman Minerals)
Diamond
Intensity (arbitrary units)
854.975 823.08
960.537
918.808
855.589 823.988
963.907
918.968
882.292
882.699
1400
1200
1000
800
600
400
200
Raman Shift (cm-1)

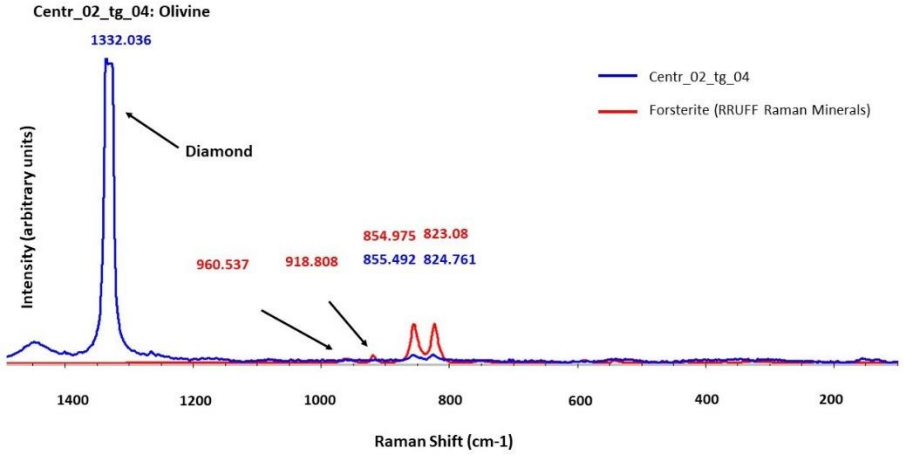
Centr_02_tg_04: Olivine
1332.036
Centr_02_tg_04
Forsterite (RRUFF Raman Minerals)
Diamond
Intensity (arbitrary units)
854.975 823.08
960.537
918.808
855.492 824.761
1400
1200
1000
800
600
400
200
Raman Shift (cm-1)

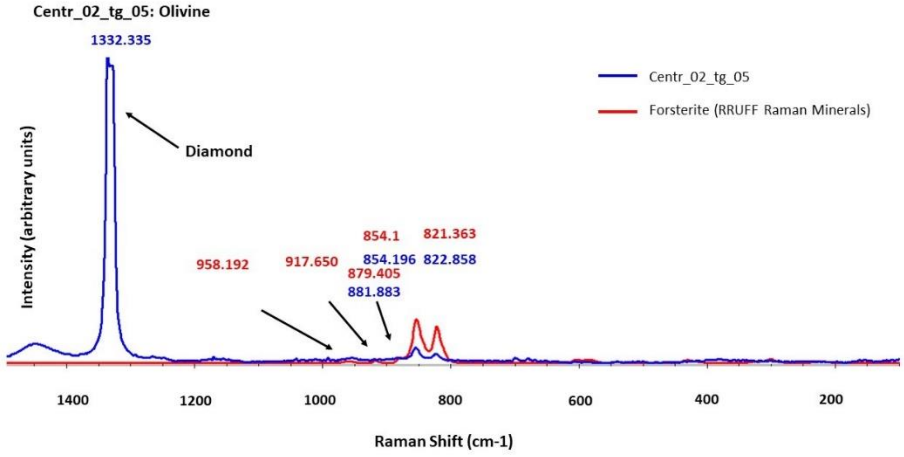
Centr_02_tg_05: Olivine
1332.335
Centr_02_tg_05
Forsterite (RRUFF Raman Minerals)
Diamond
Intensity (arbitrary units)
854.1 821.363
958.192
917.650
854.196 822.858
879.405
881.883
1400
1200
1000
800
600
400
200
Raman Shift (cm-1)

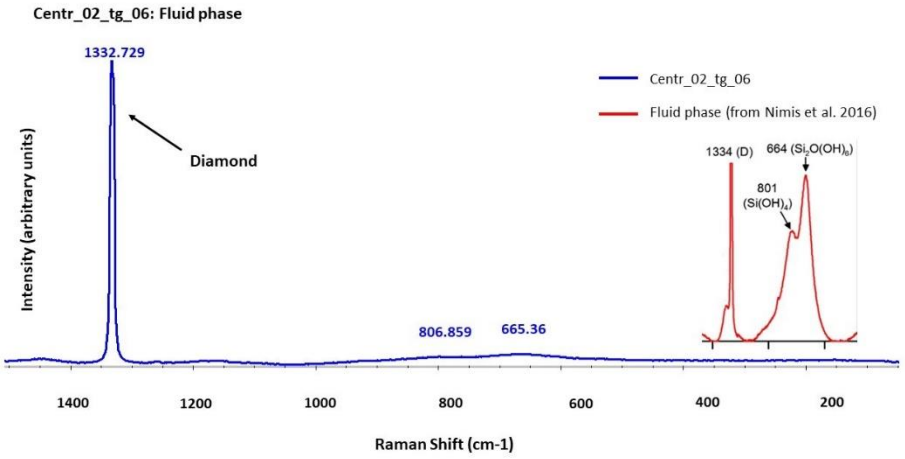
Centr_02_tg_06: Fluid phase
1332.729
Diamond
Centr_02_tg_06
Fluid phase (from Nimis et al. 2016)
1334 (D)
664 (Si2O(OH)6)
801
(Si(OH)4)
806.859
665.36
Intensity (arbitrary units)
1400
1200
1000
800
600
400
200
Raman Shift (cm-1)

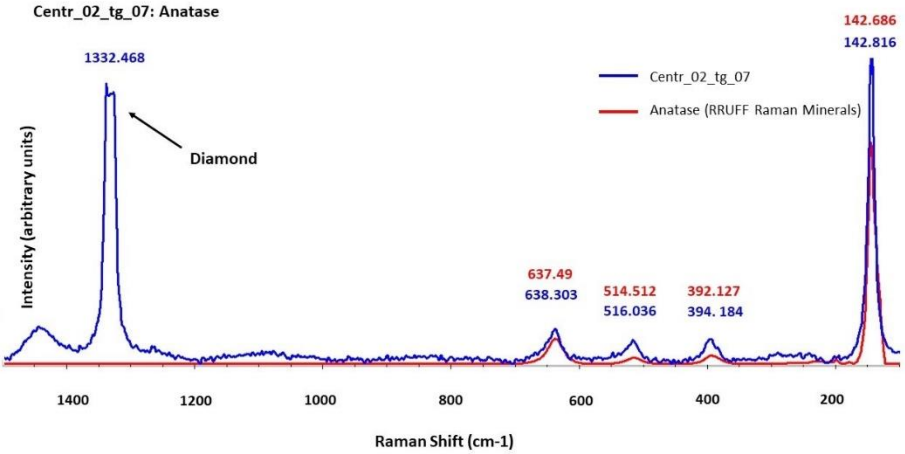
Centr_02_tg_07: Anatase
1332.468
Diamond
142.686
142.816
Centr_02_tg_07
Anatase (RRUFF Raman Minerals)
637.49
638.303
514.512
516.036
392.127
394. 184
Intensity (arbitrary units)
1400
1200
1000
800
600
400
200
Raman Shift (cm-1)

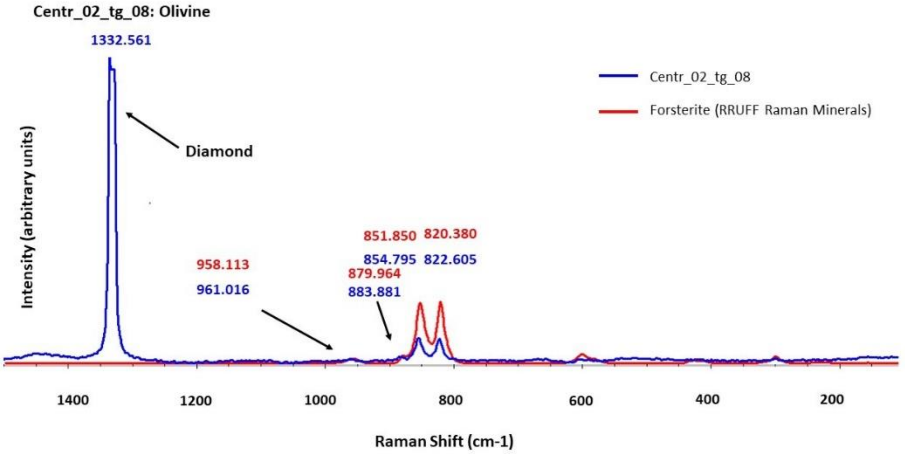
Centr_02_tg_08: Olivine
1332.561
Diamond
Centr_02_tg_08
Forsterite (RRUFF Raman Minerals)
851.850
820.380
854.795
822.605
879.964
883.881
958.113
961.016
Intensity (arbitrary units)
1400
1200
1000
800
600
400
200
Raman Shift (cm-1)

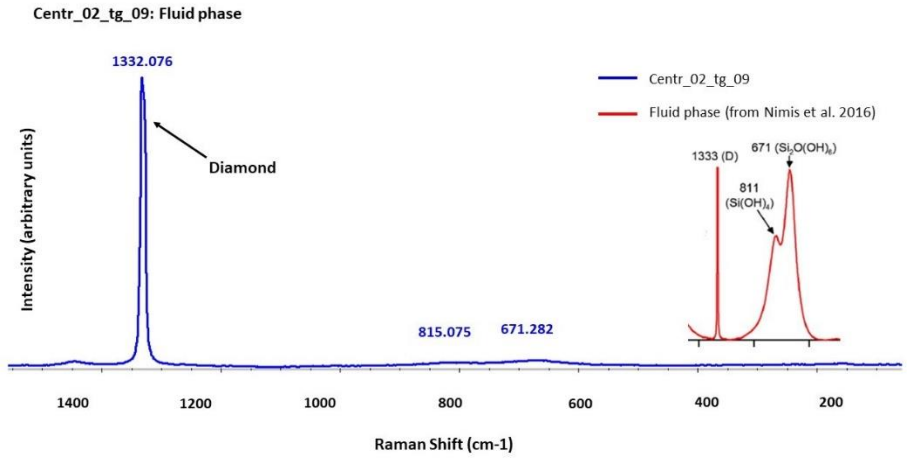
Centr_02_tg_09: Fluid phase
1332.076
Diamond
Centr_02_tg_09
Fluid phase (from Nimis et al. 2016)
1333 (D)
671 (Si3O(OH)6)
811
(Si(OH)4)
Intensity (arbitrary units)
815.075
671.282
1400
1200
1000
800
600
400
200
Raman Shift (cm-1)

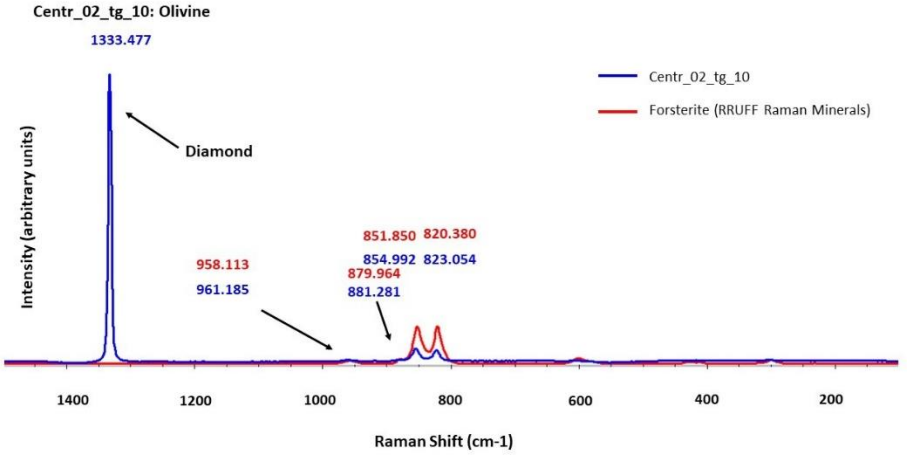
Centr_02_tg_10: Olivine
1333.477
Diamond
Centr_02_tg_10
Forsterite (RRUFF Raman Minerals)
Intensity (arbitrary units)
851.850
820.380
854.992
823.054
958.113
961.185
879.964
881.281
1400
1200
1000
800
600
400
200
Raman Shift (cm-1)

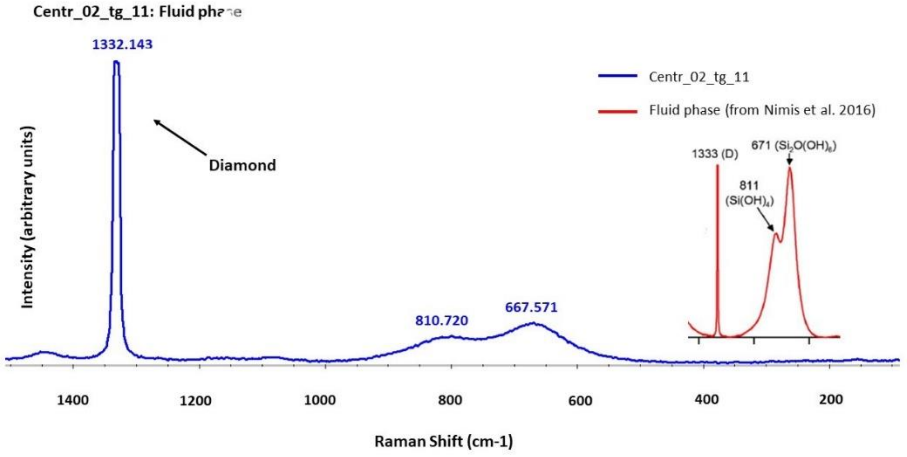
Centr_02_tg_11: Fluid phase
1332.143
Diamond
Centr_02_tg_11
Fluid phase (from Nimis et al. 2016)
1333 (D)
671 (Si3O(OH)6)
811
(Si(OH)4)
Intensity (arbitrary units)
810.720
667.571
1400
1200
1000
800
600
400
200
Raman Shift (cm-1)

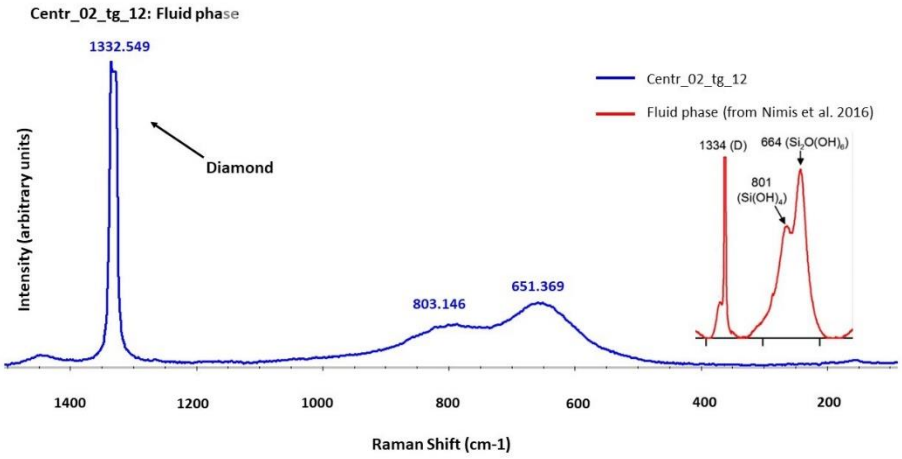
Centr_02_tg_12: Fluid phase
1332.549
Diamond
803.146
651.369
Centr_02_tg_12
Fluid phase (from Nimis et al. 2016)
1334 (D)
664 (Si2O(OH)6)
801
(Si(OH)4)
Intensity (arbitrary units)
1400
1200
1000
800
600
400
200
Raman Shift (cm-1)

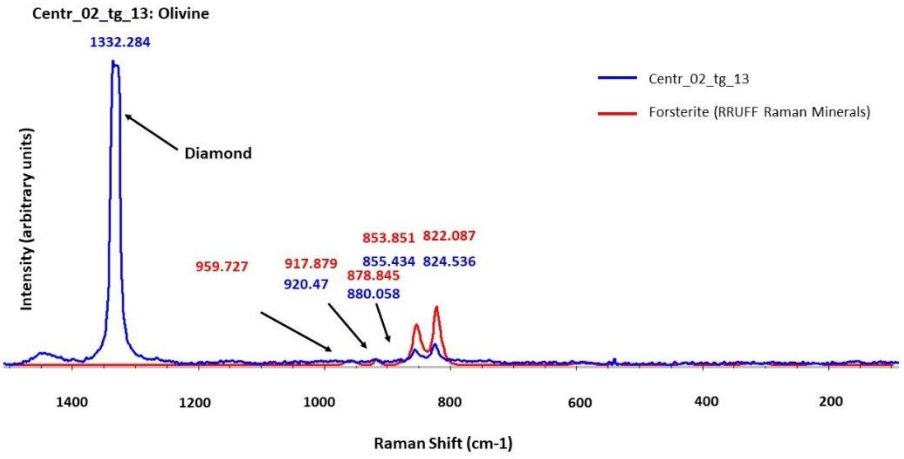
Centr_02_tg_13: Olivine
1332.284
Diamond
959.727
917.879
920.47
853.851
822.087
855.434
824.536
878.845
880.058
Centr_02_tg_13
Forsterite (RRUFF Raman Minerals)
Intensity (arbitrary units)
1400
1200
1000
800
600
400
200
Raman Shift (cm-1)

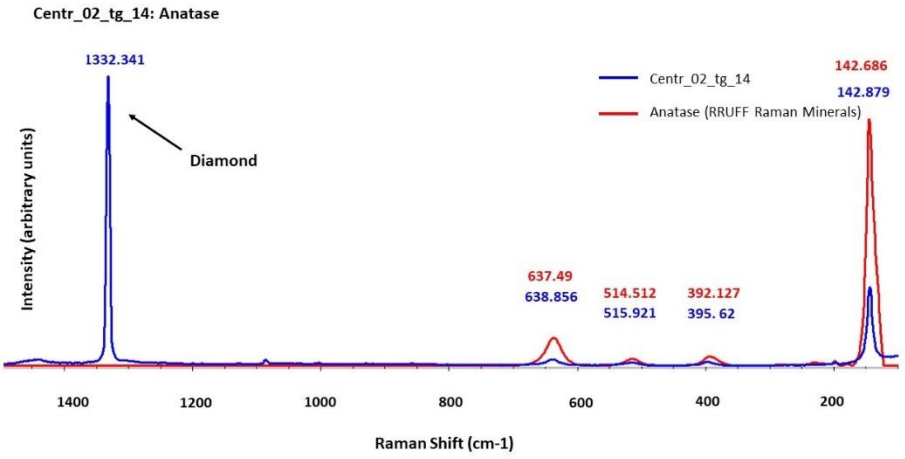
Centr_02_tg_14: Anatase
1332.341
Diamond
637.49
638.856
514.512
515.921
392.127
395. 62
142.686
142.879
Centr_02_tg_14
Anatase (RRUFF Raman Minerals)
Intensity (arbitrary units)
1400
1200
1000
800
600
400
200
Raman Shift (cm-1)

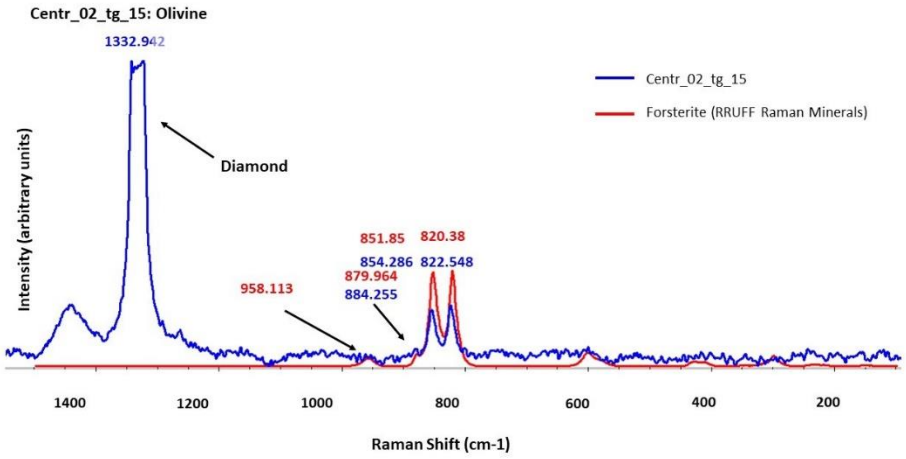
Centr_02_tg_15: Olivine
1332.942
Centr_02_tg_15
Forsterite (RRUFF Raman Minerals)
Diamond
Intensity (arbitrary units)
851.85
820.38
854.286
822.548
879.964
958.113
884.255
1400
1200
1000
800
600
400
200
Raman Shift (cm-1)

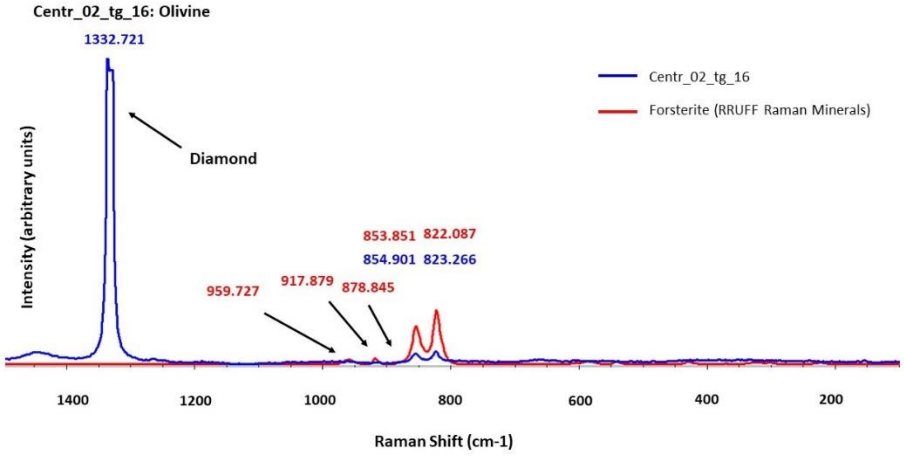
Centr_02_tg_16: Olivine
1332.721
Centr_02_tg_16
Forsterite (RRUFF Raman Minerals)
Diamond
Intensity (arbitrary units)
853.851
822.087
854.901
823.266
959.727
917.879
878.845
1400
1200
1000
800
600
400
200
Raman Shift (cm-1)

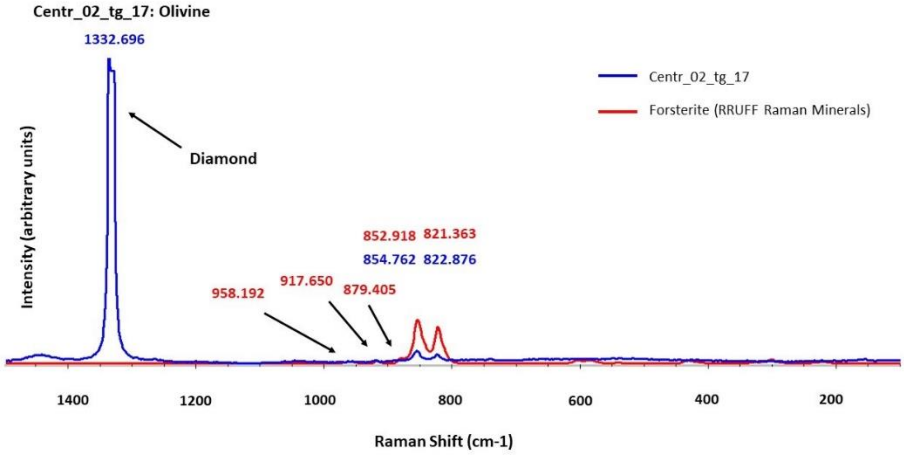
Centr_02_tg_17: Olivine
1332.696
Centr_02_tg_17
Forsterite (RRUFF Raman Minerals)
Diamond
Intensity (arbitrary units)
852.918
821.363
854.762
822.876
958.192
917.650
879.405
1400
1200
1000
800
600
400
200
Raman Shift (cm-1)

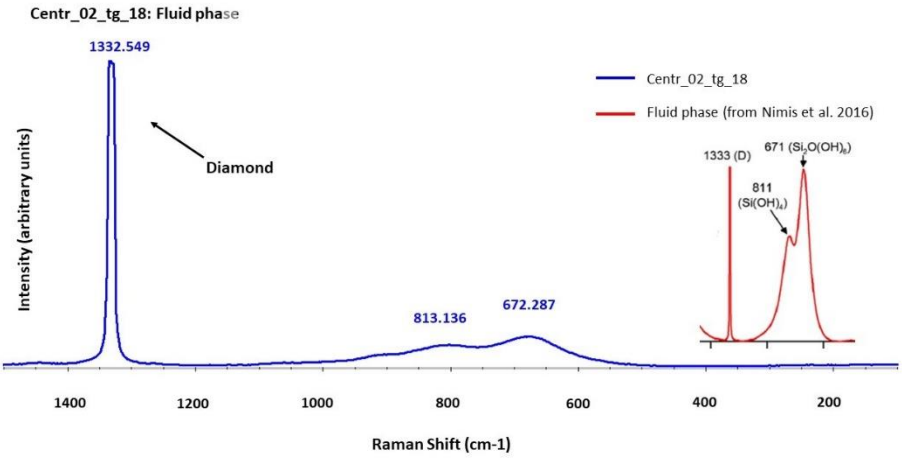
Centr_02_tg_18: Fluid phase
1332.549
Centr_02_tg_18
Fluid phase (from Nimis et al. 2016)
Diamond
1333 (D)
671 (Si2O(OH)6)
811
(Si(OH)4)
Intensity (arbitrary units)
813.136
672.287
1400
1200
1000
800
600
400
200
Raman Shift (cm-1)

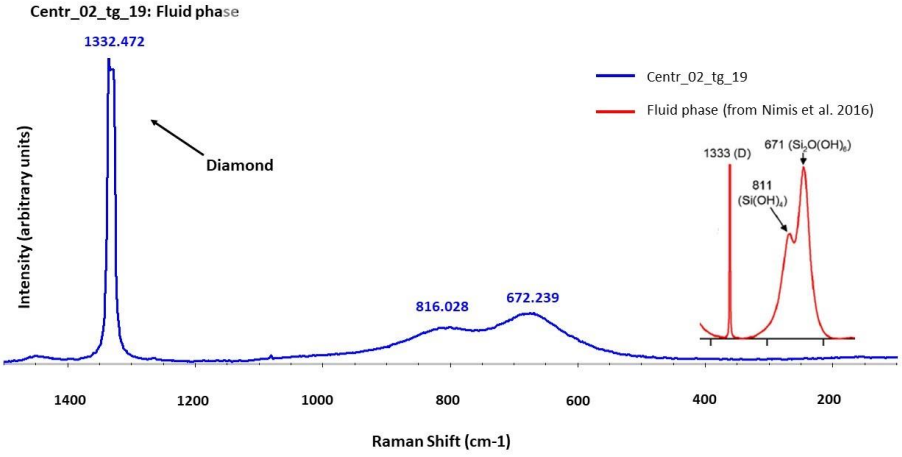
Centr_02_tg_19: Fluid phase
1332.472
Centr_02_tg_19
Fluid phase (from Nimis et al. 2016)
Diamond
1333 (D)
671 (Si2O(OH)6)
811
(Si(OH)4)
Intensity (arbitrary units)
816.028
672.239
1400
1200
1000
800
600
400
200
Raman Shift (cm-1)

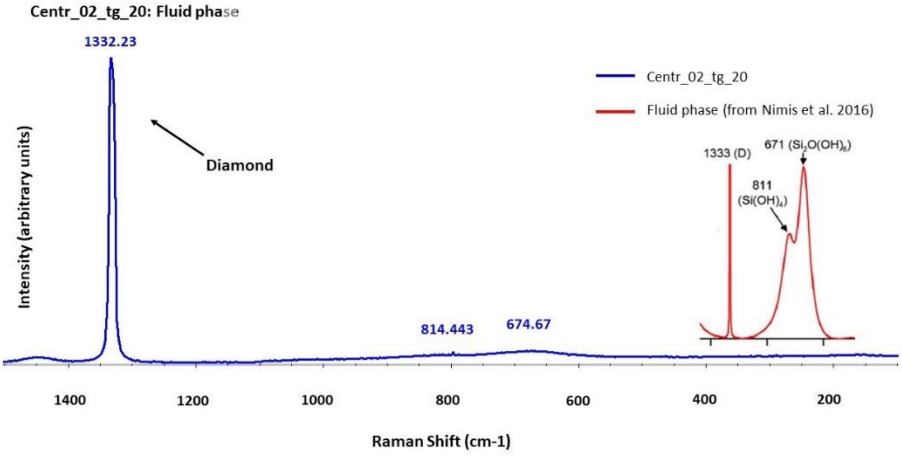
Centr_02_tg_20: Fluid phase
1332.23
Centr_02_tg_20
Fluid phase (from Nimis et al. 2016)
Diamond
1333 (D)
671 (Si2O(OH)6)
811
(Si(OH)4)
Intensity (arbitrary units)
814.443
674.67
1400
1200
1000
800
600
400
200
Raman Shift (cm-1)

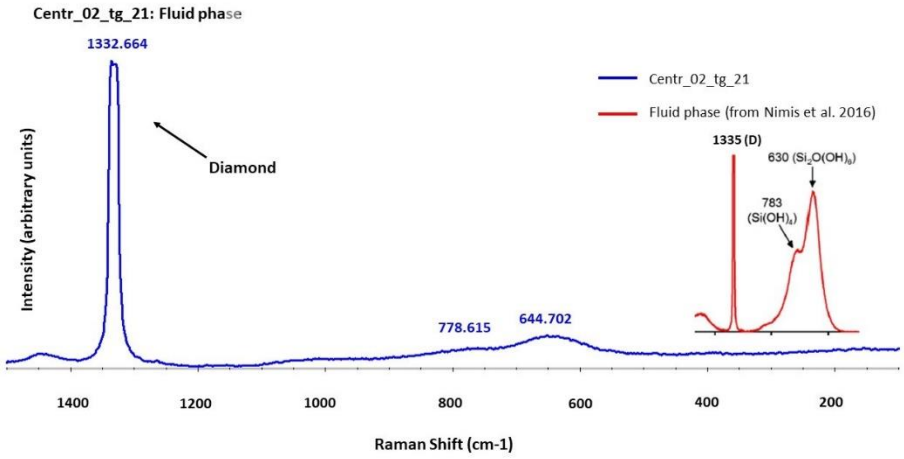
Centr_02_tg_21: Fluid phase
1332.664
Centr_02_tg_21
Fluid phase (from Nimis et al. 2016)
Diamond
1335 (D)
630 (Si2O(OH)6)
783
(Si(OH)4)
Intensity (arbitrary units)
778.615
644.702
1400
1200
1000
800
600
400
200
Raman Shift (cm-1)

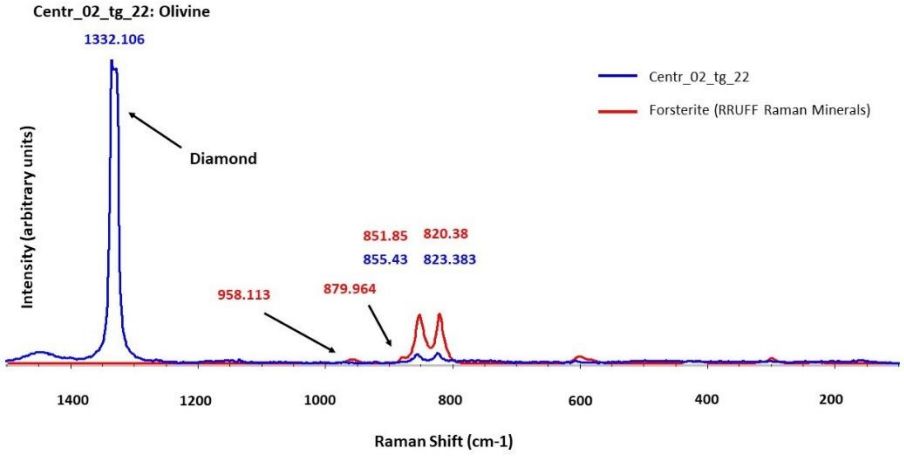
Centr_02_tg_22: Olivine
1332.106
Centr_02_tg_22
Forsterite (RRUFF Raman Minerals)
Diamond
851.85
820.38
855.43
823.383
958.113
879.964
Intensity (arbitrary units)
1400
1200
1000
800
600
400
200
Raman Shift (cm-1)

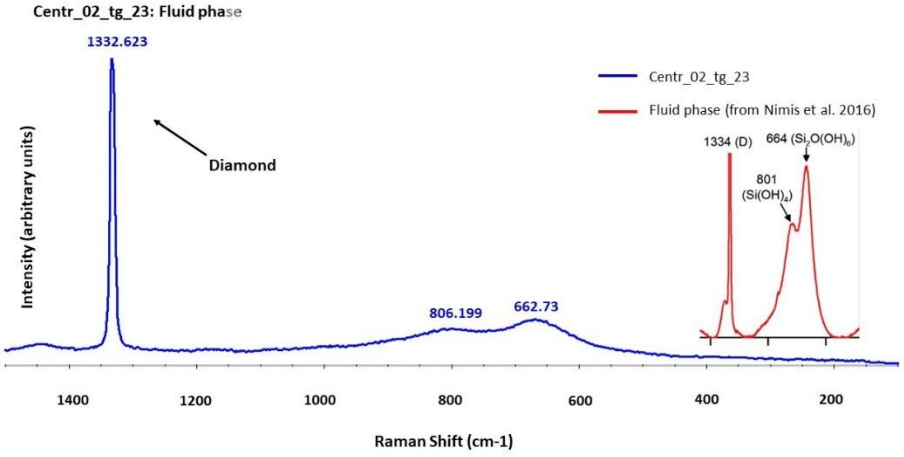
Centr_02_tg_23: Fluid phase
1332.623
Centr_02_tg_23
Fluid phase (from Nimis et al. 2016)
Diamond
1334 (D)
664 (Si2O(OH)6)
801
(Si(OH)4)
Intensity (arbitrary units)
806.199
662.73
1400
1200
1000
800
600
400
200
Raman Shift (cm-1)

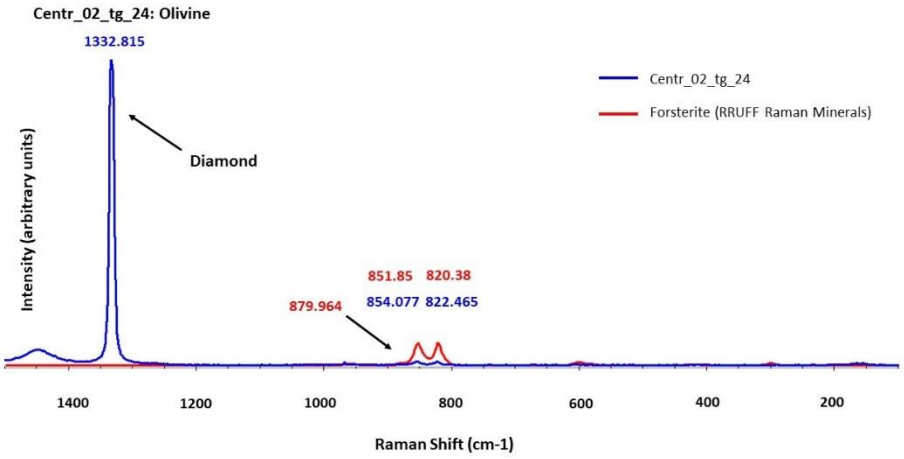
Centr_02_tg_24: Olivine
1332.815
Centr_02_tg_24
Forsterite (RRUFF Raman Minerals)
Diamond
Intensity (arbitrary units)
851.85 820.38
879.964
854.077 822.465
1400
1200
1000
800
600
400
200
Raman Shift (cm-1)

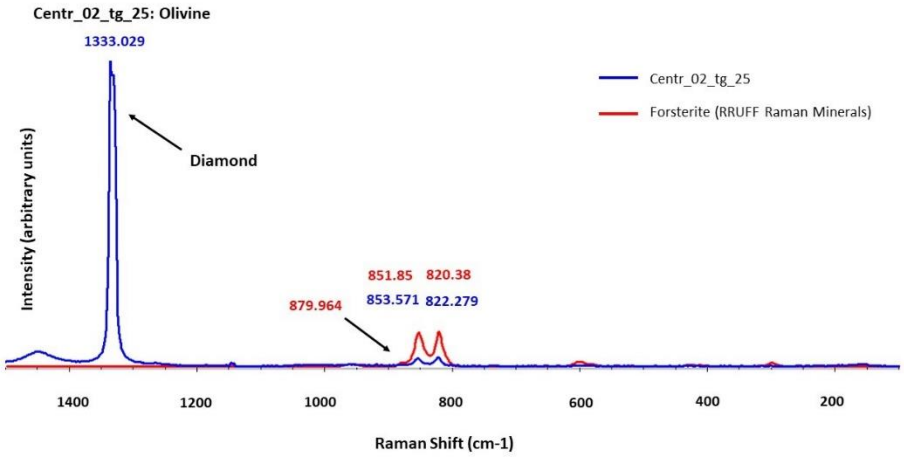
Centr_02_tg_25: Olivine
1333.029
Centr_02_tg_25
Forsterite (RRUFF Raman Minerals)
Diamond
Intensity (arbitrary units)
851.85 820.38
879.964
853.571 822.279
1400
1200
1000
800
600
400
200
Raman Shift (cm-1)

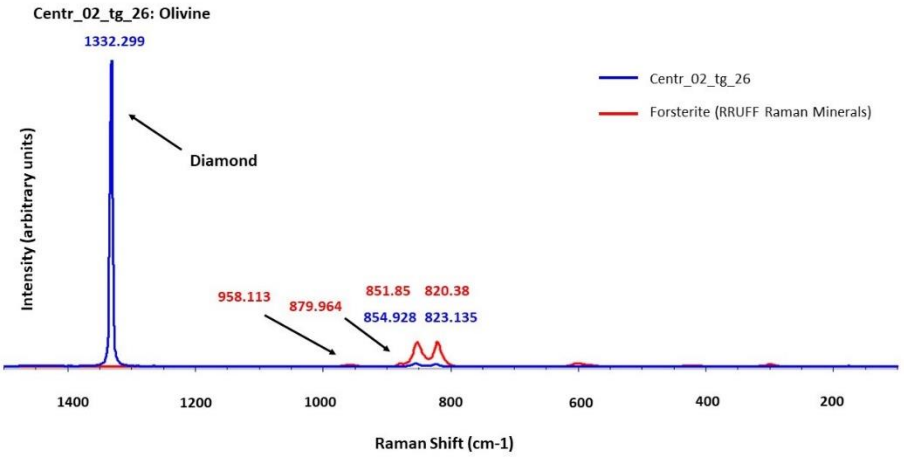
Centr_02_tg_26: Olivine
1332.299
Centr_02_tg_26
Forsterite (RRUFF Raman Minerals)
Diamond
Intensity (arbitrary units)
958.113
879.964
851.85 820.38
854.928 823.135
1400
1200
1000
800
600
400
200
Raman Shift (cm-1)

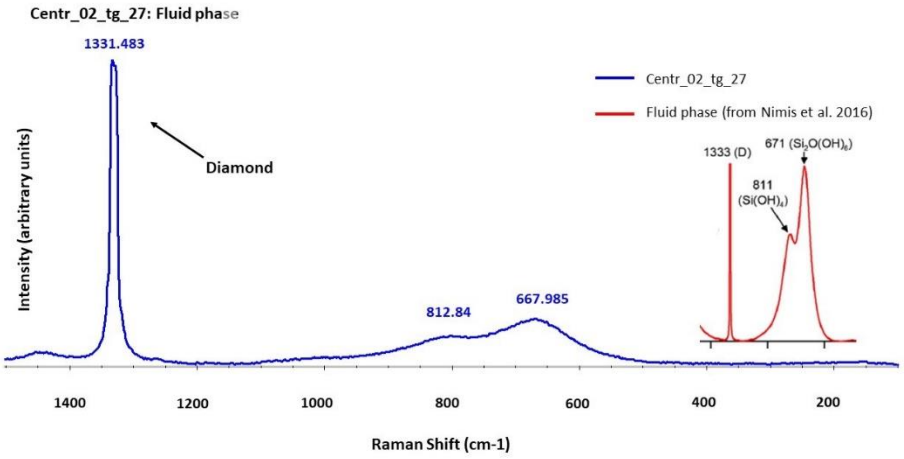
Centr_02_tg_27: Fluid phase
1331.483
Diamond
812.84
667.985
Centr_02_tg_27
Fluid phase (from Nimis et al. 2016)
1333 (D)
671 (Si2O(OH)6)
811
(Si(OH)4)
Intensity (arbitrary units)
1400
1200
1000
800
600
400
200
Raman Shift (cm-1)

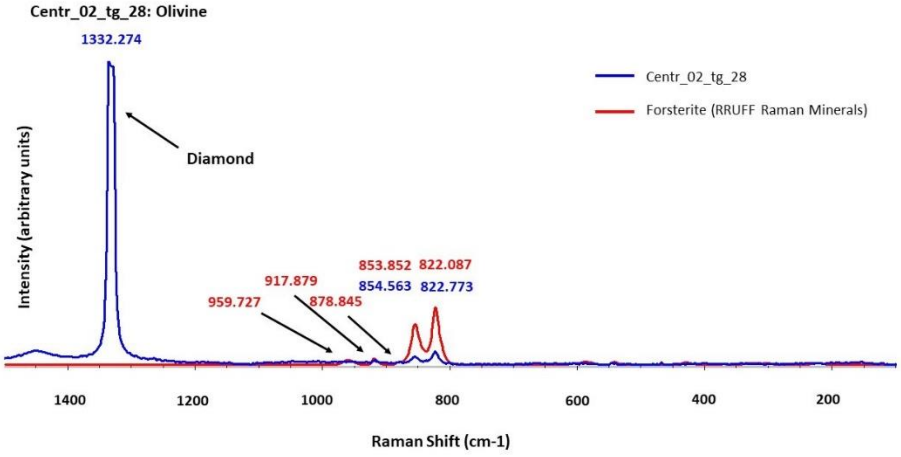
Centr_02_tg_28: Olivine
1332.274
Diamond
959.727
917.879
878.845
853.852
822.087
854.563
822.773
Centr_02_tg_28
Forsterite (RRUFF Raman Minerals)
Intensity (arbitrary units)
1400
1200
1000
800
600
400
200
Raman Shift (cm-1)

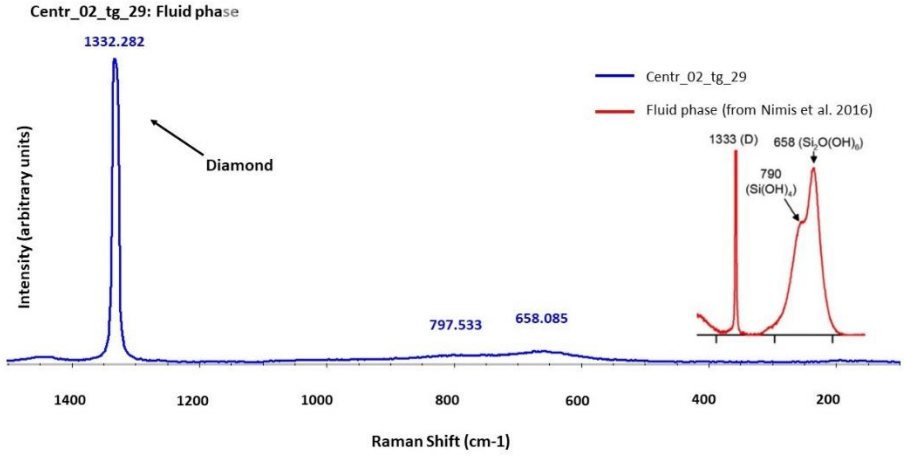
Centr_02_tg_29: Fluid phase
1332.282
Diamond
797.533
658.085
Centr_02_tg_29
Fluid phase (from Nimis et al. 2016)
1333 (D)
658 (Si2O(OH)6)
790
(Si(OH)4)
Intensity (arbitrary units)
1400
1200
1000
800
600
400
200
Raman Shift (cm-1)

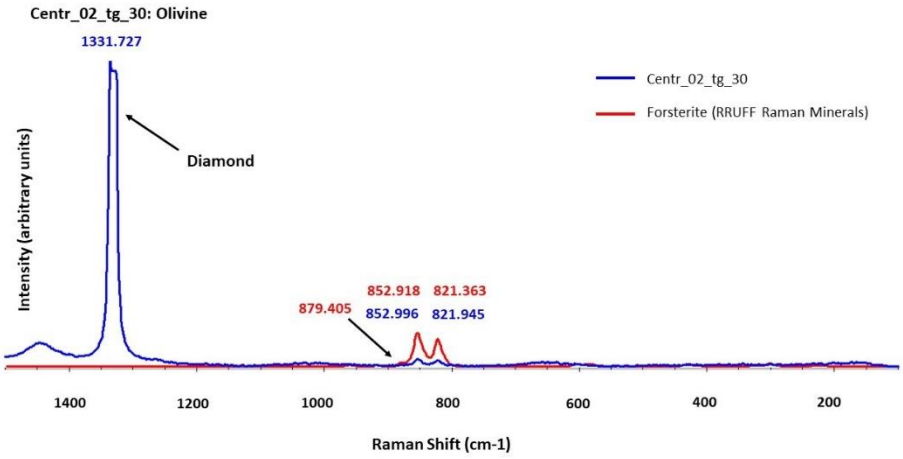
Centr_02_tg_30: Olivine
1331.727
Centr_02_tg_30
Forsterite (RRUFF Raman Minerals)
Diamond
Intensity (arbitrary units)
852.918
821.363
879.405
852.996
821.945
1400
1200
1000
800
600
400
200
Raman Shift (cm-1)

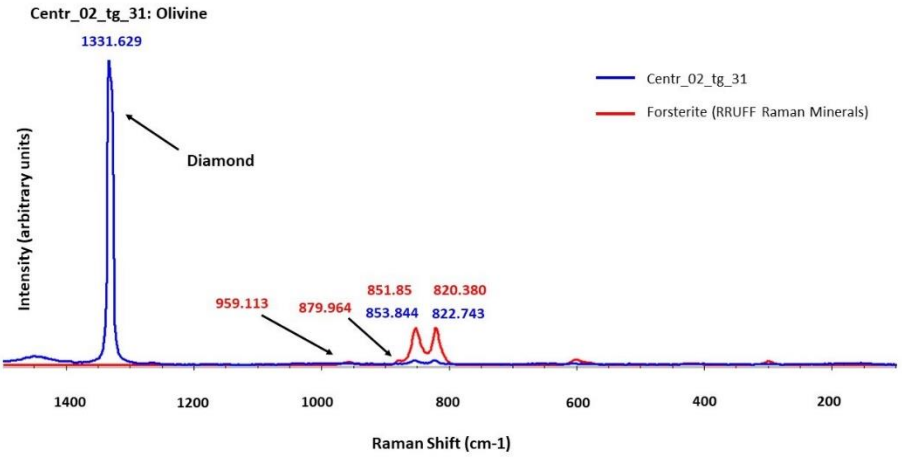
Centr_02_tg_31: Olivine
1331.629
Centr_02_tg_31
Forsterite (RRUFF Raman Minerals)
Diamond
Intensity (arbitrary units)
959.113
879.964
851.85
820.380
853.844
822.743
1400
1200
1000
800
600
400
200
Raman Shift (cm-1)

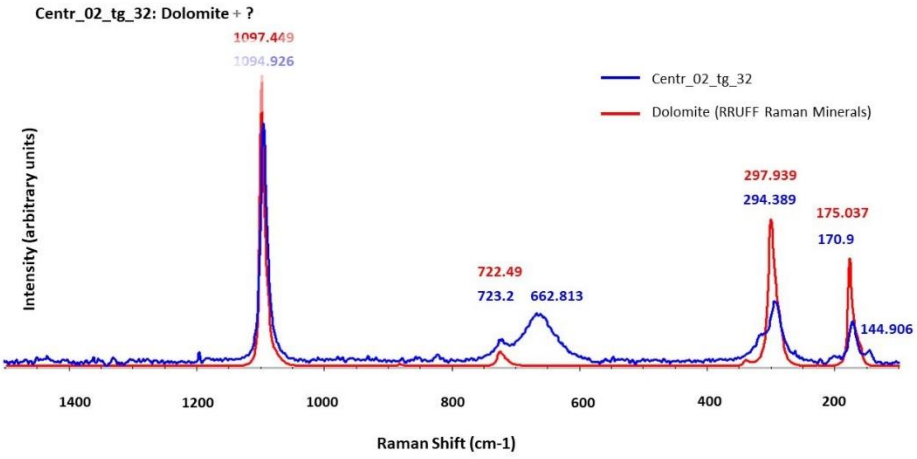
Centr_02_tg_32: Dolomite + ?
1097.449
1094.926
Centr_02_tg_32
Dolomite (RRUFF Raman Minerals)
Intensity (arbitrary units)
297.939
294.389
175.037
170.9
722.49
723.2
662.813
144.906
1400
1200
1000
800
600
400
200
Raman Shift (cm-1)

The photos of the inclusions within the sample *Centr_02_tg* (the inclusions are within the red circle):

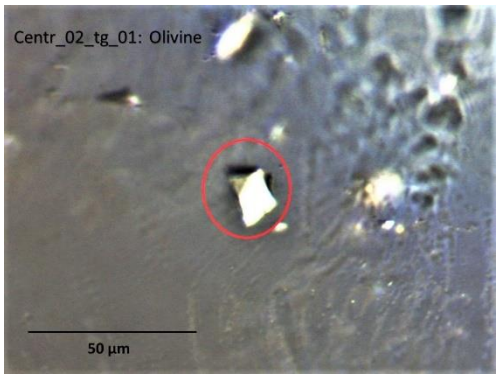

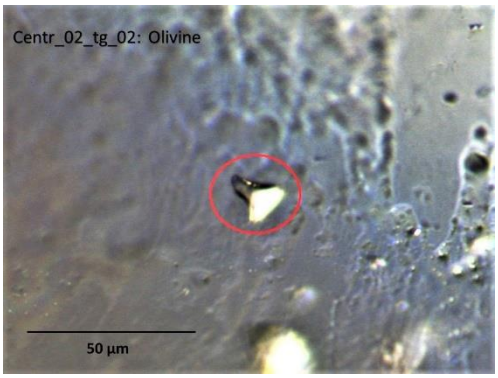

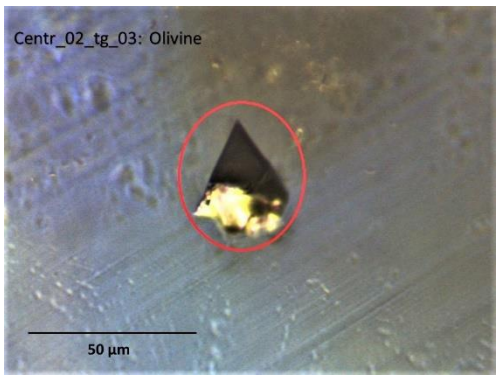

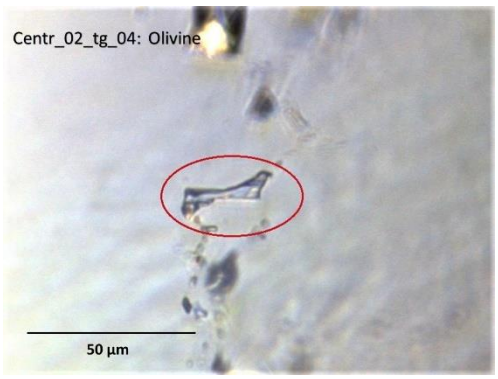

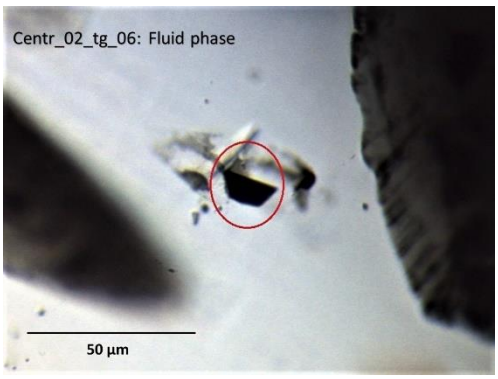

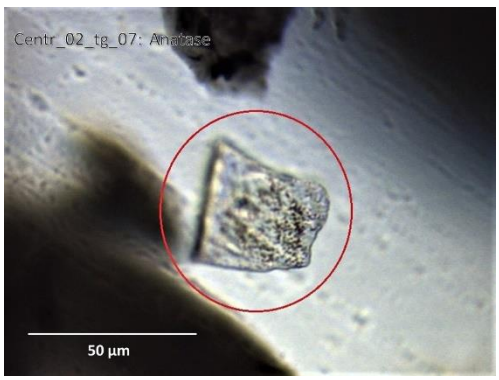

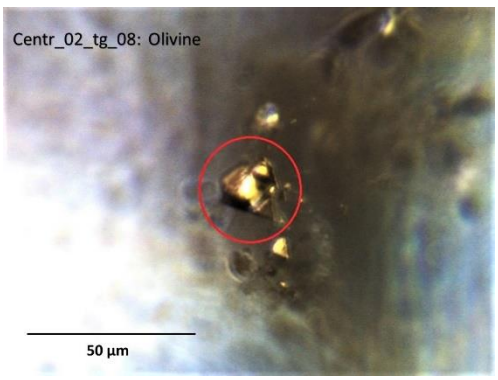

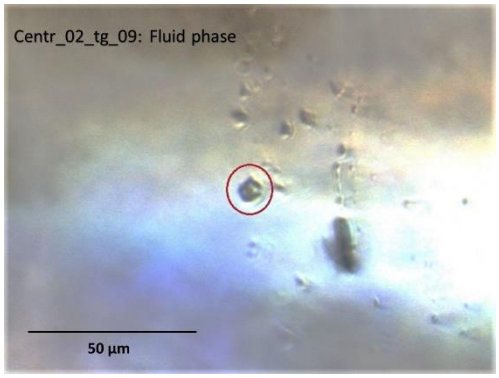
Centr_02_tg_09: Fluid phase
50 µm

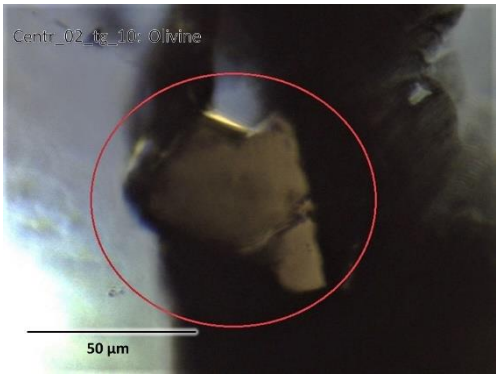
Centr_02_tg_10: Olivine
50 µm

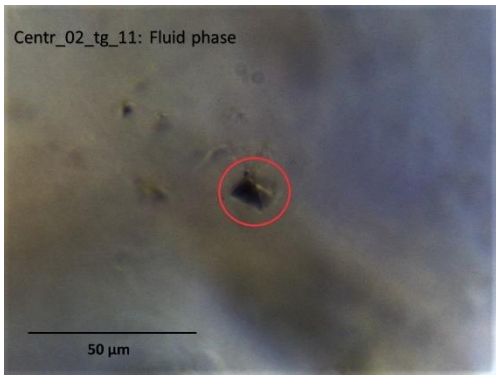
Centr_02_tg_11: Fluid phase
50 µm

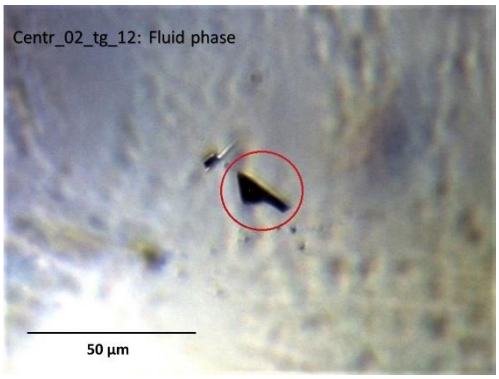
Centr_02_tg_12: Fluid phase
50 µm

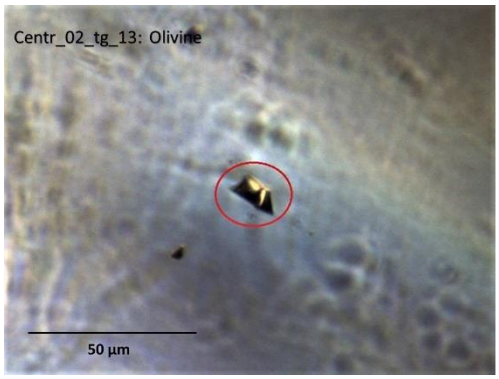
Centr_02_tg_13: Olivine
50 µm

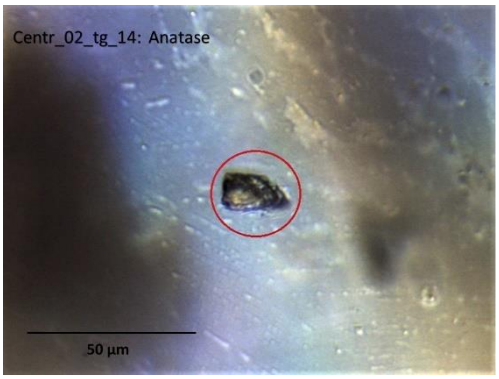
Centr_02_tg_14: Anatase
50 µm

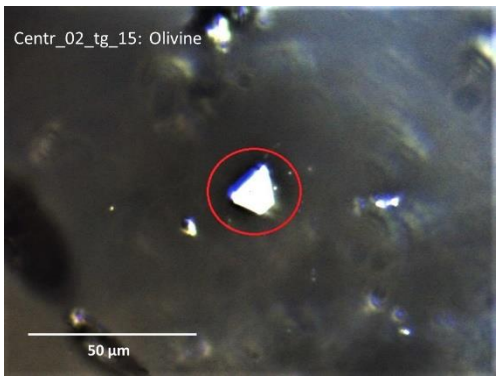
Centr_02_tg_15: Olivine
50 µm

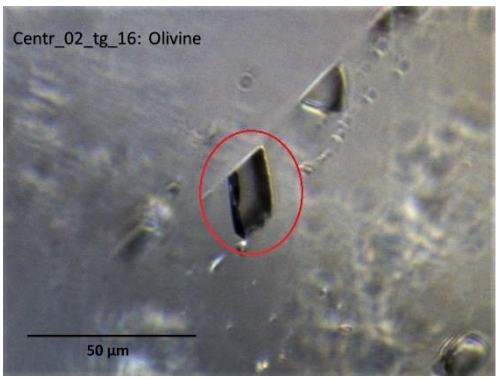
Centr_02_tg_16: Olivine
50 µm


Centr_02_tg_17: Olivine
50 µm

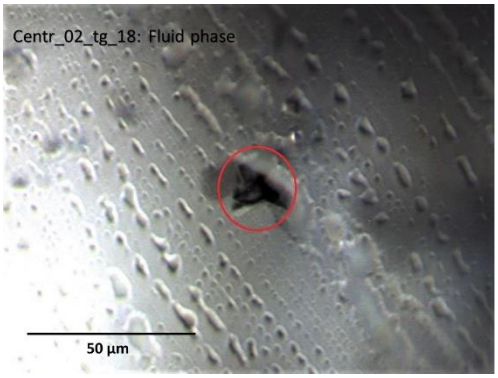
Centr_02_tg_18: Fluid phase
50 µm

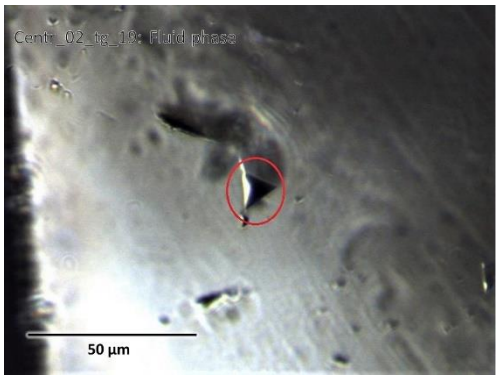
Centr_02_tg_19: Fluid phase
50 µm

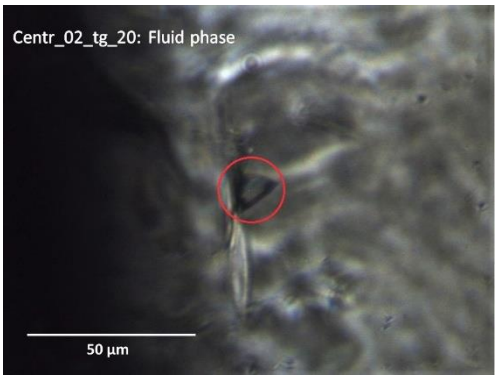
Centr_02_tg_20: Fluid phase
50 µm

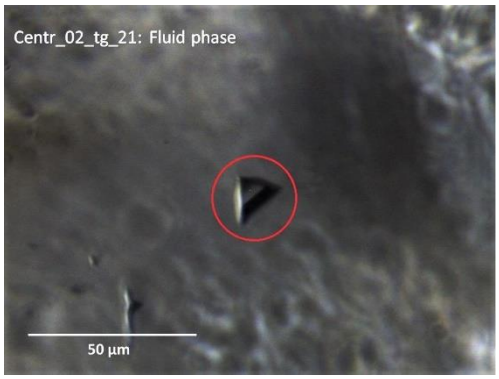
Centr_02_tg_21: Fluid phase
50 µm

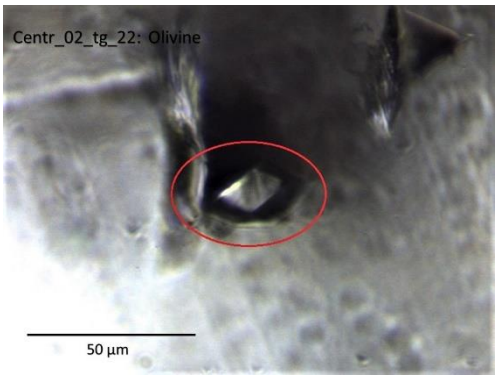
Centr_02_tg_22: Olivine
50 µm

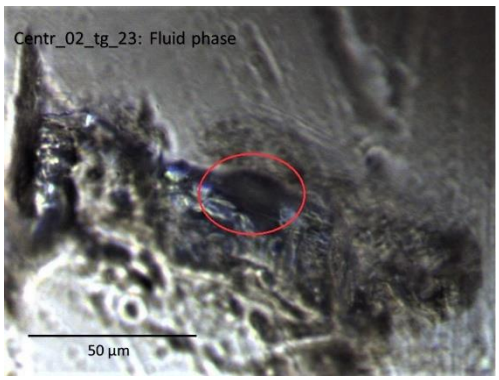
Centr_02_tg_23: Fluid phase
50 µm

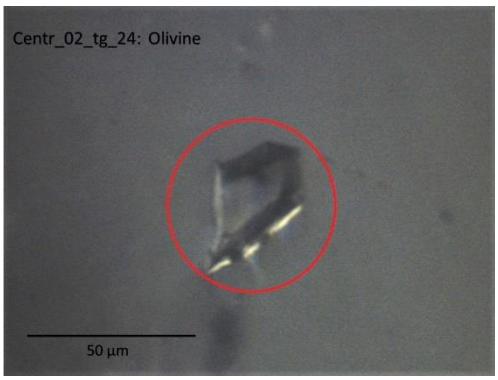
Centr_02_tg_24: Olivine
50 µm

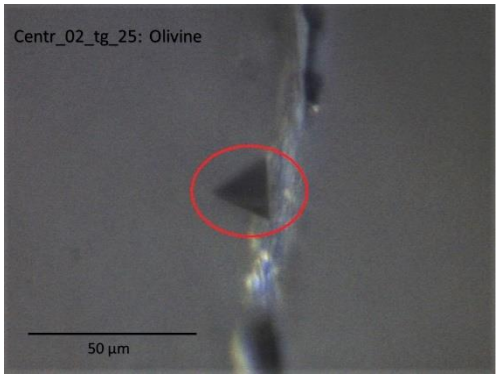
Centr_02_tg_25: Olivine
50 µm


Centr_02_tg_26: Olivine
50 µm

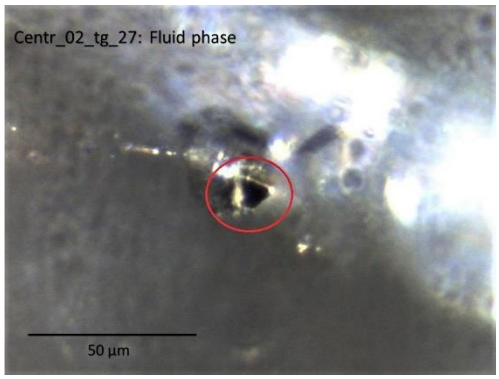
Centr_02_tg_27: Fluid phase
50 µm

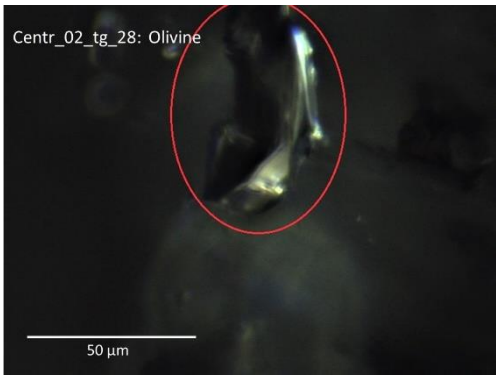
Centr_02_tg_28: Olivine
50 µm

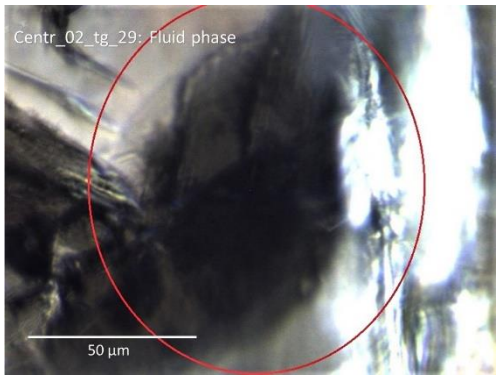
Centr_02_tg_29: Fluid phase
50 µm

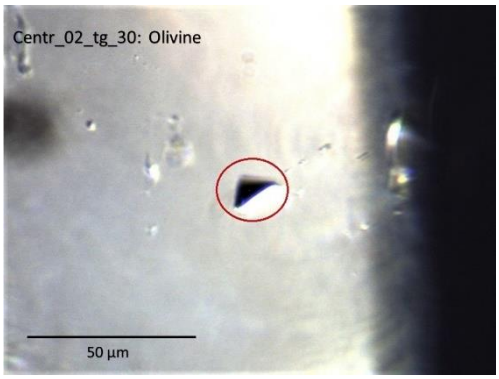
Centr_02_tg_30: Olivine
50 µm

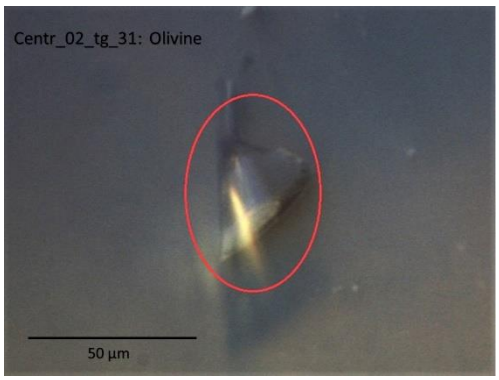
Centr_02_tg_31: Olivine
50 µm

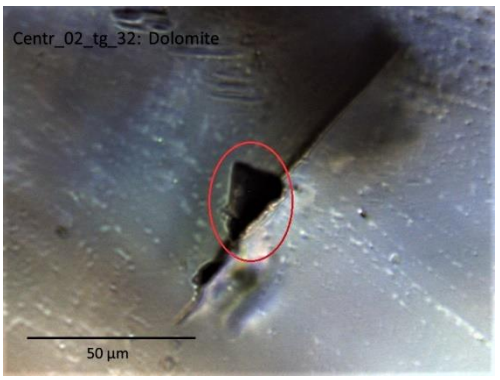
Centr_02_tg_32: Dolomite
50 µm

Ringraziamenti.

Questi ringraziamenti sono rivolti a tutte le persone che mi hanno supportato e mi sono state vicino in vari modi durante questo importante percorso e a tutte le persone che hanno reso possibile questo lavoro di tesi, collaborando con lo svolgimento delle analisi e l'aiuto nell'elaborare alcuni dati.

Prima di tutto voglio ringraziare la mia famiglia, mia madre e mio padre per aver creduto in me pagandomi gli studi in tutti questi anni (se non ci fossero stati loro ora non saremo qui a ringraziare) e per avermi sempre sostenuta durante tutto questo percorso, anche nei momenti più bui.
Inoltre, voglio ringraziare mia sorella Ginevra, che nonostante i momenti di amore e odio perenni e il continuo rinfacciarmi che sono una mantenuta e la preferita di mamma e papà, so che mi vuole bene, è orgogliosa di me e si sarà sicuramente fatta in 4 perché il giorno della mia laurea sia un giorno fantastico.

Poi voglio ringraziare tutti i miei amici da Ormelle e dintorni: Giulia, che oltre ai momenti folli passati insieme, mi ha fatto conoscere Padova e il mondo universitario, Giorgia, Anna, Sabri, Giulia e Alice per le serate, risate, uscite fuori porta e tutti i momenti passati insieme!
Anche se purtroppo ora ci si vede troppo poco, so che in ogni momento posso contare su di voi!

Un ringraziamento speciale va alle mie coinquiline attuali e passate (Marty, Giada, Hasna, Giulia, Agnese, Chiara e Arianna) per la lunghissima e bellissima convivenza in via Belzoni, le cene, le serate passate a salvare il mondo, gli aperitivi, e i momenti di sclero generale vissuti e superati insieme.

Un grazie super speciale a tutti i miei amici geologi, in particolare la vecchia squadra "Mondo Bueo", Calle, Menga, Cate ed Anna, la "Famiglia degradata", Leo, Simo, Puli, Vero e Anna e tutti i geologi generali, per tutti i campi passati insieme,

le gioie, i dolori, le sessioni, e tutti i momenti di pazzia (soprattutto durante le ultime settimane di tesi!).

Un grazie particolare ai miei inseparabili compagni di tesi, Anna e Leo, per il continuo supporto per le analisi, i momenti in laboratorio passati insieme, le notti insonni passate a scrivere la tesi e ad aggiornarci sul nostro stato psicologico sempre più instabile! Vi voglio bene ragazzi!!

Vorrei ringraziare anche il mio computer, che ha deciso di abbandonarmi 15 giorni prima della consegna della tesi!

Infine, vorrei ringraziare tutte le persone che hanno contribuito a questa tesi: il sig. Stefano Castelli e la Dr.ssa Caterina Canovaro per le foto ai campioni, il sig. Franco Salvadego per aver tagliato i diamanti, la Prof.ssa Alessandra Lorenzetti per le analisi allo spettrometro FTIR e la Dr.ssa Samantha Perrit per aver contribuito all'elaborazione di alcuni dati e aver seguito il progetto da remoto.

Ultimo, ma non per ultimo, il Prof. Nestola, che nonostante la mia follia, i "cazziatoni" e l'inglese da imparare, ha creduto in me dandomi la sua fiducia, la possibilità di lavorare con lui e tutte le opportunità che mi ha concesso e continua a concedere.

Spero di non aver dimenticato nessuno, in ogni caso grazie a tutte le persone che hanno reso questi 5 anni indimenticabili!